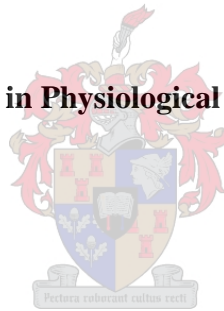


# **The hexosamine biosynthetic pathway induces gene promoter activity of the cardiac-enriched isoform of acetyl-CoA carboxylase**

**By Jamie Imbriolo**

**Submitted for the degree of PhD in Physiological Sciences at Stellenbosch University**



**Supervisor: Prof. M. Faadiel Essop**

**2013**

***I dedicate this work to my mother and my girlfriend Sophie, thank  
you for loving support that you have given me over the years***

## **Acknowledgements**

I would like to thank my supervisor, Prof. Faadiel Essop, for his support and patience. Thanks for the opportunity to acquire so many new techniques. I know that wherever I go I have a lot to offer in my next line of work.

I'd like to thank my mother for her support both financially and emotionally. Even though times were hard you helped me get this work completed.

I would like to thank Sophie for being there for 4 years. Not many have a girlfriend that is that dedicated to one person over such a long distance.

I'd like to thank NRF for the funding over the years.

I'd like to thank Dr Rob Smith for his help and constant support. Even making sure I was able to get transport to Stellenbosch to do this novel research.

I'd like to thank the coffee bean. You've seen me through two theses and without you I wouldn't have been able to stay awake.

## **Table of Contents**

	<b>Page</b>
<b>Declaration</b>	<b>i</b>
<b>Abstract</b>	<b>ii</b>
<b>Uittreksel</b>	<b>iv</b>
<b>Abbreviations</b>	<b>vi</b>
<b>List of Tables</b>	<b>x</b>
<b>List of Figures</b>	<b>x</b>
<b><u>Chapter 1: Introduction</u></b>	
1.1. Epidemiology	1
1.2. Metabolism of the heart	4
1.2.1. Fatty acid metabolism	6
1.2.2. A description of fatty acid sub classing	14

1.2.3. Glucose metabolism	15
1.2.4. Randle cycle	18
1.2.5. Hexosamine biosynthetic pathway	19
1.3. Aims of this study	26
 <b><u>Chapter 2: Methods</u></b>	
2.1. Transfections	28
2.1.1. Background to principles of the technique	28
2.1.2. Cell culture	30
2.1.3. Promoter-luciferase and DNA constructs used for transfection experiments	31
2.1.4. Preparation of plasmid DNA	32
2.1.5. Transfection procedures	37
2.1.6. Statistical analyses of Transfection results	40

2.1.7. Calculation of HOMA index	41
2.2. Real-time polymerase chain reaction	42
2.2.1 RNA extraction from Heart tissue Real Time Polymerase chain reaction	42
2.2.2. Animal model used for RNA experiments	43
2.2.3. Real-time polymerase chain reaction assay	43
2.3. Flow Cytometry	44
2.3.1. Cell preparation for flow cytometry	44
2.4. Chromatin immunoprecipitation	46
2.4.1. Chromatin immunoprecipitation of heart tissue in Wistar rats fed a high caloric diet	46
2.4.2. Western Blotting of Chromatin immunoprecipitation of heart tissue in Wistar rats fed a high caloric diet	47

2.5. Measuring fatty acid accumulation in Wistar rats fed a high caloric diet	48
---	----

## **Chapter 3: Results**

3.1. <i>In Vitro</i> Experiments	49
3.1.1. Transfections	49
3.2. Flow Cytometry	53
3.3. <i>In Vivo</i> Experiments	59
3.3.1. Animal model	59
3.3.2 Real-Time Polymerase Chain Reaction	63
3.3.3. Chromatin immunoprecipitation of heart tissue	65
3.3.4. Measuring USF2 O-GlcNAcylation with Immunoprecipitation and Western blotting	67
3.3.5. Fatty acid measurements	69

## **Chapter 4: Discussion**

4.1 Discussion	76
4.2. Conclusion	83
4.3. Limitations of this study	85
4.4. References	86

## **Chapter 5: Appendix**

Appendix	111
----------	-----

## **Declaration**

**I, the undersigned, hereby declare that the work contained in this thesis is my own original work and has not previously in its entirety or in part been submitted at any university for a degree.**

Jamie Imbriolo

---

Signature

12 February 2013

---

Date

**Copyright ©2013 Stellenbosch University**

**All rights reserved**

## **Abstract**

The cardiac isoform of acetyl-CoA carboxylase (ACC $\beta$ ) produces malonyl-CoA, a potent inhibitor of mitochondrial fatty acid (FA) uptake; thus increased ACC $\beta$  activity decreases fatty acid utilization thereby potentially leading to intracellular myocardial lipid accumulation and insulin resistance (IR). Previous studies show that greater flux through the hexosamine biosynthetic pathway (HBP) contributes to the development of IR. In light of this, we hypothesize that increased HBP flux induces ACC $\beta$  gene expression thereby contributing to the onset of IR. Our initial work focused on ACC $\beta$  gene promoter regulation and suggest that the HBP modulates upstream stimulatory factor 2 (USF2) thereby inducing ACC $\beta$  gene expression. Here, we further investigated HBP-mediated regulation of ACC $\beta$  gene expression by transiently transfecting cardiac-derived H9c2 cells with an expression vector encoding the rate-limiting HBP enzyme (GFAT)  $\pm$  the full length ACC $\beta$  and 4 truncated promoter-luciferase constructs, respectively. GFAT overexpression increased ACC $\beta$  gene promoter activity for the full length and 3 larger deletion constructs ( $p < 0.001$  vs. controls). However, GFAT-mediated and USF2-mediated ACC $\beta$  promoter induction was blunted when co-transfected with the -38/+65 deletion construct suggesting that USF2 binds to the proximal promoter region (near start codon). Further investigation proves that USF2 binds to ACC $\beta$  promoter and activates it, but that USF2 is not O-GlcNAc modified even though there is a strong correlation between increased O-GlcNAc levels and USF2 activation of ACC $\beta$ . This would suggest that there is another O-GlcNAc modified factor involved in this regulatory pathway. Our study demonstrates that increased HBP flux induces ACC $\beta$  gene promoter activity via HBP modulation of USF2. We propose that ACC $\beta$  induction reduces fatty acid oxidation, thereby leading

to intracellular lipid accumulation (FA uptake $\gg$ FA oxidation) and the onset of cardiac IR.

## Uittreksel

Die kardiaale isoform van asetiel-CoA karboksilase (ACC $\beta$ ) produseer maloniel-CoA, 'n kragtige inhibeerder van mitochondriale vetsuur (VS) opname, en om hierdie rede sal verhoogde ACC $\beta$  aktiwiteit, vetsuur gebruik verlaag en potensieel aanleiding gee tot intrasellulêre miokardiale lipiedophoping en insulienweerstand (IW).

Vorige studies toon dat groter fluks deur die heksosamienbiosintetiese weg (HBW) bydra tot die ontwikkeling van IW. In die lig hiervan hipotetiseer ons dat verhoogde HBW fluks, ACC $\beta$  geenuitdrukking induseer, en sodoende tot die ontstaan van IW bydra. Ons aanvanglike werk het op ACC $\beta$  geenpromotorregulering gefokus, en voorgestel dat die HBW die opstroom stimuleringsfaktor 2 (USF2) moduleer en dus ACC $\beta$  geen uitdrukking induseer.

Hier het ons verder die HBW-gemedieërde regulering van ACC $\beta$ -geenuitdrukking deur kortstondige tranfeksie van kardiaalverkrygde H9c2 selle met 'n uitdruktingsvektor wat kodeer vir die tempo-bepalende HBW ensiem (GFAT)  $\pm$  die volle lengte ACC $\beta$ , en vier afgestompte promotor-lusiferase konstrunkte onderskeidelik, te ondersoek. GFAT ooruidrukking het ACC $\beta$  geenpromotor aktiwiteit vir die volle lengte, en drie groter uitwissingskonstrukte verhoog ( $p < 0.001$  vs. kontrole).

Hoewel GFAT- en USF2-gemedieërde ACC $\beta$  promotorinduksie tydens ko-transfeksie van die -38/+65 uitwissingskonstruk versag was, is dit voorgestel dat USF2 aan die proksimale promotor area (naby die beginkodon) bind. Verdere ondersoek bewys ook dat USF2 aan die ACC $\beta$  promotor bind en dit aktiveer, maar dat USF2 nie O-GlcNAc gemodifiseer word nie ten spyte van 'n sterk korrelasie tussen verhoogde O-GlcNAc vlakke en USF2 aktivering van ACC $\beta$ . Dit kan dus voorgestel word dat daar 'n alternatiewe O-GlcNAc gemodifiseerde faktor betrokke is in hierdie reguleringsweg. Ons studie demonstreer dat verhoogde HBW fluks ACC $\beta$  geenpromotor aktiwiteit *via*

HBW modulering van USF2 veroorsaak. Ons stel voor dat ACC $\beta$  induksie vetsuuroksidasie verlaag en so tot intrasellulêre lipiedophoping (VS opname >> VS oksidasie) en die ontstaan van kardiaal I $\omega$  lei.

## **Abbreviations**

ACBP	Acyl-CoA binding protein
ACC	Acetyl-CoA carboxylase
acetyl-CoA	Acetyl-Coenzyme A
Acyl-CoA	Acyl-Coenzyme A
AMP	adenosine monophosphate
AMPK	AMP-activated protein kinase
ATP	Adenosine triphosphate
BSA	Bovine serum albumin
CACT	Carnitine/acylcarnitine transferase
ChREBP	Carbohydrate response element-binding protein
CPT	Carnitine palmitoyl transferase
CTD	Carboxyl-terminal domain
dGFAT	Dominant negative GFAT
dH <sub>2</sub> O	Distilled water
DMEM	Dulbecco's modified Eagle's medium
DNA	Deoxyribonucleic acid
DNL	<i>De novo</i> lipogenesis
DON	6-Diazo-5-oxo-L-norleucine
ECL	Enhanced chemiluminescence
EDTA	Ethylene diamine tetraacetic acid
eIF	Eukaryotic factor
ER	Estrogen receptor
F-6-P	Fructose-6-phosphate

FA	Fatty acids
FABP	Fatty acid binding protein
FADH <sub>2</sub>	Flavin adenine dinucleotide
FAS	Fatty acid synthase
FAT	Fatty acid transporter
FATP	Fatty acid transport protein
FCS	Fetal calf serum
FFA	Free fatty acids
GFAT	Glutamine: fructose 6-phosphate amidotransferase
Glc-6-P	Glucose-6-phosphate
GlcN-6-P	Glucosamine-6-phosphate
GlcNAc	<i>N</i> -acetylglucosamine
GLUT	Glucose transporter
GP	Glycogen phosphorylase
GS	Glycogen synthase
H <sub>2</sub> O	Water
HBP	Hexosamine biosynthetic pathway
HCl	Hydrogen chloride
H-FABP	Heart-type fatty acid binding protein
HK	Hexokinase
HRP	Horse-radish peroxidase
IRS-1	Insulin receptor 1
kDa	kilodaltons
LCFAs	Long-chain fatty acids
LAR	Luciferase assay reagent

malonyl-CoA	Malonyl-Coenzyme A
MCD	Malonyl-Coenzyme A decarboxylase
mg	Milligrams
ml	Millilitre
mM	Millimolar
mRNA	Messenger ribonucleic acid
n	Numbers
NADH	Nicotinamide adenine dinucleotide
nm	Nanometer
O-GlcNAc	O-linked $\beta$ - <i>N</i> -acetylglucosamine
O-GlcNAcase	$\beta$ - <i>N</i> -acetylglucosaminidase
OGT	O-linked $\beta$ - <i>N</i> -acetylglucosaminyl transferase
PBS	Phosphate Buffer Saline
PDH	Pyruvate dehydrogenase
PFK	Phosphofructokinase
PI-3 kinase	Phosphoinositide 3-kinase
PMSF	Phenylmethylsulfonyl fluoride
PPARs	Peroxisome proliferator-activated receptors
PPP	Pentose phosphate pathway
Pro	Proline
PUGNAc	O-(2-acetamido-2-deoxy-D-glucopyranosylidene) amino- <i>N</i> -phenylcarbamate
PVDF	Polyvinylidene difluoride
RIPA	Radio immuno precipitation assay
RNA	Ribonucleic acid

RNA Pol	Ribonucleic acid polymerase
rpm	Revolutions per minute
RT	Room temperature
RT-PCR	Real-time polymerase chain reaction
SBT	Strontium bismuth tantalate
SDS	Sodium dodecyl sulphate
Ser	Serine
STZ	Streptozotocin
TBS	Tris-buffered saline
Thr	Threonine
Tyr	Tyrosine
UDP	Uridine diphospho
UDP-GlcNAc	Uridine diphospho- <i>N</i> -acetylglucosamine
μl	Microlitre
USF	Upstream stimulatory factor
VLDLs	Very-low density lipoproteins

## **List of Tables**

Table 1: Measurements of glucose, insulin and HOMA on the day of sacrifice of animals in this study	59
Table 2: Quantitative fatty acid composition: $\mu\text{g}$ FA/gram heart (tissue)	73
Table 3: Total sum of each carbon form of fatty acids for each time point of high fat vs low fat diet (measured FA/gram heart tissue)	74

## **List of Figures**

Figure 1: Diagram of fatty acid metabolism	8
Figure 2: Diagram representing the different pathways of glucose metabolism (reproduced from (53))	16
Figure 3: Description of the hexosamine biosynthetic pathway.	20
Figure 4: Schematic diagram of our findings in the previous MSC study.	27

Figure 5: Sketch of human GFAT gene cloned into pcDNA3.1 vector.	33
Figure 6: Diagram of pcDNA3	34
Figure 7: Diagram of pPII $\beta$ -1,317 construct	35
Figure 8: Diagram of pTransLucent construct	36
Figure 9: USF2 overexpression promotes ACC $\beta$ expression in response to HBP flux and not USF1	50
Figure 10: GFAT overexpression enhances USF transcriptional Activation	51
Figure 11: ACC $\beta$ Deletion Construct induction by GFAT	52
Figure 12: The effects of USF2 on ACC $\beta$ promoter activity (deletion constructs)	53
Figure 13: The effects of HBP flux on O-GlcNac expression represented per 10000 transfected cells measured with Flow Cytometry	54
Figure 14: The effects of HBP flux on USF2 expression represented per 10000 transfected cells measured with Flow Cytometry	55

Figure 15: The effects of HBP flux on USF2 expression represented per 10000 transfected cells Flow Cytometry result	56
Figure 16: The effects of L-glutamine mediated HBP flux on USF2 expression	57
Figure 17: The effects of HBP flux on USF2 expression can be blunted with the use of a dominant negative inhibitor of GFAT	58
Figure 18: HOMA index values of male Wistar rats in response to a high fat diet versus controls (low fat)	62
Figure 19: ACC $\beta$ expression in male Wistar rats in response to a high fat diet versus controls (low fat)	63
Figure 20: USF2 expression in transfected H9C2 myoblasts cells	64
Figure 21: DNA of sonicated of tissue from male Wistar rats with bursts 4, 8 and 12	65
Figure 22: ACC $\beta$ PCR of isolated DNA with ChIP of USF2 antibody using control primers outside the region of binding	66

Figure 23: ACC $\beta$ PCR of isolated DNA with ChIP of USF2 antibody using signal primers in the region of binding	67
Figure 24: USF2 O-GlcNAcylation with Immunoprecipitation and Western blotting for USF2 and O-GlcNAc separately	68
Figure 25: Total Phosphatidylcholine (PC) Fatty Acids ( $\mu$ g FA per g heart tissue)	69
Figure 26: Total Phosphatidylethanolamine (PE) Fatty Acids ( $\mu$ g FA per g heart tissue)	70
Figure 27: Total Phospholipid Fatty Acids ( $\mu$ g FA per g heart tissue)	70
Figure 28: Total Triacylglycerol Fatty Acids ( $\mu$ g FA per g heart tissue)	71
Figure 29: Total Free Fatty Acids ( $\mu$ g FA per g heart tissue)	72
Figure 30: Total quantitative sum of fatty acid composition per $\mu$ g of FA/gram heart (tissue) represented in different fatty acid subtypes	74

Figure 31: Schematic diagram of hypothesis and findings

84

# **Chapter 1**

## **Introduction**

## 1.1 Epidemiology

Obesity is defined as an excess of body fat which accumulates in adipose tissue, associated with increased fat cell size and number (69). Obesity has become more prevalent worldwide, resulting in an increase in related diseases such as type-2 diabetes (4). Although obesity is especially common in industrialised countries, its prevalence is also dramatically increasing in developing countries such as South Africa. The movement of populations from a rural type to a more “western-based” lifestyle with its increased availability of high-caloric diets is a key factor that has led to a higher incidence of obesity. It is believed 346 million people worldwide have diabetes and the World Health Organization predicts that diabetes-related deaths will double between 2005 and 2030 (126, 130).

Individuals who are obese develop insulin resistance which is characterised as an impairment of insulin to mediate glucose uptake and metabolism by muscle and adipose tissue. Cardiovascular disease is the primary cause of morbidity and mortality in obese individuals and in patients diagnosed with type-2 diabetes mellitus (61, 70, 115, 131). Although the heart plays a small role in the development of insulin resistance throughout the whole body, cardiovascular complications are the main causes of death in insulin resistant obese and type-2 diabetes patients (23). Diabetes mellitus is a cluster of metabolic perturbations characterized by high blood glucose levels or hyperglycaemia, which result from defects in insulin secretion, or action, or both. Diabetes mellitus can easily be identified with high glucose levels found in urine, and excessive muscle loss (125). There are three types of diabetes. Type 1 diabetes mellitus is loss of beta cell function of the islets of Langerhans in the pancreas

resulting in the inability of the pancreas to produce insulin. Type 1 diabetes mellitus can affect children or adults, but a majority of these diabetes cases are in children and can be genetically inherited (125). Type 2 diabetes mellitus is characterized by insulin resistance and a failure of the body to use insulin properly or a deficiency in its function or availability to the body. Type 2 diabetes can eventually develop into type 1 diabetes but can be managed by diet and exercise and is mostly linked to the life-style of the individual. The other main type of diabetes is gestational diabetes mellitus which resembles type 2 diabetes mellitus but is only present in some women during pregnancy. It is treatable although the main concern is its effect on the fetus or the mother (68).

South Africa has a unique, heterogeneous population originating from a diverse range of ethnic backgrounds. The ~ 46 million individuals that reside in South Africa largely consist of African (79%), Caucasoid (9.6%), mixed ancestry ("coloured") (8.9%) and Indian backgrounds (2.5%) (4). This diverse cultural and ethnic diversity makes it difficult to elucidate trends with respect to changes in diet and health behaviours of the entire population. There are also limited studies performed to assess the prevalence of metabolic syndrome (a precursor to obesity and diabetes) in South Africa. However, recent data show that mortality rates from ischaemic heart disease among whites, coloureds and Indians were found to be more than 2x the rate for blacks, while stroke death rates among blacks and coloureds were double compared to whites (4).

There are many sociological implications why the prevalence of cardiovascular diseases has become more common. For example, for the black community, the highest incidences of obesity are observed in black women (4). This may, in part,

depend on the cultural background in the black population where obesity is often regarded as a reflection of health and wealth (4).

Other associated lifestyle risk factors may also influence the epidemiology of cardiovascular diseases. Risk factors such as physical inactivity, increased smoking, hypertension and hypercholesterolemia may play an important role in the increase in cardiovascular disease and type-2 diabetes (115, 135). For example, although measures were adopted to reduce smoking (higher retail prices and a smoking ban) a recent South African report found that the prevalence of young smokers (14 years) increased by 30% (115). The survey was performed from 1998 to 2003 among a population of 15,124 school children in South Africa. Furthermore, the prevalence of sedentary behaviour has increased in recent years and is continuing to grow as a problem (115). Together these data highlight the increased burden of diabetes and cardiovascular diseases faced by developing nations such as South Africa.

In light of this, our laboratory has begun to investigate the basic mechanisms underlying the development of diabetes and cardiovascular diseases. In particular, we are focusing on the role of altered metabolism in the pathogenesis of type-2 diabetes and heart diseases. For the next part of this Introduction, I will now review some basics aspects of the heart's metabolism and thereafter focus on my particular interest, i.e. the hexosamine biosynthetic pathway.

## 1.2 Metabolism of the heart

The heart pumps blood continuously for the complete lifespan of an individual. This constant workload demands a high and very adaptive capacity for energy production in the form of adenosine triphosphate (ATP), produced by mitochondria of the heart. In terms of its fuel substrate preferences, the heart is like an omnivore that utilises fatty acids, glucose, lactate and ketone bodies. The heart is able to switch substrate priority easily depending on each substrate's availability, and the conditions of stress it is placed under (23). The normal adult mammalian heart obtains ~70% of its energy from fatty acid oxidation with the remainder provided by glucose and lactate (23). In the foetal heart carbohydrates are favoured as major substrates.

The heart utilises ketone bodies as a fuel source during fasting conditions. Metabolism of ketones generates  $\text{NADH}_2$  and  $\text{FADH}_2$  which can be used to generate energy by the electron transport chain (37). It has been shown that ketone bodies are able to suppress cardiac fatty acid oxidation during diabetes (47). In support Ruderman et al (1974) investigated arteriovenous differences for glucose, lactate, acetoacetate and 3-hydroxybutyrate in brain tissue of anaesthetized starved and diabetic rats. Here glucose represented the sole oxidative fuel of the brain during the fed state. They concluded that cerebral glucose uptake is decreased with diabetic ketoacidosis due to an inhibition of phosphofructokinase by elevated brain intracellular citrate levels.

Studies have shown that under certain conditions e.g. increased exercise, hypoxia, and anoxia; excess pyruvate from glycolysis is converted into lactate (37). Moreover, Brooks et al. (2000) introduced the hypothesis of a “lactate shuttle” (9). This hypothesis proposes that lactate formation and its distribution throughout the body can act as a mechanism to coordinate metabolism in different tissues. It is also known that during intense exercise lactate flux can exceed glucose flux (9, 37). Hashimoto et al (2007) hypothesized that in addition to its role as a fuel source and gluconeogenic precursor, lactate anion ( $\text{La}^-$ ) functions as a signaling molecule. Furthermore, polymerase chain reaction (PCR) and electrophoretic mobility shift assays (EMSA) showed that lactate can increase reactive oxygen species (ROS) production. It was also found to up-regulate 673 genes, of which many are known to be responsive to ROS and  $\text{Ca}^{2+}$  (9, 37). Here, lactate is linked to the regulation of expression of monocarboxylate transporter-1 (*MCT1*) and cytochrome c oxidase (*COX*) mRNA. Increases in *COX* expression coincided with increased peroxisome proliferator activated-receptor  $\gamma$  coactivator-1 $\alpha$  (*PGC1 $\alpha$* ) and nuclear respiratory factor (NRF)-2 levels. These data therefore demonstrate that lactate in itself can have a wide range of effects on the regulation of a vast number of intracellular metabolic, signalling and transcriptional pathways (9, 37).

### 1.2.1. Fatty acid metabolism

Fatty acids have four major physiological roles in metabolism. Firstly, it forms building blocks in the formation of phospholipids and glycolipids; secondly it is involved in the modification of proteins that are targeted to the cell membrane; thirdly it can serve as hormones and intracellular messengers; and finally fatty acids are utilised as fuel substances (116). Fatty acids are stored as triacylglycerol in adipose tissue until it is needed, i.e. then to be broken down by lipolysis (116).

Long-chain fatty acids (LCFAs) enter the circulation in two forms, either in a complex with albumin or esterified in a lipid core of very-low density lipoproteins (VLDLs) and chylomicrons (23, 112, 122). Free fatty acids (FFA) are released into the bloodstream by adipose tissue and taken up by non-adipose tissue via sarcolemmal transporters. It was first believed that LCFAs were transported across the sarcolemma into cardiomyocytes by passive diffusion, but it is now accepted that most of LCFAs are taken up by membrane transporters (40, 74, 75, 94). Two such fatty acid transporters are fatty acid translocase, a rat homologue of human CD36 (FAT/CD36) and fatty acid binding protein (FABP) (8, 84). There are also two isoforms of the fatty acid transport protein (FATP) family, i.e. FATP1 and FATP6 present in cardiomyocytes (112). Both exhibit acyl-CoA synthetase activity. FATP6 is found exclusively and in higher abundance in the heart. FATP has been found to colocalise with FAT/CD36 and both these LCFA transport proteins act in concert with each other.

Once inside the cardiac myocyte, LCFAs bind to a cytoplasmic heart-type fatty acid binding protein (H-FABP). This protein transports non-esterified LCFAs towards a site where they are converted and activated by acyl-Coenzyme A (acyl-CoA) synthetase to form fatty acyl-CoA. Acyl-CoA binding protein (ACBP) then binds to acyl-CoAs and can either incorporate them into intracellular lipid pools or shuttle it to the mitochondria to be metabolised (Figure 1).

After uptake is complete acyl-CoAs are oxidised by  $\beta$ -oxidation producing acetyl-CoA as a by-product. Acetyl-CoA from  $\beta$ -oxidation enters the citric acid cycle to be degraded along with acetyl-CoA from glucose oxidation (23, 34, 105). The result is the generation of  $\text{FADH}_2$  and  $\text{NADH}$  that enter the mitochondrial respiratory chain. In oxidative phosphorylation, ATP synthesis is coupled to the flow of electrons from  $\text{NADH}$  or  $\text{FADH}_2$  to oxygen by a proton gradient across the inner mitochondrial membrane (116).

A proton gradient is created by pumping protons out of the mitochondrial matrix into the inter-mitochondrial membrane space. Thus a proton gradient is formed which creates a membrane potential. The protons then flow back into the mitochondrial matrix through ATP synthase which drives ATP production (Figure 1).

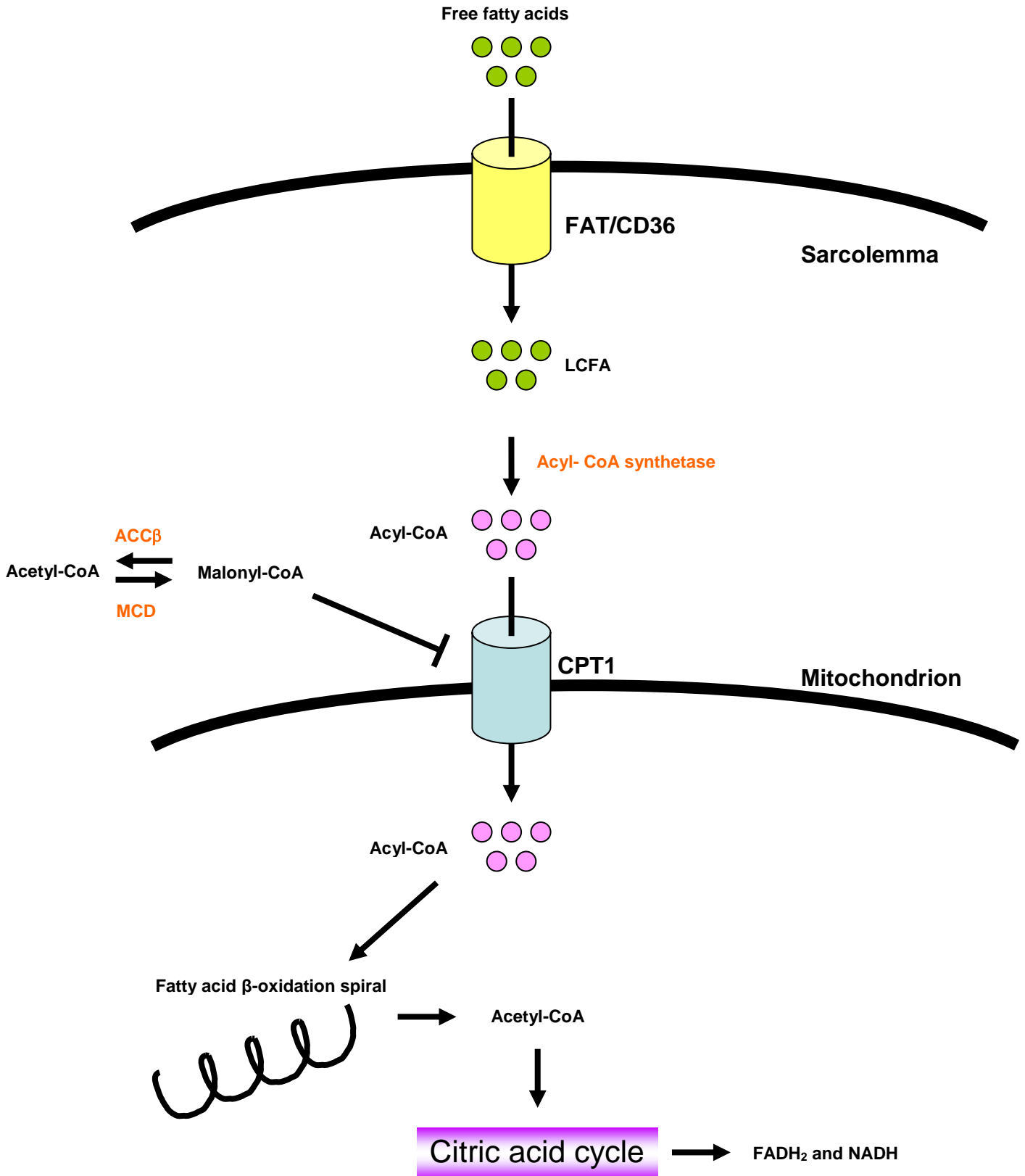


**Figure 1: Diagram of fatty acid metabolism.**

(CPT1: carnitine palmitoyl transferase, ACC $\beta$ : acetyl-coenzyme A carboxylase  $\beta$ , LCFA: long-chain fatty acid).

Even though LCFAs are utilised for energy production they also play a role in the regulation of genes involved in their own metabolic pathway. LCFAs can induce genes that increase fatty acid oxidation by activating a family of ligand-activated nuclear receptors called the peroxisome proliferator-activated receptors (PPARs) (117, 121). There are three isoforms of PPARs, i.e. PPAR $\alpha$ ,  $\beta/\delta$  and  $\gamma$  (117, 121). PPAR $\alpha$  and  $\beta/\delta$  are the main isoforms expressed in cardiomyocytes and activation of target genes results in an increased expression of regulators of fatty acid oxidation and fatty acid uptake, i.e. fatty acid transport protein (FAT/CD36) and carnitine palmitoyl transferase (CPT1) (35).

Fatty acid oxidation is regulated depending on fatty acid availability, its uptake by mitochondria and by its breakdown. Fatty acid uptake is a strongly regulated process involving a number of membrane transporters both on the outer membrane and mitochondrial membrane. In particular, fatty acyl-CoAs are transported into the mitochondrion by the action of three proteins which function as a complex. At the outer membrane is CPT1 which catalyses the formation of acylcarnitine (23, 29). Connected to CPT1 is carnitine/acylcarnitine transferase (CACT) which transports acylcarnitine into the mitochondria. The final enzyme (CPT-II) is found on the inner mitochondrial membrane and releases acyl-CoA into the mitochondrial matrix (23).

The process of mitochondrial LCFA uptake is regulated by CPT1 which is the rate-limiting enzyme for this process. A key molecule responsible for the regulation of CPT1 is malonyl-CoA (67, 70, 91, 102, 114, 134). Malonyl-CoA is a potent inhibitor of CPT1 and is produced from acetyl-CoA by an enzyme known as acetyl-CoA

carboxylase (ACC) (67, 70, 91, 102, 114, 134). Another enzyme, malonyl-CoA decarboxylase (MCD) degrades malonyl-CoA into acetyl-CoA (28, 114).

ACC has two isoforms, ACC $\alpha$  and ACC $\beta$ , that have different physiological roles based on their distinct subcellular distributions (44). ACC $\alpha$  is a cytosolic enzyme (molecular mass of 265 kDa) that supplies malonyl-CoA to fatty acid synthase (FAS) and is committed to *de novo* lipogenesis (DNL) in many tissues via subsequent nutritional and hormonal regulation (3, 39, 44, 62, 99). In contrast, ACC $\beta$  (molecular mass of 280 kDa) is anchored to the mitochondrial surface via a unique N-terminal domain that includes 20 hydrophobic amino acids and an additional 136 amino acids relative to ACC $\alpha$ , 114 of which constitute the unique N-terminal sequence of ACC $\beta$  (1, 2, 39, 44). ACC $\beta$  is responsible for malonyl-CoA production in the heart with ACC $\alpha$  localized to the cytosol.

In studies performed with ACC $\beta$  knockout mice there was an increase in fatty acid oxidation in skeletal muscle and a reduction in body weight fat content. However, mice with a mutation in the ACC $\alpha$  gene were embryonic lethal. It has also been shown that ACC $\beta$ -deficient mice do not develop diabetes when fed a high caloric diet. Furthermore, an increased ACC $\beta$  gene expression was found in skeletal muscle of diabetic patients. Conversely, ACC $\beta$  overexpression increases malonyl-CoA production resulting in a decrease in fatty acid uptake (28, 67, 91, 102, 114, 135). Since ACC $\beta$  is responsible for malonyl-CoA production, its overexpression increases malonyl-CoA production and thereby results in a decrease in fatty acid uptake. These data therefore strongly indicate the importance of ACC $\beta$  in the development of

diabetes. Since the focus of this study is on transcriptional regulation of ACC $\beta$  gene expression, I will now discuss previous studies in this regard.

.ACC $\beta$  is expressed abundantly in heart, skeletal muscle, and liver (1, 62, 89, 138). ACC $\beta$  transcripts contain two species of 5'-UTRs, which contain either the sequence of exon 1a or of exon 1b via the alternative usage of two promoters, i.e. promoter 1 and promoter 2 (P1 and P2). Exon 1a and exon 1b are located ~ 15 kilobases apart in human genome but are both connected to exon 2 in mRNA after splicing. However, they both use the same ATG start codon for translation, which is found in exon 2 and therefore the two transcripts encode for the same protein (39, 69, 89). A differential regulation of ACC $\beta$  gene expression originates from alternative usage of promoters, such as P1 and P2 in different tissues (89). P1 is the sole promoter found in the heart and skeletal muscle of rats, although both P1 and P2 are active in human skeletal muscle. Metabolic changes occur rapidly in skeletal and cardiac muscle and therefore rapid regulation of enzyme activity by phosphorylation or dephosphorylation is important in ACC $\beta$  expression. In comparison, the liver's response to changes in environment is less immediate with more emphasis on transcriptional regulation of ACC $\beta$ .

It was reported that sterol regulatory element-binding protein-1 regulates hepatic ACC $\beta$  expression through the P2, in response to feeding status. Moreover P2 is also regulated by myogenic regulatory factors (MRF's) in human skeletal muscle (69, 89). These include MyoD(myogenic differentiation 1), myogenin, MRF4 and Myf5 (Myogenic factor 5) which are basic helix-loop-helix transcription factors involved in myogenic differentiation. All of these transcription factors recognize the same

consensus sequence, i.e. E-box (CANNTG), but are expressed at different times resulting in different modes of action and varying regulation patterns of ACC $\beta$  (89).

Myogenin and MRF4 play a major role in the expression of muscle genes in fully differentiated myotubes, while Myf5 and MyoD establish the myogenic lineage during embryogenesis (89, 100, 101, 104, 110). It is important to note that myogenic regulatory factor-binding sites found in the human ACC $\beta$  P2 are not conserved in rat P2. This would contribute to this difference in P2 usage between human and rat skeletal muscle (89).

The level of ACC $\beta$  expression is higher in the heart than in skeletal muscle. It is currently not known which promoter controls ACC $\beta$  expression in the heart. Cardiomyocyte-specific transcription factors, such as homeobox protein Nkx-2.5 (Csx/Nkx2.5), transcription factor GATA-4 (GATA4), myocyte enhancer factor-2 (MEF2), and Heart- and neural crest derivatives-expressed protein 1 (eHand) have been implicated in cardiac development and cardiac gene expression. Unlike in skeletal muscle MRFs have not been shown to be involved in ACC $\beta$  regulation in the heart (59, 64, 86, 89, 90).

The nucleotide sequence of the cDNA of the human liver ACC $\beta$  carboxylase has an open reading frame of 7,449 nucleotides that encode 2,483 amino acids. The nucleotide sequences and the predicted amino acid sequences from the cDNA of ACC $\beta$ , has ~60 and 80% in similarity to that of ACC $\alpha$ , respectively. Ser77 and Ser79 are critical for the phosphorylation of rat ACC $\alpha$  (Ser78 and Ser80 of human ACC $\alpha$ ) (1, 89). These amino acids are conserved in ACC $\beta$  and are represented as Ser219 and

Ser221, respectively. Another phosphorylation site, Ser1200, in rat ACC $\alpha$  (Ser1201 of human ACC $\alpha$ ) is absent in ACC $\beta$ .

Most of the homology between the amino acid sequences of the human ACC isoforms is found downstream of residues Ser78 and Ser81 in human ACC $\alpha$  and their equivalent residues in ACC $\beta$ , i.e. Ser219 and Ser22. It has been suggested that the first 218 amino acids at the N terminus of ACC $\beta$  represents a unique peptide that may be responsible for the variation between the two carboxylases. Despite the similarities between these two isoforms, studies with rat liver ACC $\alpha$  and ACC $\beta$  showed that the two isoforms do not cross-react immunochemically. It was shown that when the amino acid sequences of the human ACC $\alpha$  and ACC $\beta$  are aligned, an extra 142 amino acids can be found in ACC $\beta$  (i.e. 426 bp in ACC $\beta$  cDNA). It is believed that the extra 142 amino acids are involved in controlling the localisation of ACC $\beta$  in the cell, i.e. to the mitochondrion.

AMP-activated protein kinase (AMPK) plays an important role in the regulation of CPT1 by phosphorylating and inhibiting ACC $\beta$ , resulting in an increase in fatty acid oxidation (27, 54). Phosphorylation of ACC $\beta$  by AMPK is well documented. It has been suggested that MCD is also phosphorylated by AMPK (27, 54). Therefore, AMPK plays a distinct and important role in regulating both malonyl-CoA levels and fatty acid oxidation in the heart.

## 1.2.2 A description of fatty acid sub classing

A fatty acid is described as a carboxylic acid with a long unbranched aliphatic tail. This aliphatic tail is saturated or unsaturated. Most fatty acids that occur naturally contain a chain with an even number of carbon atoms that varies from 4 to 28 carbon atoms. Fatty acids usually derive from triglycerides or phospholipids. Triglycerides are esters which form from glycerol and three fatty acids. Unsaturated fatty acids are typically found in vegetable oils, while saturated fats are in abundance in animal fats. By contrast, phospholipids are found in cell membranes and play a major role in the formation of lipid bilayers. The hydrophilic head contains a negatively charged phosphate group while the tail is hydrophobic. When they are not attached to other molecules, they are known as "free" fatty acids.

Fatty acids are classed according to the length of its tail and whether it contains a double bond. Fatty acids that have double bonds are known as unsaturated fatty acids while those without double bonds have hydrogen atoms bound in place of the double bonds and are saturated. Fatty acids are divided into categories according to tail length as short, medium and long. A short-chain fatty acid is a fatty acid with aliphatic tails with fewer than six carbon atoms. Medium-chain fatty acids have tails between six and twelve carbon atoms, while long-chain fatty acids have more than twelve carbon atoms. Very long chain fatty acids are defined as fatty acids with an aliphatic tail longer than 22 carbon atoms.

Unsaturated fatty acids can be divided into two types, namely by the two carbon atoms in the chain that are bound next to either side of the double bond which can occur in

a *cis* or *trans* configuration. Those in *cis* conformation are found naturally while those in *trans* (known as trans fats) are not found in nature and are the result of human processing. Trans fats are known for their ability to clog cell membranes in tissues because of the bodies inability to process them.

### **1.2.3. Glucose metabolism**

The uptake of extracellular glucose by myocytes is mediated by glucose transporters (GLUTs). There are two glucose transporters that can be found in the heart, i.e. GLUT1 and GLUT4 that are located not only in the sarcolemma but also in intracellular storage compartments (6, 23, 48-50, 63, 79, 80, 82, 108). GLUT1 is the foetal isoform and can be found in less abundance than the adult, insulin-stimulated glucose transporter (GLUT4). Insulin regulates glucose uptake into these cells by recruiting membrane vesicles containing the GLUT4 glucose transporters from the interior of cells to the cell surface. GLUT4 then allows for the uptake of glucose into the cell. After an hour of insulin stimulation the GLUT4 is translocated back into the cell in vesicles and stored to be reused again. A dysfunction in GLUT4 trafficking is a key factor that has been linked to type 2 diabetes mellitus and the development of insulin resistance (6, 23, 48-50, 63, 79, 80, 82, 108). After glucose has entered the cardiomyocytes it is rapidly phosphorylated by hexokinase into glucose-6-phosphate.

Once converted to glucose-6-phosphate, glucose can be metabolised in six different ways (Figure 2). Firstly, glycogen synthesis can take place and glucose-6-phosphate can be converted by glycogen synthase (GS) into glycogen for storage. This process is reversible and when required glycogen phosphorylase (GP) can convert glycogen

back into glucose-6-phosphate (115). Some of the glucose-6-phosphate can enter the pentose phosphate pathway (PPP) where it has been proposed that xylulose-5-phosphate activates a specific isoforms of protein phosphatase 2A which, in turn, dephosphorylates the transcription factor carbohydrate response element-binding protein (ChREBP) (53, 131). In the liver ChREBP translocates from the cytosol to the nucleus where it regulates the expression of glycolytic and lipogenic enzymes (58).

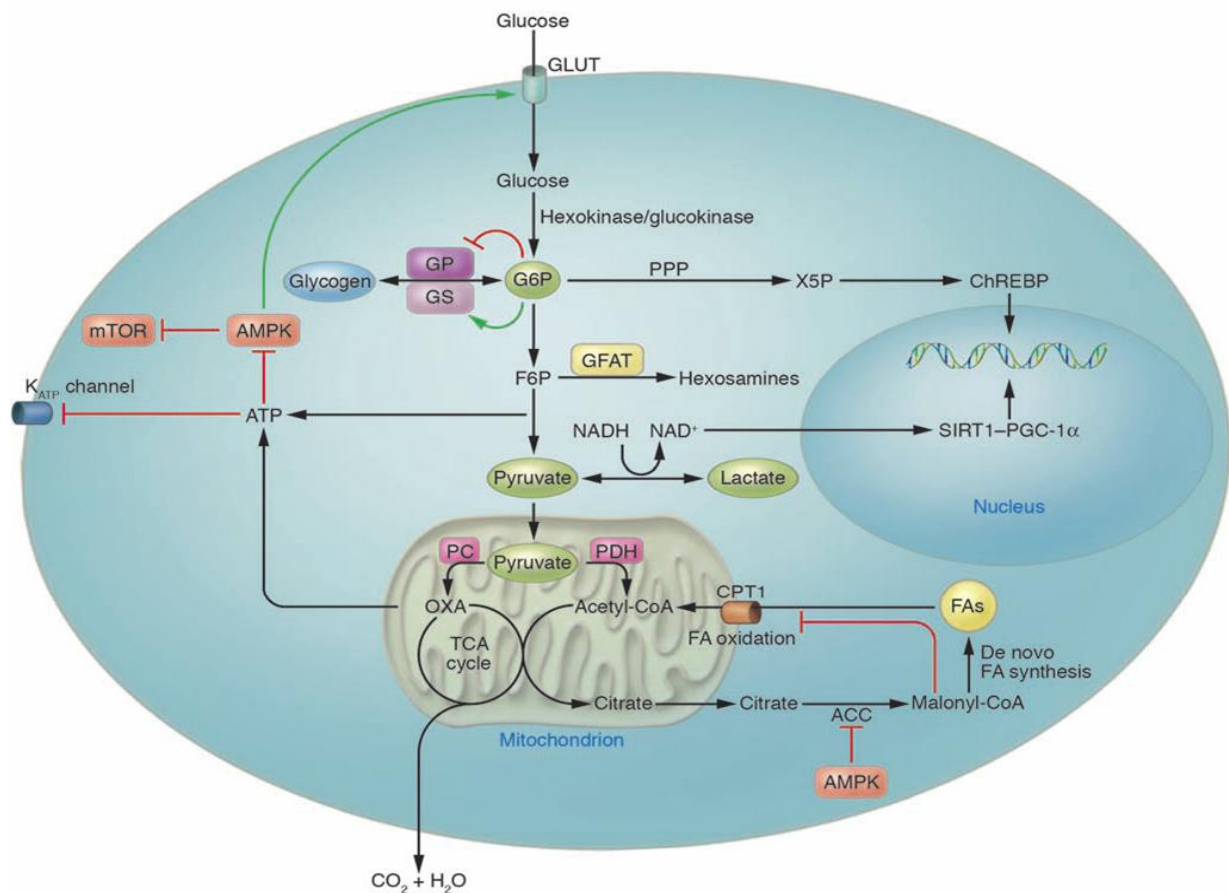


**Figure 2: Diagram representing the different pathways of glucose metabolism (reproduced from (53)).**

Most of the glucose-6-phosphate enters glycolysis. After the first step of glycolysis, phosphoglucose isomerase converts glucose-6-phosphate into fructose-6-phosphate. At this point most of the fructose-6-phosphate continues down the glycolytic pathway where it is converted to pyruvate after a long series of steps. However, a small

percentage of the fructose-6-phosphate is diverted to another pathway responsible for nutrient sensing, i.e. the hexosamine biosynthetic pathway (79, 97).

In the glycolytic pathway, fructose-6-phosphate is converted into fructose-1,6-bisphosphate by phosphofructokinase which is the rate-limiting enzyme of glycolysis (116). The production of pyruvate marks the end of the glycolytic pathway. In the absence of oxygen pyruvate can be reversibly converted to lactate. Under aerobic conditions pyruvate is transported into the mitochondrion by pyruvate dehydrogenase (PDH), the rate limiting enzyme of glucose oxidation, where it undergoes oxidative decarboxylation into acetyl-CoA. Acetyl-CoA from glucose metabolism, together with acetyl-CoA from fatty acid oxidation, enters the citric acid cycle (Krebs cycle) where it is oxidised to carbon dioxide, NADH and FADH<sub>2</sub>. The NADH and FADH<sub>2</sub> produced are then used in oxidative phosphorylation to produce ATP after donating their electrons to oxygen (116).

Another pathway that utilizes glucose is the polyol pathway. The polyol pathway consists of two steps in which glucose is converted to sorbitol and then converted into fructose (72). During this process NADPH is converted to NADP<sup>+</sup> (72). The polyol pathway mainly functions to remove excess glucose from glycolysis and then return it to the glycolytic pathway again (72).

The glyoxylate pathway is found mainly in plants and yeast (71). This pathway converts acetyl-CoA into oxaloacetate by bypassing the steps in the citric acid cycle. It can therefore use fats for the synthesis of carbohydrates (71).

The last pathway that utilises carbohydrates is the biosynthesis of oligosaccharides and glycoproteins which are then expressed on the surface of cell membranes (20).

Another pathway which can affect glucose metabolism is the phosphatidylinositol 3-kinase (PI 3-kinase) pathway. PI 3-kinases have been linked to a diverse group of cellular functions, including cell growth, proliferation, differentiation, motility, survival and intracellular trafficking. PI 3-kinases are important regulators involved in the insulin signaling pathway and play a role in the development in diabetes mellitus. PI 3-kinase binds to tyrosyl-phosphorylated insulin receptor substrate-1 (IRS-1), and this step plays a central role in the regulated movement of the glucose transporter, GLUT4, from intracellular vesicles to the cell surface. It has been shown that PI 3-kinase inhibitors, such as wortmannin, and LY294002 inhibit insulin-stimulated glucose transport and translocation of GLUT4 to the cell surface (107).

#### **1.2.4 The Randle cycle**

The Randle cycle (named after Philip Randle, its first proposer), which has been used to explain the reciprocal relationship between fatty acid oxidation and glucose oxidation, has long been implicated as a potential mechanism for hyperglycaemia and type-2 diabetes mellitus (109). The Randle cycle states that increased fatty acid oxidation causes a decrease in glucose oxidation. Thus in the setting of excess FFA and glucose supply (insulin resistant state), this is thought to lead to lower glucose uptake and eventually lead to hyperglycaemia. Here, acetyl-CoA and NADH derived from fatty acid oxidation can suppress pyruvate oxidation by inhibiting pyruvate dehydrogenase (33, 87). Increased fatty acid oxidation has also been shown to result

in the inhibition of phosphofructokinase and attenuate glycolysis. This would increase accumulation of upstream glycolytic metabolites through other glucose pathways and result in glucose accumulation (87). In my previous study I had proposed a “reverse Randle cycle” where by glucose metabolism could regulate fatty acid metabolism as a negative feedback and therefore provide an alternate mechanism for nutrient switching within the cell.

### **1.2.5. Hexosamine biosynthetic pathway**

Since the focus of my thesis is on the hexosamine biosynthetic pathway (HBP), I will now discuss this in more detail. HBP is a relatively small branch glucose utilising pathway. Only ~3-5% of the total glucose utilised in the cell enters the HBP depending on the tissue or cell type (79, 97). The pathway is catalysed by the rate-limiting enzyme glutamine: fructose 6-phosphate amidotransferase (GFAT). During this first step, fructose-6-phosphate and glutamine is converted to glucosamine-6-phosphate and glutamate (Figure 3). Thereafter, through a series of steps glucosamine-6-phosphate is converted to glucosamine-1-phosphate. After the addition of uridine, it is converted into uridine diphospho-*N*-acetylglucosamine (UDP-GlcNAc) and CMP-sialic acid. UDP-GlcNAc is the end product of the HBP pathway and also functions as an inhibitor of GFAT (12).

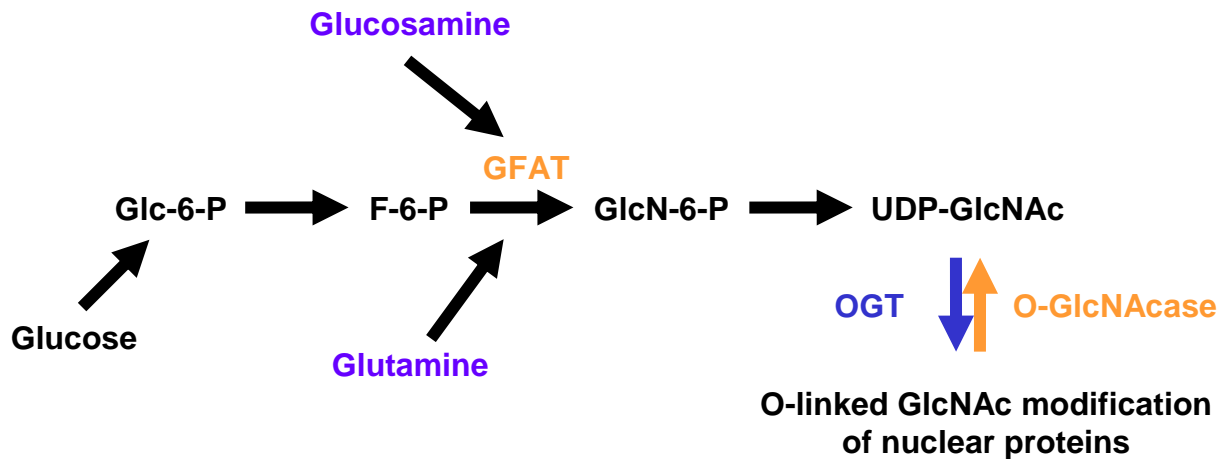


**Figure 3: Description of the hexosamine biosynthetic pathway.**

(GFAT: glutamine:fructose-6-phosphate amidotransferase, OGT: O-linked  $\beta$ -*N*-acetylglucosaminyl transferase, O-GlcNAcase:  $\beta$ -*N*-acetylglucosaminidase).

UDP-GlcNAc functions as the substrate for O-linked  $\beta$ -*N*-acetylglucosamine transferase (OGT). OGT catalyses the reversible modification of various proteins and transcription factors by cleaving UDP from GlcNAc and transferring GlcNAc in O-linkage to serine/threonine residues on proteins. O-GlcNAc modification has two novel mechanisms of action (12, 65, 73).

O-GlcNAc modification is a unique form of glycosylation found in plants and animals found to be different to normal glycosylation in that it is not elongated to more complex structures and that it is not restricted to only cell surface and luminal faces of secreted proteins. It has been shown in lymphocytes that a majority of O-GlcNAc modification can be found inside the cell and even localised within the nucleocytoplasm. It has a nucleoplasmic distribution instead of being localised to the cell surface like other glycoproteins (45, 52). O-GlcNAc modification has been implicated in modulating different mechanisms that include (i) regulating protein phosphorylation and function; (ii) altering protein degradation; (iii) altering the localisation of proteins; (iv) modulating

protein-protein interactions and (v) mediating transcription (135). The modification of proteins with O-GlcNAc has been linked to the regulation of a wide variety of protein to protein interactions and the localization of these proteins within the cell (12, 129). To date all known proteins that are modified by the hexosamine biosynthetic pathway can be phosphorylated as well but both forms of modification have been described as mutually exclusive with no protein found to possess both modifications at the same time.

A decrease in phosphorylation has been shown to increase O-GlcNAcylation (21). In one study it was observed that inhibition of protein kinase A and protein kinase C resulted in increased O-GlcNAc levels. Also by increasing the overall level of O-GlcNAc modification by inhibiting O-GlcNAcase expression in NIH-3T3 cells, it was shown that the levels of phosphorylation in a majority of regulatory proteins decreased drastically (21). Contrary to this, specific phosphorylation sites on some proteins actually increased. These findings have suggested a crosstalk between phosphorylation and O-GlcNAcylation whereby each process communicates with each other to add a new level of intracellular regulation that is dynamic and varies between proteins. It is unknown how interplay between these two modifications occurs but at the moment there are two theories. The first is that each modification could regulate each other's pathways or cycle times. The second is that phosphorylation and O-GlcNAcylation compete for proximal or the same target sites (threonine and serine) and through steric hindrance can affect each other's affinity for the protein (24, 26, 136). This is plausible despite O-phosphate being negatively charged and O-GlcNAc moieties being neutral, the latter are larger in size. Interference between

phosphorylation and O-GlcNAc modification may arise from their proximity to each other in tertiary protein structure.

The sites of O-GlcNAc modification are often identical or adjacent to known phosphorylation sites, suggesting that “O-GlcNAcylation” plays a role in regulation of a wide range of pathways. It has been shown that O-GlcNAc regulation can modify proteins in competition with phosphorylation. In some instances O-GlcNAc and phosphorylation can exist on separate and distinct subsets of a protein (21). For example, c-Myc and RNA polymerase both contain threonine or tyrosine sites that can be phosphorylated or glycosylated, but although, there has been no proof that the two modifications can exist on one protein, there is a possibility that this dual-protein modification can occur. In particular, RNA polymerase II exists in two distinct forms, i.e. RNA Pol IIA and RNA POL IIO (21, 135). RNA polymerase II contains a highly conserved carboxyl-terminal domain (CTD) consisting of 52 tandem repeats of the consensus sequence Tyr-Ser-Pro-Thr-Ser-Pro-Ser (21, 24, 26, 137). The CTD of the IIO isoforms is found to be phosphorylated on the serine and threonine residues. In contrast, the IIA isoform is non-phosphorylated and exhibits extensive O-GlcNAc modification. The existence of both O-GlcNAc and phosphorylation site implies a precise regulation of protein activity (21).

The modifications of proteins by OGT with O-GlcNAc are also closely regulated. Another enzyme responsible for the regulation of O-GlcNAcylation is  $\beta$ -N-acetylglucosaminidase (O-GlcNAcase). Although OGT is responsible for binding O-GlcNAc to serine/threonine residues of proteins, O-GlcNAcase functions to remove O-

GlcNAc. O-GlcNAc modification is thus regulated in the same manner as phosphorylation.

O-GlcNAc modification targets numerous proteins, including transcription factors (21, 136). For example, Sp1, an important transcription factor in the regulation of several target genes, has been shown to have multiple O-GlcNAc residues (12, 21, 137). O-GlcNAc has been shown to alter protein degradation by two different mechanisms, i.e. (i) by altering the targeting of proteins to the proteasome O-GlcNAc modification could act as a protective signal against proteasomal degradation by modifying target substrates or (ii) by altering the activity of the proteasome. O-GlcNAc modifies eukaryotic factor (eIF) 2 $\alpha$ -p67, Sp1 and estrogen receptor (ER)- $\beta$  prolonging the half-life of these proteins (135). Insulin has been reported to increase O-glycosylation and nuclear content of Sp1 (76).

Incubation with high glucose or increasing flux through HBP by overexpressing GFAT increased the expression of upstream stimulatory factor 1 and 2 (USF1 and 2), although these transcription factors are apparently not O-GlcNAc modified (12, 126). The gene encoding OGT (O-linked  $\beta$ -N-acetylglucosamine transferase) is essential for embryonic and stem cell development in mammals, making it difficult to produce a transgenic knockout model to investigate HBP regulation (42). Hanover et al. (2005) examined the role of OGT using an *ogt-1* deletion strain of *Caenorhabditis elegans* (42). This strain exhibited no obvious developmental phenotype that was found in homozygous animals and could be used successfully as a model for nutrient-driven insulin resistance. One of the main findings of this model was that homozygous (rat/mouse) lacking *ogt-1* had increased levels of glucose and glycogen, accompanied

by a decrease in fat stores (42). This would imply that the HBP was involved in the regulation glycogen synthesis and fatty acid oxidation.

Studies in adipocytes suggest that glucose-induced insulin resistance is caused by impaired translocation of insulin-responsive glucose transporters to the cell membrane (such as GLUT4) and that an increase in glucose flux through the HBP plays a major role in the development of insulin resistance (10-12, 81, 100). There are several observations to suggest that the HBP increases the development of insulin resistance (6, 13, 18, 47, 48, 55, 79, 83, 108, 124). For example, pre-exposure to glucosamine inhibits basal and insulin-stimulated glucose transport and decreases insulin-stimulated glycogen synthesis in rat muscles without affecting insulin receptor signaling (6, 13, 18, 47, 48, 55, 79, 83, 108, 124). Moreover, increasing HBP flux can alter glucose uptake due to increased O-GlcNAc modification of proteins involved in the regulation of the insulin-signaling cascade, i.e. IRS-1, PI-3 kinase and Akt (31, 92, 136).

A much lower concentration of glucosamine than glucose is required to elicit insulin resistance. The main difference between these two substrates is that glucose is utilised by several pathways whereas glucosamine is utilised only by HBP but may bypass the rate limiting enzyme GFAT (glutamine:fructose-6-phosphate amidotransferase) and increase HBP flux. Glutamine or a mixture of amino acids is also an important requirement for the development of glucose-induced insulin resistance of glucose transport in adipocytes (55). When transamidases are added to adipocytes treated with a mixture of amino acids, the effect is reversed (55).

Several studies have shown that by increasing the concentration of extracellular glucose and glucosamine, or by increasing glucose uptake by overexpressing glucose transporters (GLUTs), this results in insulin resistance (6, 48-50, 63, 79, 80, 82, 96, 108). For example, it was shown that by blocking GFAT with pharmacological agents inhibited glucose-mediated insulin resistance (77). Moreover, other studies found that GFAT overexpression mimicked the effect of treating cells or rats with elevated glucose/glucosamine(18, 22, 25, 82). Also by increasing O-GlcNAc levels in mice and in cell culture genetically or by pharmaceutical intervention, resulted in insulin resistance (5, 14, 42, 83, 92, 124). Together these studies therefore support a strong link between increased HBP flux and the development of insulin resistance/type-2 diabetes.

### 1.3. Aims of this study

In my previous study we investigated the link between glucose metabolism and fatty acid metabolism. It was revealed that with increased glucose or glutamine there was increased flux through the hexosamine biosynthetic pathway which resulted in an increase in acetyl CoA carboxylase  $\beta$  promoter expression. It was also shown that there is a high level of control of ACC $\beta$  expression from HBP flux when we changed the level of flux through this pathway by making use of varying levels glutamine, various pharmaceutical inhibitors at different points of the pathway and by making use of dominant negative inhibitors of GFAT. At the end of the study we identified a novel transcription factor that could be involved in the link between HBP flux and ACC $\beta$  regulation, i.e. upstream stimulatory factor 2 (USF2) (Figure 4). It had also become apparent toward the end of the study that this form of regulation became important in the development of insulin resistance possibly at the stage of metabolic syndrome. We hypothesized that in metabolic syndrome when there is increased glucose there would be an increase in flux through HBP and that this would lead to an increase in ACC $\beta$  expression and the reduction of fatty acid uptake. Glucose metabolism would therefore regulate fatty acid metabolism in these conditions. We had already shown that USF2 was involved in this regulation by responding to HBP flux and upregulating ACC $\beta$  (Figure 4). In this study we aim to strengthen this finding. We also aim to investigate the downstream effects of this change and apply this hypothesis to an animal model of high caloric diet induced insulin resistance. We also aim to find the time point for when the dysregulation of this pathway will become relevant which may provide possible therapeutic interventions as diagnostic technique for identifying metabolic syndrome. This diagnostic technique could prove useful because it is at this moment of metabolic

syndrome that we can still treat patients and prevent insulin resistance from happening. Once this time point has been surpassed it is impossible to reverse. In this study we aimed to target the site of USF2 binding to ACC $\beta$  and prove its responsiveness to hexosamine flux. We also want to prove that USF2 is modified by O-GlcNAc which would show a mechanism of action. We also aim to measure fatty acid metabolism or accumulation, together with ACC $\beta$  expression and HBP flux in response to a high fat diet in an animal model.

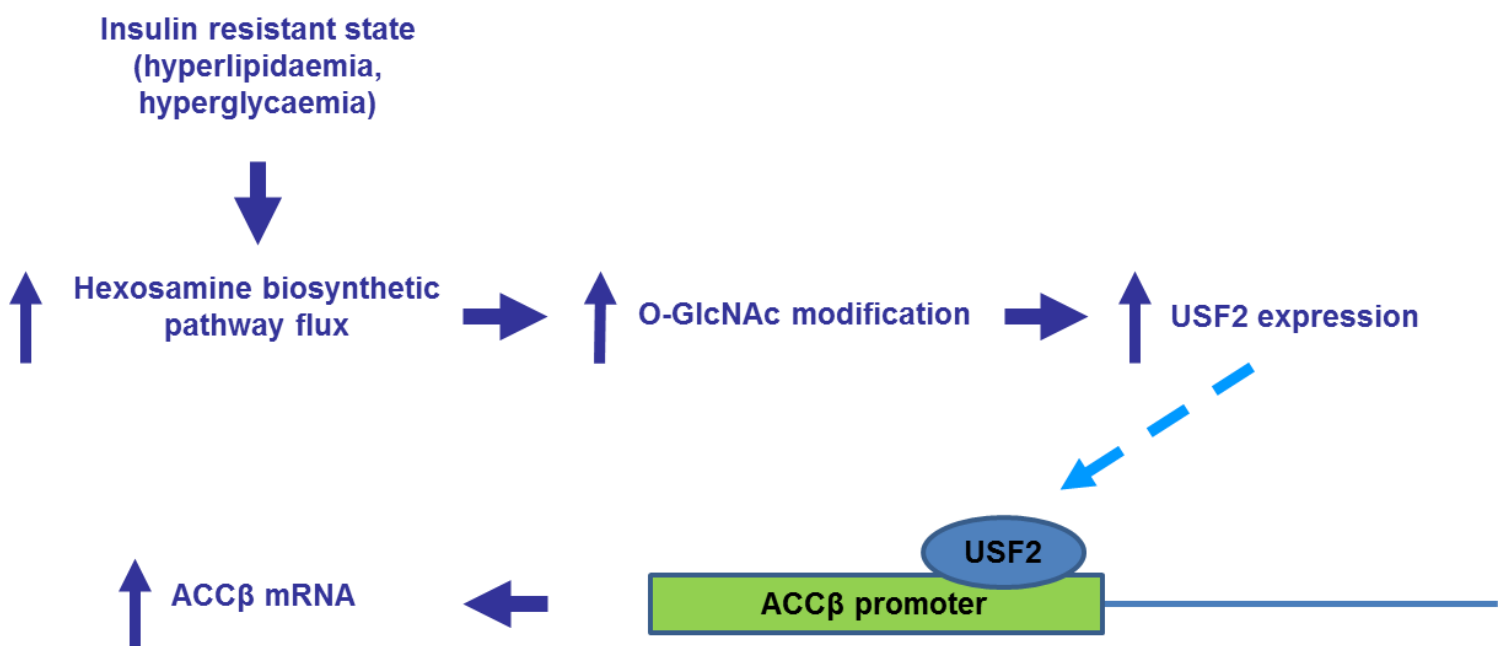


Figure 4: Schematic diagram of the findings in the previous MSC study.

# **Chapter 2**

# **Methods**

## 2.1. Transfections

### 2.1.1. Background to principles of the technique

Transfection, i.e. experimental exogenous transfer of DNA into a target cell is a useful method to exploit in order to measure gene promoter activity (Appendix 1). Two components are required for a successful transfection. Firstly, a transfection reagent is required that will bind to plasmid DNA to be transferred into the cytosol of cells. For this study Fugene 6 transfection reagent (Roche, Penzberg, Germany) was employed. The second requirement is a plasmid DNA that will be transfected together with the promoter-luciferase construct. The former is constitutively expressed and used to normalise transfection results according to cell number and transfection efficiency. We seeded 35, 000 cells per well on day one and let them double over 2 days before transfection. Measurements would be taken two days later when they reached approximately 80-90% confluency.

The gene promoter of interest is bound to a firefly luciferase gene, allowing promoter activity to be measured by the amount of luciferase protein synthesized by the cell. The normalising construct employed for this thesis was pRL-CMV (Promega, Fitchburg, WI, USA). The luciferin protein expressed by the pRL-CMV construct is isolated from *Renilla reniformis*. After transfection, luciferin protein is extracted by cell lysis. Thereafter a substrate called luciferase assay reagent II (LAR II) is added to activate the luciferin protein, resulting in light emission. The latter can be measured using a luminometer. Since the luciferin protein produced by the normalising agent and the promoter construct are different, each can be measured separately from the

same sample. Thus, a Dual-Luciferase Reporter Assay Kit (Promega, Fitchburg, WI, USA) was used where two substrates were added to the same sample, i.e. Luciferase Assay Reagent II (LAR II) (measuring promoter activity) and “Stop and Glo” (neutralizes LAR II substrate and activates the *Renilla* luciferin).

Transfections were performed as a 5-day experiment (Appendix 2). On the first day cells were seeded on 12-well plates. On day 2 cells were transfected, while media of myoblasts was replaced on day 3. This ensured that myoblasts were supplied with sufficient nutrients and also to remove excess transfection reagent. At this stage inhibitors/drugs that were being tested were added (to be discussed later). On day 4, after 24 hours treatment, cells were lysed and the lysate stored at -80°C. The samples were rapidly thawed on day 5 to further enhance cell lysis. Samples were subsequently plated on a 96-well luminometer plate and promoter activity measured (Appendix 2).

## 2.1.2. Cell culture

H9c2 rat cardiac-derived myoblasts were chosen for experiments because they are a precursor cell line to cardiomyocytes. H9c2 is a subclone of the original clonal cell line derived from embryonic BD1X rat heart tissue. These cells do however; exhibit many of the properties of skeletal muscle. H9c2 myoblasts can be differentiated to will fuse and form multinucleated myotubes (57). Precursor cells are also easier to differentiate than terminally differentiated myotubes. This cell line has its weaknesses that although it was originally characterised as being closely related to cardiac myocytes lacks some morphological properties of cardiomyocytes such as gap junctions caveolae, T tubules, or myofibrils (57). H9c2 myoblasts were cultured in T75 culture flasks with Dulbecco's modified Eagle's medium (DMEM) (Sigma, St. Louis, Missouri, USA) with 10% GibCo foetal calf serum (Invitrogen, Carlsbad, CA, USA) and 4 mM GibCo L-glutamine (Invitrogen, Carlsbad, CA, USA). Cells were not allowed to grow to a confluency greater than 70-80% and were cultured for a maximum of 8 passages before growing new cells. We used passages 9-15 for transfection experiments. In our initial optimizing experiments passages 9-15 were used and it was decided to continue using them in order to ensure consistency between results. In the beginning of our experiments cells were checked for viability under light microscope and trypan blue.

Myoblasts were grown as described and plated at 35, 000 cells per well on 12-well culture plates (Greiner, Kremsmünster, Austria) in 1 ml of completed DMEM with 10% foetal calf serum and 4 mM L-glutamine. The cells were incubated for 24 hours at 5% CO<sub>2</sub>, 20% O<sub>2</sub> and 95 % humidity at 37°C prior to transfection. The main limitation of using a precursor cell line is that it isn't the same morphologically as differentiated

cells or tissue. To generate reliable data cell culture conditions have to remain the same for each experiment which can create a challenge depending on reagents, media and the skill of the researcher. It is, however, useful at investigating pilot studies and investigating direct mechanisms. Precursor cells can be maintained and grown which allows for fast generation of results and plenty of available sample and is cheaper to maintain than an animal model.

### **2.1.3. DNA Promoter-luciferase and over-expressing constructs used for transfection experiments**

pGL3-Control (Promega, Madison, WI, USA) was used in all transfection experiments to normalise results according to cell number and transfection efficiency. pGL3-Control is a plasmid constitutively expressing luciferase from an SV40 promoter. pGL3-Basic is a plasmid lacking a promoter and therefore expresses only baseline levels of luciferase. The latter was used to normalise the total amount of DNA used per transfection to ensure comparable transfection efficiency between experiments. The total amount of DNA transfected for each experiment was 0.75 µg, and pGL3- Basic was used to make up the remaining DNA needed. H9c2 myoblasts were transiently transfected with a 1,317 bp human ACC $\beta$  promoter-luciferase reporter construct (pPII $\beta$ -1,317) previously described (Makaula et al., 2006). 0.25 µg of pPII $\beta$ -1,317 was transfected  $\pm$  0.25 µg of a human pcDNA3-GFAT expression vector. Two dominant negative constructs, i.e. pcDNA3-GFAT577 and pcDNA3-GFAT667 were also employed in this study. Both dominant negative constructs were separately transfected with pPII $\beta$ -1,317 and GFAT. There is a great amount of sequence homology between the rat and human isoforms of GFAT (91%) and ACC $\beta$  (90%) and

therefore it is unlikely that this would represent a problem when expressing human constructs in a rat cardiac-derived cell line.

#### **2.1.4. Preparation of plasmid DNA**

##### **Description of plasmid constructs:**

1. pcDNA3-GFAT (see Figure 5) contains a full-length human GFAT cDNA generated by RT-PCR and cloned into the expression vector pcDNA3.1 (see Figure 6) (Invitrogen, Inchinnan, Scotland). The PCR product was verified by sequencing and shows identity to human GFAT (also known as GFAT1 = glutamine:fructose-6-phosphate transaminase 1, GenBank accession number M90516). This construct was kindly donated to us by Dr. Cora Weigert (University of Tübingen, Germany).

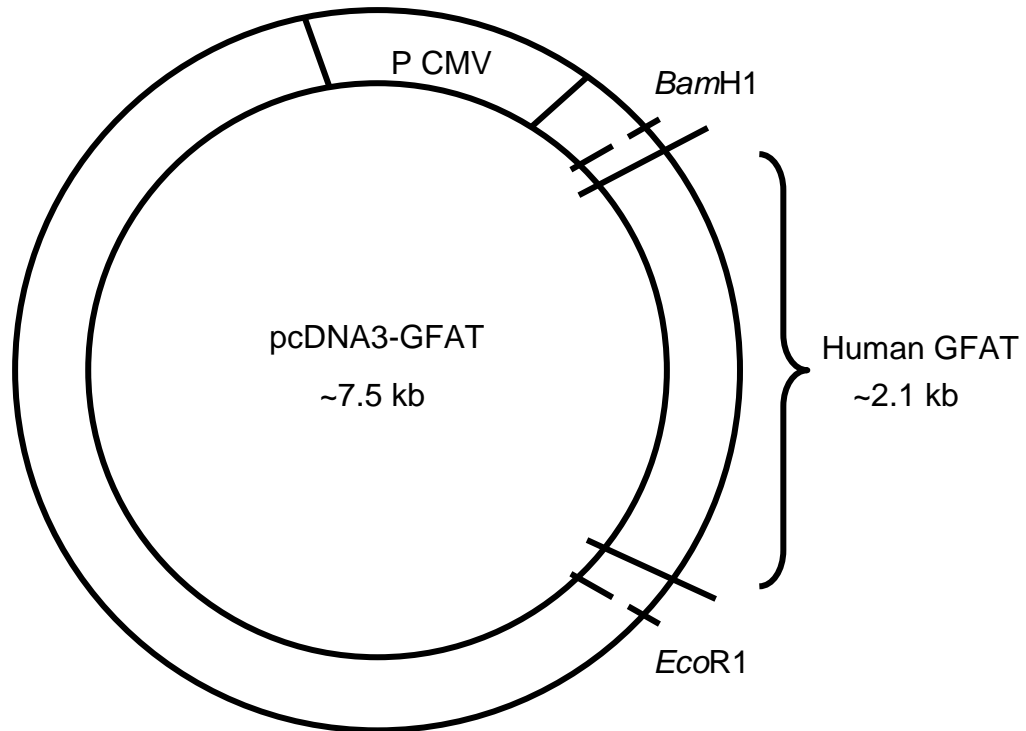


**Figure 5: Sketch of human GFAT gene cloned into pcDNA3.1 vector.**

(from Weigert et al., 2003) (pRL-CMV: Vector, GFAT: glutamine:fructose-6-phosphate amidotransferase, *EcoR1* and *BamH1* are restriction splice sites).

2. pcDNA3-GFAT/577 contains human GFAT1 cloned into the pcDNA3.1 vector but with histidine 577 mutated to alanine, resulting in the complete loss of GFAT enzyme activity (127).
3. pcDNA3-GFAT/677 contains human GFAT1 cloned into the pcDNA3.1 vector but with lysine 667 mutated to alanine, leading to complete loss of GFAT enzyme activity (127).

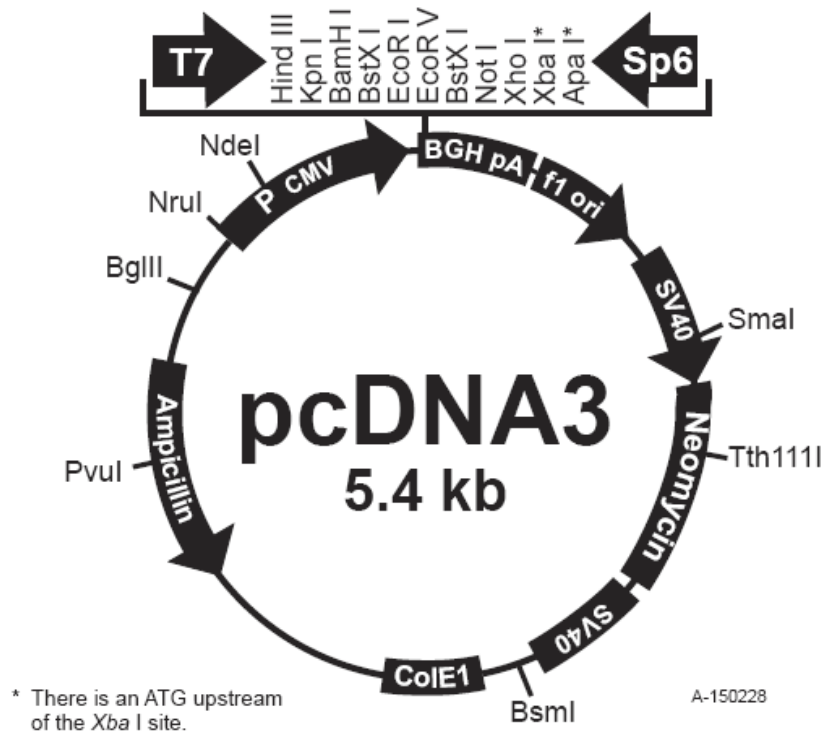
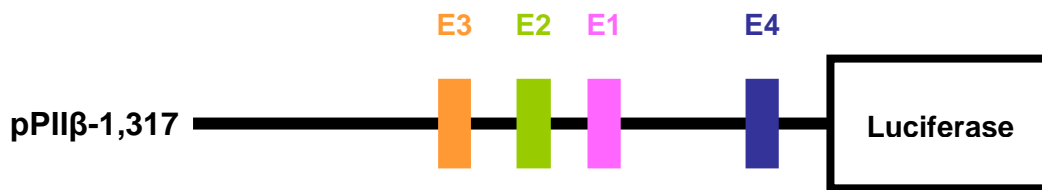


**Figure 6: Diagram of pcDNA3 vector** (from brochure supplied by Invitrogen, Carlsbad, CA, USA).

4. pPII $\beta$ -1,317 is a full-length human ACC $\beta$  promoter reporter luciferase construct that contains 4 E-boxes (CANNTG) (Figure 7) (76).



ACC $\beta$  promoter region = 1,317 bp

Four “E-boxes” identified (E1-E4): important regulatory elements for transcription factors such as upstream stimulatory factor (USF)

**Figure 7: Diagram of pPII $\beta$ -1,317 construct** (modified from Makaula et al., 2006).  
(E1: Ebox 1, E2: Ebox 2, E3: Ebox 3, E4: Ebox 4, pPII $\beta$ -1317: human ACC $\beta$  pomoter-reporter construct).

5. TransLucent USF Reporter Vector (USF-L) contains promoter recognition sites for both upstream stimulatory factor 1 (USF1) and upstream stimulatory factor 2 (USF2) cloned into a pTransLucent Vector (catalog number LROO86, Panomics, Redwood City, USA) (Figure 8).

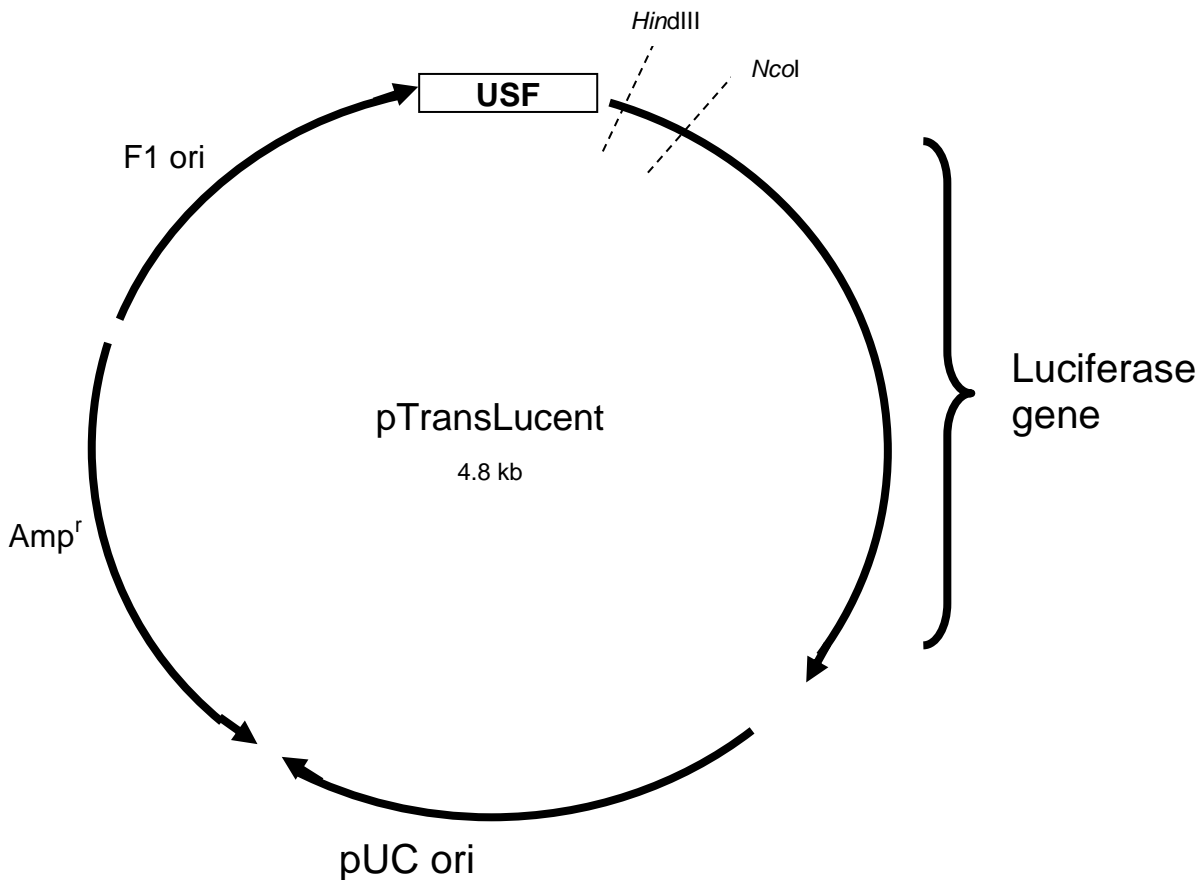


**Figure 8: Diagram of pTransLucent construct.** (Panomics, Redwood City, USA). (*HindIII* and *NcoI* are restriction sites where the USF promoter is cloned).

## Preparation of plasmid DNA

Each expression vector was amplified in *Escherichia coli* cultures (JM109 competent cells, Promega, Madison, WI, USA) and extracted using the Qiagen<sup>®</sup> Plasmid Purification Maxi Kit (Qiagen, Invitrogen, Carlsbad, CA, USA). Purified DNA was quantified using a spectrophotometer (wavelengths of 260 nm and 280 nm) and its quality checked by restriction enzyme analysis. The DNA was electrophoresed on a 1% agarose gel to check for the quality of the DNA.

### 2.1.5. Transfection procedures

On Day 2 of transfection experiments (one day after seeding) the cells were transfected with the DNA of interest (Appendix 2). Transfections were performed in triplicate for each experiment and repeated to generate the necessary numbers for statistical analysis. First, a stock solution of pGL3-Control DNA (pRL-CMV) was made in media concentration of 10 ng/ml (see step 1 of Appendix 3). The media contained DMEM and 4 mM L-glutamine. The stock solution was aliquoted into separate microfuge tubes to a final volume of 165  $\mu$ l for every transfection experiment (consisting of three replicates for each experiment) (see step 2 of Appendix 3). DNA was aliquoted into its respective microfuge tubes with pGL3-Basic making up the total DNA mass to 0.75  $\mu$ g (step 3 of Appendix 3).

A second stock solution was then prepared with an equal volume of media containing Fugene 6 Transfection Reagent (Roche, Penzberg, Germany). Here, a 2:1 ratio of Fugene 6: DNA (with DMEM and 4 mM L-glutamine) was used. 165  $\mu$ l of the Fugene 6 solution was then added to each of the microfuge tubes containing DNA and incubated at room temperature for 15 minutes (steps 4, 5 of Appendix 3).

Meanwhile, 0.9 ml of fresh medium (containing DMEM, 10% FCS and 4 mM L-glutamine) was added to the H9c2 cells before the transfection. The final volume of the DNA/Fugene 6 cocktail therefore equalled 330  $\mu$ l in each microfuge tube for each transfection experiment.

The DNA/Fugene 6 solution was added to the H9c2 myoblasts (100 µl per well to make a final volume of 1 ml per well). The solutions were applied in triplicate (step 6 of Appendix 3). The plates were gently rocked and then incubated at 37°C for 24 hours.

After 24 hours the media on the cells was changed. During this media change, various drugs of interest were added to cells. My previous experiments in my master's thesis employed other pharmacological inhibitors which proved the concept for this study, thus we chose to employ the most reliable of these. For this study we only treated with 40 µM Diazo-5-oxo-L-norleucine (DON) (Sigma-Aldrich, St. Louis, Missouri). DON is a pharmaceutical inhibitor of GFAT which is the rate-limiting enzyme of the hexosamine biosynthetic pathway. Twenty-four hours later cells were lysed, protein extracted and expression of luciferase measured using the Glomax luminometer (Promega, Fitchburg, WI, USA).

The protocol and reagents used were as stipulated in the manual of the Dual-Luciferase Reporter Assay Kit (Promega, Fitchburg, WI, USA). First, the cells were washed with phosphate buffer saline and then 200 µl of Passive Lysis Buffer (Promega, Fitchburg, WI, USA) was added to each well. The 12-well plate was then incubated on a shaker at room temperature for 15 minutes. The lysis buffer and cells from each well were transferred to microfuge tubes. A separate microfuge tube was used for each well of the 12-well plate. The microfuge tubes carrying the cells and lysis buffer were stored at -80°C (Appendix 4). On Day 5 the lysate was thawed in water and vortexed. The microfuge tubes were centrifuged at 12,000 rpm at 4°C for 2 minutes with a ALC multispeed refrigerated centrifuge PK 121R (Intergrated Services,

New Jersey, USA). 10  $\mu$ l of each sample was aliquoted into a separate well on a 96-well luminometer plate (Amersham, Buckinghamshire, UK).

Two reagents had to be prepared. Reagent 1 contained Luciferase Assay Reagent II (LAR II) and reagent 2 Stop and Glo reagent (Appendix). Both reagents were provided with the Dual-Luciferase Reporter Assay Kit (Promega, Fitchburg, WI, USA). The luminometer plate, together with the two reagents, was placed in the luminometer. Only half the amount of reagent recommended by the kit manual was used in the measurements since this was adequate enough to give a very sensitive reading. The luminometer was set up to add 50  $\mu$ l of LAR II, delay for 2 seconds and then take a reading for 8 seconds. This gave a measurement for human ACC $\beta$  promoter (pPII $\beta$ -1,317) activity. The luminometer then added “Stop and Glo” to the same well and delayed for 2 seconds before measuring the light released (for another 8 seconds). This yielded the measurement for the Renilla construct (pRL-CMV) of the same sample. The process was repeated for each well, providing two readings for each sample (Appendix 5).

### **2.1.6. Statistical analyses of transfection results**

Luminometer firefly readings for each experiment were normalised against its respective Renilla luminometer reading by dividing the firefly reading by its renilla reading. Luminometer readings referred to the measurement from the sample when the first reagent was added to the sample and is a measure of the amount of luciferin protein expressed by the promoter of interest. Renilla readings referred to the measurement from the sample when the second reagent was added to the sample and is a measure of the amount of renilla protein expressed by a constitutively expressed control vector that we use to normalise our results according to cell number and transfection efficiency. Each experiment was performed in triplicate each time a transfection was carried out. Each replicate of an experiment was added together and then divided by three to give a mean value for each experiment. This provided a mean value for each experiment that was normalised according to transfection efficiency and cell number. To eliminate any vector effects (i.e. in which the construct were cloned) on the experiment, each of the mean values were divided by the vector's mean value.

The transfection experiments were repeated numerous times to provide a larger number of replicates for each experiment. Measurements from all the same experiments were combined and Graphpad Instat version 3.01 (GraphPad Software Inc., San Diego, CA, USA) used to perform statistical analyses of these values. First, the mean, standard error of the mean and standard deviation were calculated. A 95% confidence interval was also calculated. Replicates of an experiment that were outside the 95% confidence interval or were not within two standard errors of the mean were discarded. The remaining replicates were used to plot a graph. The Student-Newman

statistical test was used to check if there were significant differences between controls and the experiments in each set of experiments. Values  $p < 0.05$  were taken as being significant. When we began our experiments we calculated both standard deviation and standard error of the mean because the statistical program offered this option. We chose to go with standard error of the mean because subtle differences in results can be detected (that standard deviation ignores). Physiological data is lost and overlooked when errors are too large. To make sure that there were few outliers, we performed numerous experimental repeats and thus increased the quality of the data.

### **2.1.7. Calculation of HOMA index**

On the day the animal was sacrificed glucose was measured from glucometer readings and from tail cuts. Insulin was measured from blood plasma. HOMA index was calculated as the product of (overnight) fasting insulin and fasting glucose divided by a normalising factor. This factor can be 405 or 22.5. The US formula uses 405 while the accepted international formula uses 22.5. We chose to follow the international formula:

$$\text{HOMA-IR} = (\text{fasting Glucose}(\text{mmol/L}) \times \text{fasting Insulin}(\text{mU/L})) / 22.5$$

Animals that were stressed had abnormal values for glucometer readings and were not included in the final results. An  $n$  of as high as 7 was used with Student Newman Keuls statistical analysis used to calculate standard error of the mean to plot a graph.

## 2.2. Real-time polymerase chain reaction

### 2.2.1 RNA extraction from Heart tissue Real Time Polymerase chain reaction

Tissue was shaven off using a scalpel after being frozen in liquid nitrogen and then added directly to the PureZol RNA isolation reagent (Bio-RAD Laboratories, Hercules, California, USA) with homogenization beads in each tube. The samples were then homogenized for 2 minutes at 30 Hz using a rotor–stator homogenizer (Qiagen, Invitrogen, Carlsbad, CA, USA). The tube was then flicked to release the tissue pellet from under the bead and then homogenized again for another 2 minutes at 30 Hz. RNA was extracted from Wistar rat heart muscle using the Aurum™ Total RNA Fatty and Fibrous tissue kit (Bio-RAD Laboratories, Hercules, California, USA) (Appendix 6). At the end of the extraction the RNA sample was analysed for integrity and concentration using the Experion™ RNA StdSens Analysis Kit (Bio-RAD Laboratories, Hercules, California, USA). 2 µl of RNA sample was added to 2 µl of RNase free water, heated to 70°C for 2 minutes. An RNA ladder was also heated to 70°C. 1 µl of each sample was used to measure RNA concentration and integrity with the Agilent RNA 6000 Nano Kit (Bio-RAD Laboratories, Hercules, California, USA). 1 µg RNA was reverse transcribed to cDNA using the iScript™ cDNA Synthesis Kits (Bio-RAD Laboratories, Hercules, California, USA) for RT-PCR.

### **2.2.2. Animal model used for RNA experiments**

Male Wistar rats were fed a high fat and high glucose diet versus controls (low fat). The rats were fed a high-fat diet (39.8, Harlan Teklad, WI, Madison, USA). for 86 days and compared to matched controls (9.5% fat, TD.06683, Harlan Teklad, WI, Madison, USA). Rats were housed in a room with a controlled temperature (22 °C) with a 12 h/12 h light-dark cycle and free access to food and water (119). On the final day of the experiment animals anaesthetised by an intramuscular injection of 3 IL ketamine per g<sup>1</sup> body weight (119). Tissue was isolated at 14, 56 and 86 days and myocardial RNA prepared using standard methods. The number of animals in each group was 14 but we used a n of 7 for experiments. The high fat rats were shown to be insulin resistant at Day 86 (refer to Results section [HOMA index]). Any rats that might have been stressed during the sacrificing procedure were excluded from experimental numbers as the insulin measurements changed accordingly, making any data that followed from successive experiments unreliable. Due to how small rat hearts are and the number of experiments we wanted to test within the same sample, the hearts were crushed before use in all in vivo experiments. Results can therefore be defined as that compared between whole heart tissue rather than one section of the heart.

### **2.2.3. Real-time polymerase chain reaction assay**

RT-PCR was performed (in duplicate) testing the relative expression of the ACC $\beta$  gene in isolated male Wistar rat heart tissue. Primers for the ACC $\beta$  gene were designed to measure the expression of ACC $\beta$  gene promoter activity with RT-PCR. (Inqaba Biotechnical Industries, Pretoria, South Africa). Three house keeper genes

were used to normalize the data namely, ribosomal protein L13 (RPL13), beta-2 microglobulin (B2M) and ubiquitin C (UBC). House keepers were selected from 8 possible genes that we expected would not be influenced too greatly by our experimental conditions. Three were chosen to increase the statistical power of our results and were chosen using the geNORM housekeeping gene selection kit (PrimerDesign, Southampton, United Kingdom). RT-PCR was performed using SYBR® green detection on a 96 well iCycler thermal cycler PCR machine (Bio-RAD Laboratories, Hercules, California, USA). Results were analysed using new geNORM analysis software.

## **2.3. Flow Cytometry**

### **2.3.1. Cell preparation for flow cytometry**

H9C2 Cells were seeded in T75 flasks in equal numbers and grown to about 60% confluency prior to transfection. Cells were transfected as described earlier but in 3 times the dose used for cells seeded in 12-well plates. The next morning we added fresh media ± pharmacological agents or appropriate substrates. Six hours after treatment the cells were harvested with trypsin, centrifuged and washed with phosphate buffered saline (PBS) with a centrifuge step of 1,500 rpm for 3 minutes. We then permeabilized the cell membranes by incubating for 10 minutes with a solution of acetone:methanol (1:1 ratio). We centrifuged off the fixing solution and resuspend the cells in 5% Donkey serum in PBS, and incubated overnight at 4°C.

Cells were thereafter washed with PBS and incubated with primary antibody (1:50 for O-GlcNAc or 1:500 for USF2) at room temperature (overnight). The samples were then split in half, i.e. into two separate tubes to be treated by primary antibodies of interest namely, O-GlcNAc and USF2. The samples were washed and centrifuged with PBS and then incubated with 1:200 PE/Alexa Fluor 610 anti-goat secondary antibody (Invitrogen, Carlsbad, CA, USA) in PBS for 30 minutes at room temperature. The same secondary antibody was used for both primary antibodies used per sample. The samples were then washed 2-3 times with PBS before resuspended in 300  $\mu$ l of PBS and measured on the BD FACSAria Flow Cytometer (BD Biosciences, Franklin Lakes, New Jersey, USA). To ensure that our antibodies were at a strong enough concentration to bind to all available proteins, we titrated it at twice the normal concentration. Samples were measured after being excited at 488 nm channel by an argon laser. Our results indicated no increase in the titrated samples and thus demonstrated enough primary antibody available (data not shown). Samples gated for cell debris and dead cells. Experiments were repeated 3 times until a total of 10, 000 events measured per sample. We took a measure of the geometric mean for all samples.

## 2.4. Chromatin immunoprecipitation

### 2.4.1. Chromatin immunoprecipitation of heart tissue in Wistar rats fed a high caloric diet

100 mg of male Wistar rat heart tissue was fixed using formaldehyde to crosslink protein bound to DNA and then washed with PBS before placed in lysis buffer for isolation using a *Chromatin immunoprecipitation (ChIP) Assay kit* (catalog number 17-295, Millipore, Massachusetts, USA). The samples were sonicated to shear the tissue and DNA into appropriate sizes. We optimized the sonication by using varying numbers of bursts 4, 8 and 12 and running the lysate on a gel after de-crosslinking to ensure that the number of bursts was adequate for our experiments. We found that 8 bursts at 33% power for 15 seconds was optimum. We pre-cleared the sample with Protein A agarose/salmon sperm DNA (catalog number 16-157C, Millipore, Massachusetts, USA), then incubate the samples with either USF2 or O-GlcNac primary antibody. We isolated from the USF2 samples DNA for PCR of two regions on the ACC $\beta$  gene. One set of primers was designed for the region inside where USF2 is expected to bind called the signal primers, another region was designed to bind to a region outside the binding region to be a control (called the control primers). The primers were designed and bought from Inqaba biotech (Pretoria, South Africa). For the control primers the sequences were: forward 5' TCAGGGAGGGCATTCTAACTT 3' and reverse 5' CAGAGATAATTTAACTGATGGG 3'. For the signal primers the sequences were: forward 5' AGTAGGGCTAAGTACAGAAA 3' and reverse 5' ATTCTTGAGTGAGGCTG 3'. The PCR was performed using thermopol taq with buffer (catalog number M0267, New England Biolabs, Massachusetts, USA) and

using conditions: initial 95°C 5 mins, 35 cycles of 95°C for 30 seconds, 56°C for 45 seconds, and 68°C for 1 minute. The PCR product was electrophoresed on a 1% agarose gel with loading dye (catalog number R0631, Fermentas, ThermoScientific, Massachusetts, USA) and a O'GeneRuler 1000 bp DNA ladder (catalog number SM1143, ThermoScientific, Massachusetts, USA).

#### **2.4.2. Western Blotting of Chromatin immunoprecipitation of heart tissue in Wistar rats fed a high caloric diet**

We also isolated from the USF2 samples protein for western blotting for O-GlcNAc to prove whether USF2 is modified directly by the hexosamine pathway or possibly regulated by another protein which is O-GlcNAc modified. These protocols for DNA ChIP and protein isolation were performed using the *Chromatin immunoprecipitation(ChIP) Assay kit* (catalog number 17-295, Millipore, Massachusetts, USA). A Western blot was then performed for the opposing target. Firstly USF2 and O-GlcNAc were immunoprecipitated separately from the same samples and western blotted for O-GlcNAc. The membrane was then stripped and reprobed for USF2. For O-GlcNAc, 2% BSA in PBS - Tween as a blocking agent was used and for USF2 we used milk powder in TBS-Tween a blocking agent. Membranes were developed using HRP (catalog number 34077, ThermoScientific, Massachusetts, USA) (Appendix 7 and 8).

## **2.5. Measuring fatty acid accumulation in Wistar rats fed a high caloric diet**

100 mg of male Wistar rat heart tissue was taken from our stored samples in liquid nitrogen to preserve the rest of the heart sample for other experiments. The sample to be used for fatty acid extraction could then be stored in -20°C or on ice if used immediately. The fatty acids were then extracted in collaboration with the Medical Research Council (Dr. van Jaarsveld and Johanna van Wyk, Tygerberg, Cape Town, South Africa). The method we used is described in Appendix 9. The samples were measured for phospholipids, triglycerides and free fatty acids, as percentage fat and per gram of heart tissue.

# **Chapter 3**

# **Results**

## 3.1 *In Vitro* Experiments

### 3.1.1. Transfections

Carrying on with my hypothesis in my master's thesis my initial focus was to strengthen my assumptions of USF2 as a possible candidate as a transcription factor for ACC $\beta$  promoter response to hexosamine biosynthetic pathway flux. I transiently transfecting H9c2 myoblasts with the human ACC $\beta$  promoter-luciferase reporter construct (pPII $\beta$ -1317/+65)  $\pm$  a USF1 and USF2 expression vector. Results showed that ACC $\beta$  responded to USF2 overexpression but not USF1. The white bar represents the empty vector described in the methods section (Figure 5) used as a control to normalize against any affects the vector might have on our statistical results. The black bar represents cells only treated with ACC $\beta$  while the grey bar represents samples only transfected with ACC $\beta$  and GFAT. I further co-transfected with GFAT and this saw no greater increase in ACC $\beta$  activity (Figure 9).

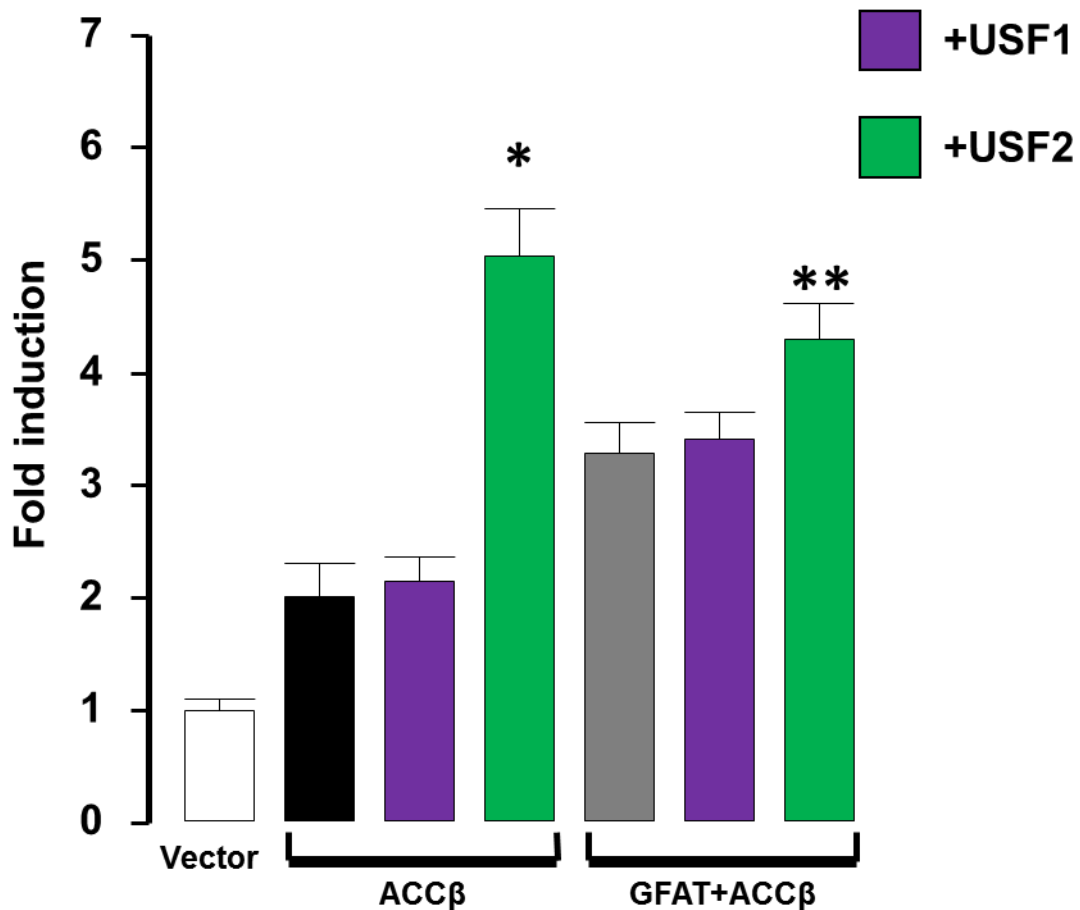


**Figure 9: USF2 overexpression promotes ACC $\beta$  expression in response to HBP flux and not USF1.**

\* $p < 0.001$  vs ACC $\beta$  [n=6]

\*\* $p < 0.05$  vs ACC $\beta$  [n=6]

We further investigated USF-mediated regulation of the ACC $\beta$  promoter by proving the affects of hexosamine biosynthetic pathway flux on USF2 expression by co-transfecting a GFAT expression construct together with a USF luciferase reporter construct (USF-L = Upstream Stimulatory Factor TransLucent™ Reporter Vector) that contains multiple promoter binding sites for USFs. Here, we found a marked induction of the USF-L reporter construct by  $80 \pm 12\%$  ( $p < 0.001$ , n=5) compared to the control (Figure 10).

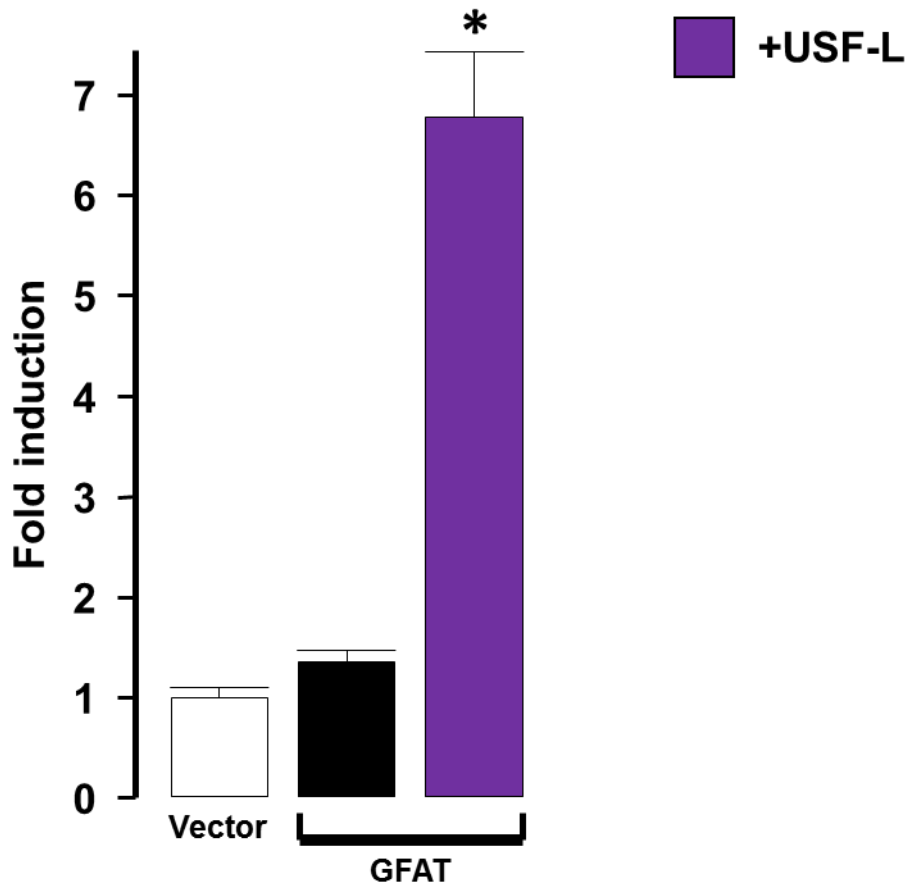


**Figure 10: GFAT overexpression enhances USF transcriptional activation.**

\*  $p < 0.001$  vs. GFAT [n=6]

We then turned our attention to the USF2 and its HBP-mediated mechanisms of regulation of the ACC $\beta$  promoter. Firstly we identified where the region of ACC $\beta$  regulation would occur in response to GFAT overexpression with the use of deletion constructs of ACC $\beta$  promoter (-1317/+65). Here in this experiment GFAT overexpression vector was also transfected with various truncated versions of the ACC $\beta$  and it was found that the effects of GFAT overexpression was lost at -18/+65 deletion construct. This would indicate that the binding region of transcription factors that respond to HBP flux can be found between -38/+65 and -18/+65 on the ACC $\beta$  promoter (Figure 11).

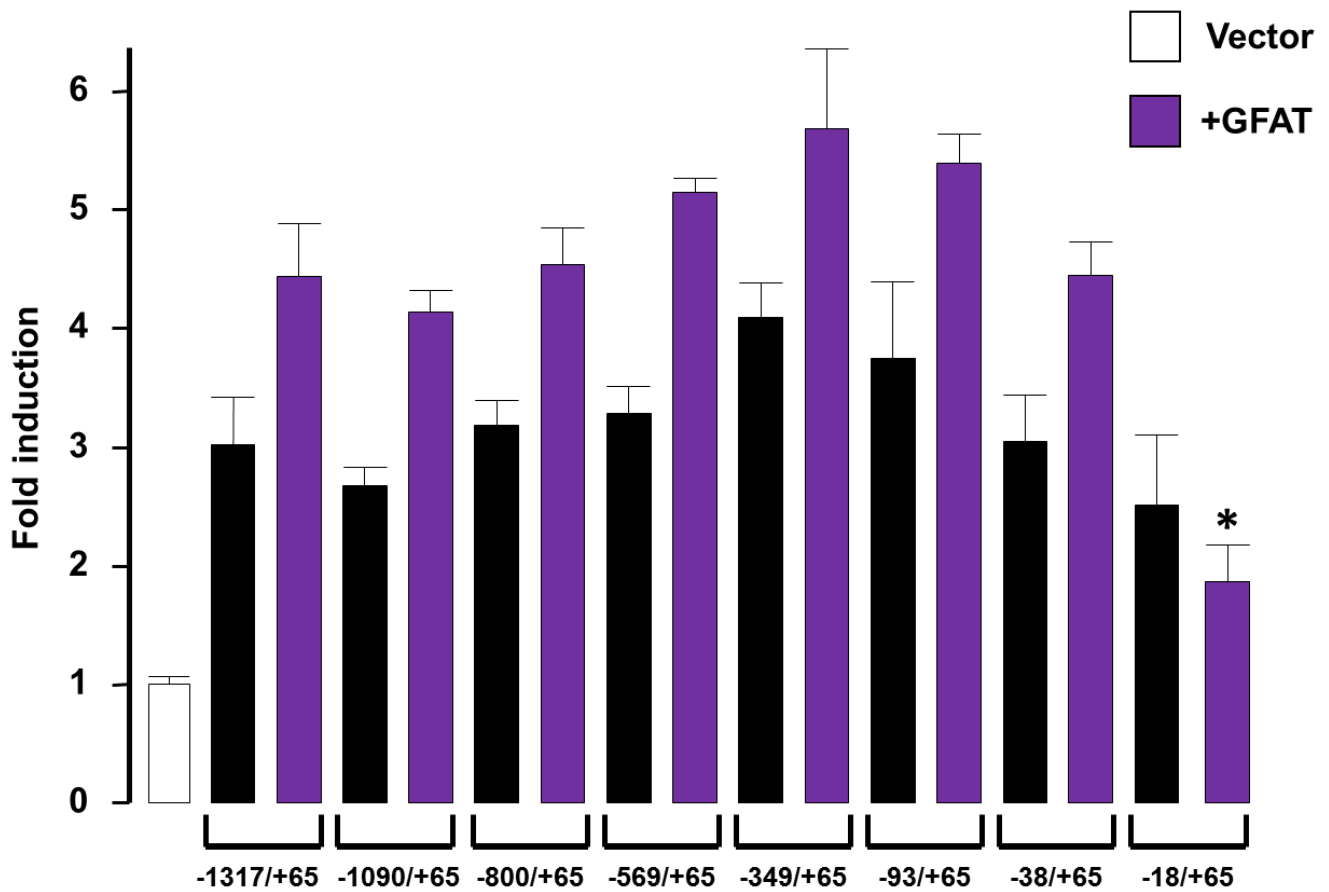


**Figure 11: ACC $\beta$  Deletion Construct induction by GFAT**

\* $p < 0.001$  vs -1317/+65 to -38/+65 [n=6]

We then repeated this experiment but co-transfected with USF2 instead of GFAT and found the same pattern of a binding region in response to USF2 overexpression between -38/+65 and -18/+65 on the ACC $\beta$  promoter (Figure 12).

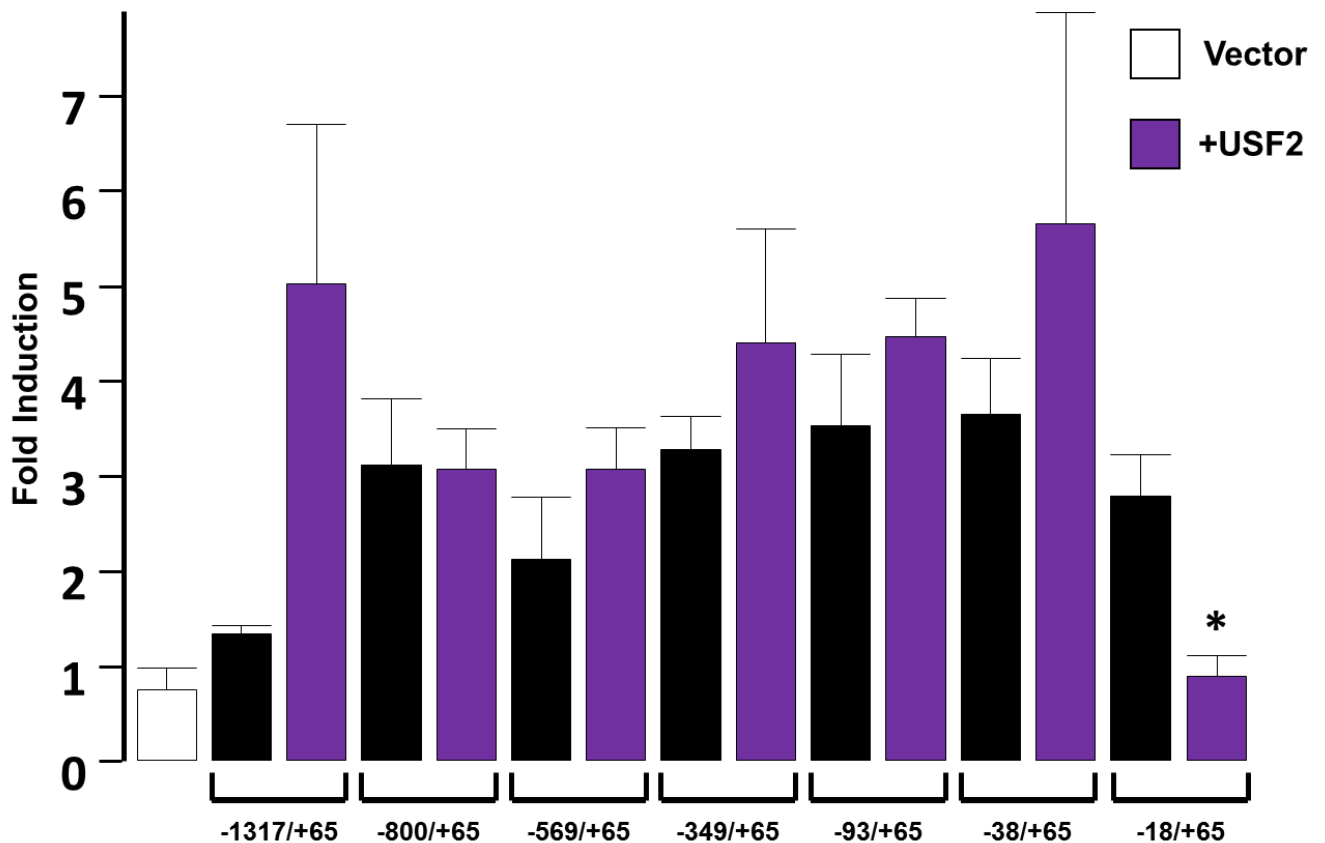
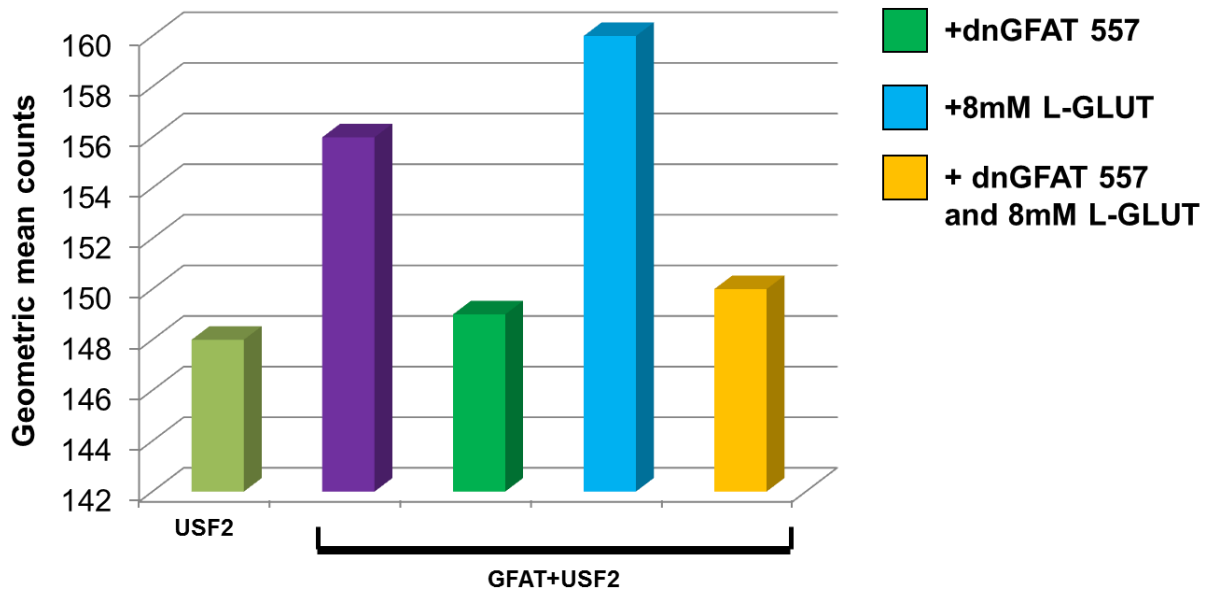


Figure 12: The effects of USF2 on ACC $\beta$  promoter activity (deletion constructs)  
 \*  $p < 0.01$  vs -1317/+65 to -38/+65

### 3.2. Flow Cytometry

In order to strengthen the hypothesis that hexosamine flux was linked to USF2 expression we transiently co-transfected H9c2 myoblasts with GFAT overexpression vector with USF2 expression vector and then co-transfected with a dominant negative inhibitor of GFAT (GFAT557). The cells were permeabilised and probed with an O-GlcNAc primary antibody and a USF2 primary antibody. USF2 and O-GlcNAc expression was measured by flow cytometry with a PE/Alexa Fluor 610 anti-goat secondary antibody. Results showed per 10000 cells that O-GlcNAc levels rose in response to GFAT and USF2 expression and fell when GFAT was inhibited. We also

treated cells with 8mM L-glutamine (a substrate of HBP). This rise in L-glutamine resulted in increased O-GlcNAc levels, which was ameliorated with the addition of the inhibitor (Figure 13).



**Figure 13: The effects of HBP flux on O-GlcNAc expression represented per 10000 transfected cells measured with Flow Cytometry [n=10000]**

In the same sample we measured USF2 expression using flow cytometry. The same pattern was seen as before in the O-GlcNAc results. Results showed an increase in USF2 expression when co-transfected with GFAT (Figure 13 and 14). This effect was decreased when co-transfected with dominant negative GFAT. Treatment with 8 mM L-glutamine increased USF2 expression greatly (Figure 13 and 14) and this effect was lost when co-transfected with the dominant negative GFAT (Figure 13 and 14). This gave strong indication that USF2 and O-GlcNAc modification is related but not proof that USF2 is being modified by the hexosamine biosynthetic pathway. Later we would look to investigate whether USF2 is modified by O-GlcNAc (Figures 13 to 17).

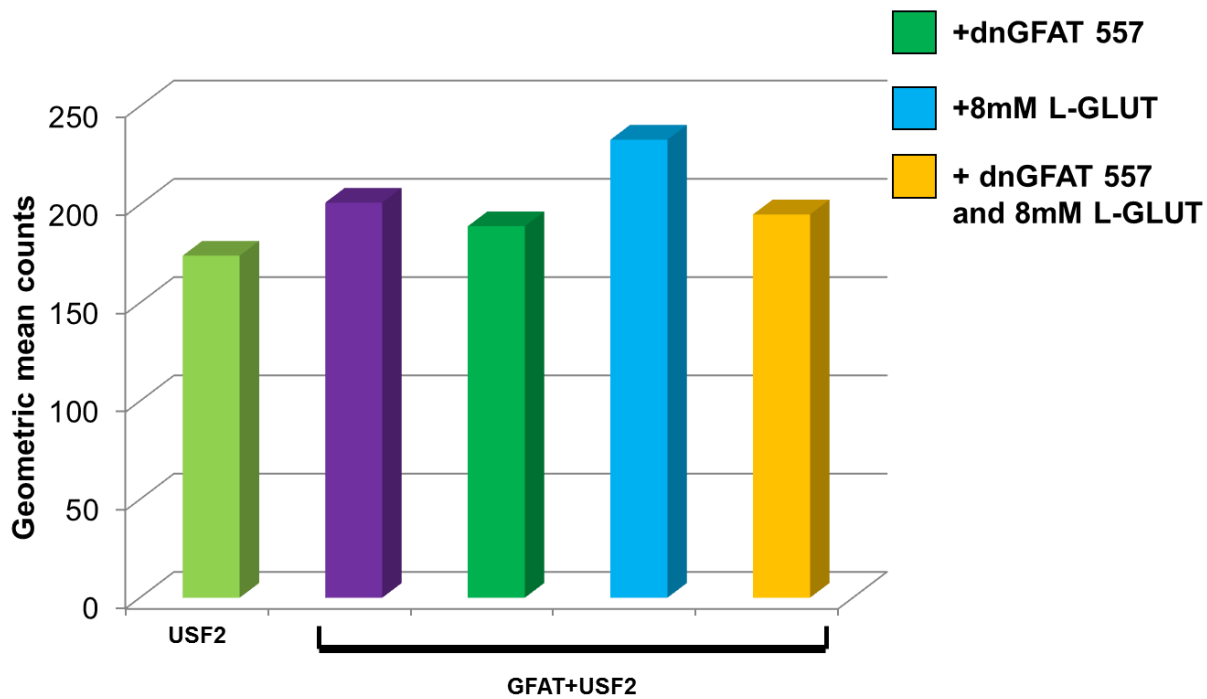


**Figure 14: The effects of HBP flux on USF2 expression represented per 10000 transfected cells measured with Flow Cytometry [n=10000]**

It can be noted that with the addition of GFAT to USF2 there was an increase in side-scatter (SSC) in the cells. This may indicate a change in morphology or change in response to GFAT overexpression. Increased GFAT expression would increase O-GlcNAc modification and result in modification of a wide variety of proteins and transcription factors. These cells do not appear morphologically different under the microscope; however there must be a morphological shift due increased hexosamine flux that we haven't been able to observe without the use of flow cytometry (Figures 15-17).

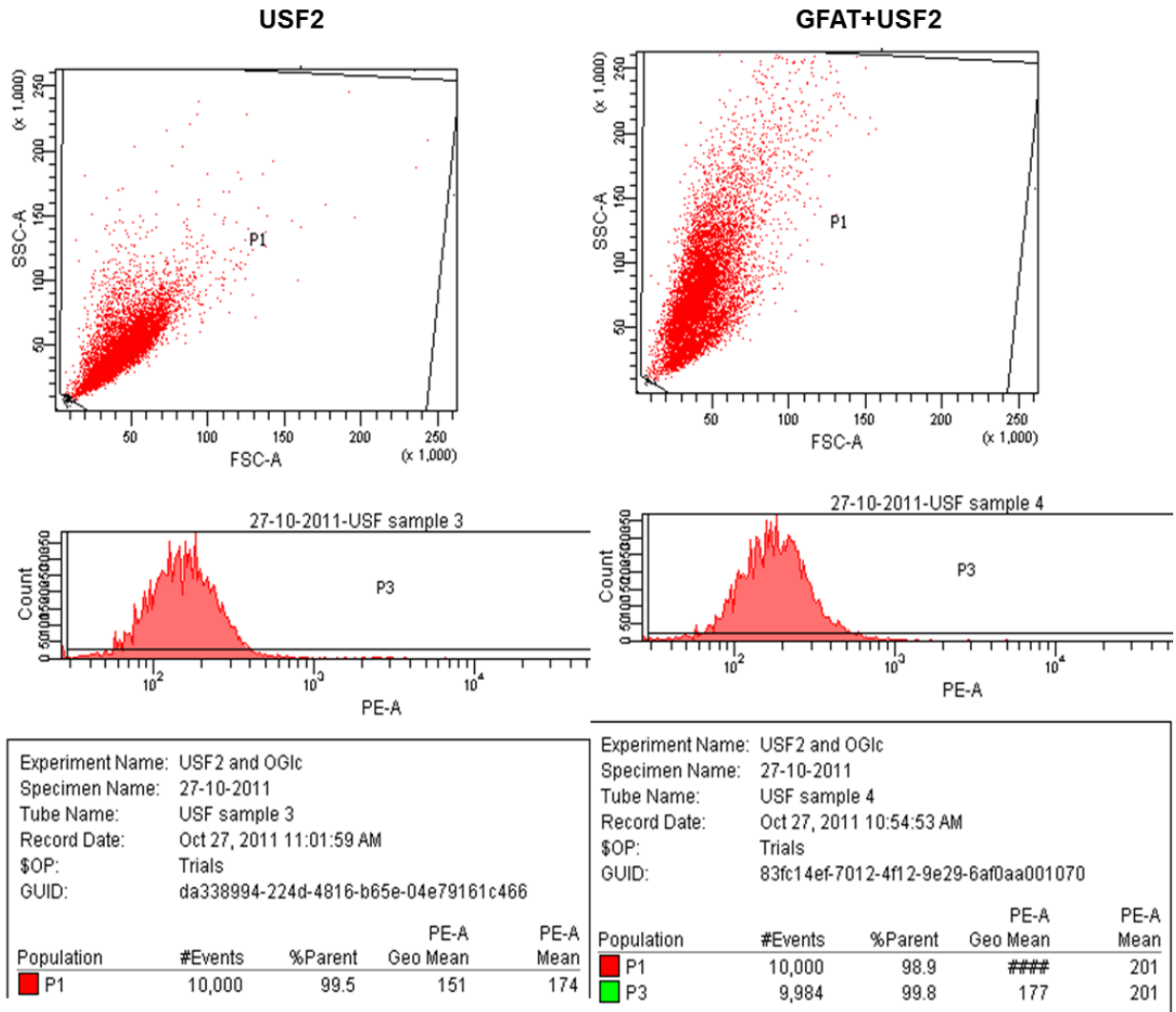


**Figure 15: The effects of HBP flux on USF2 expression represented per 10000 transfected cells Flow Cytometry result [n=10000]**

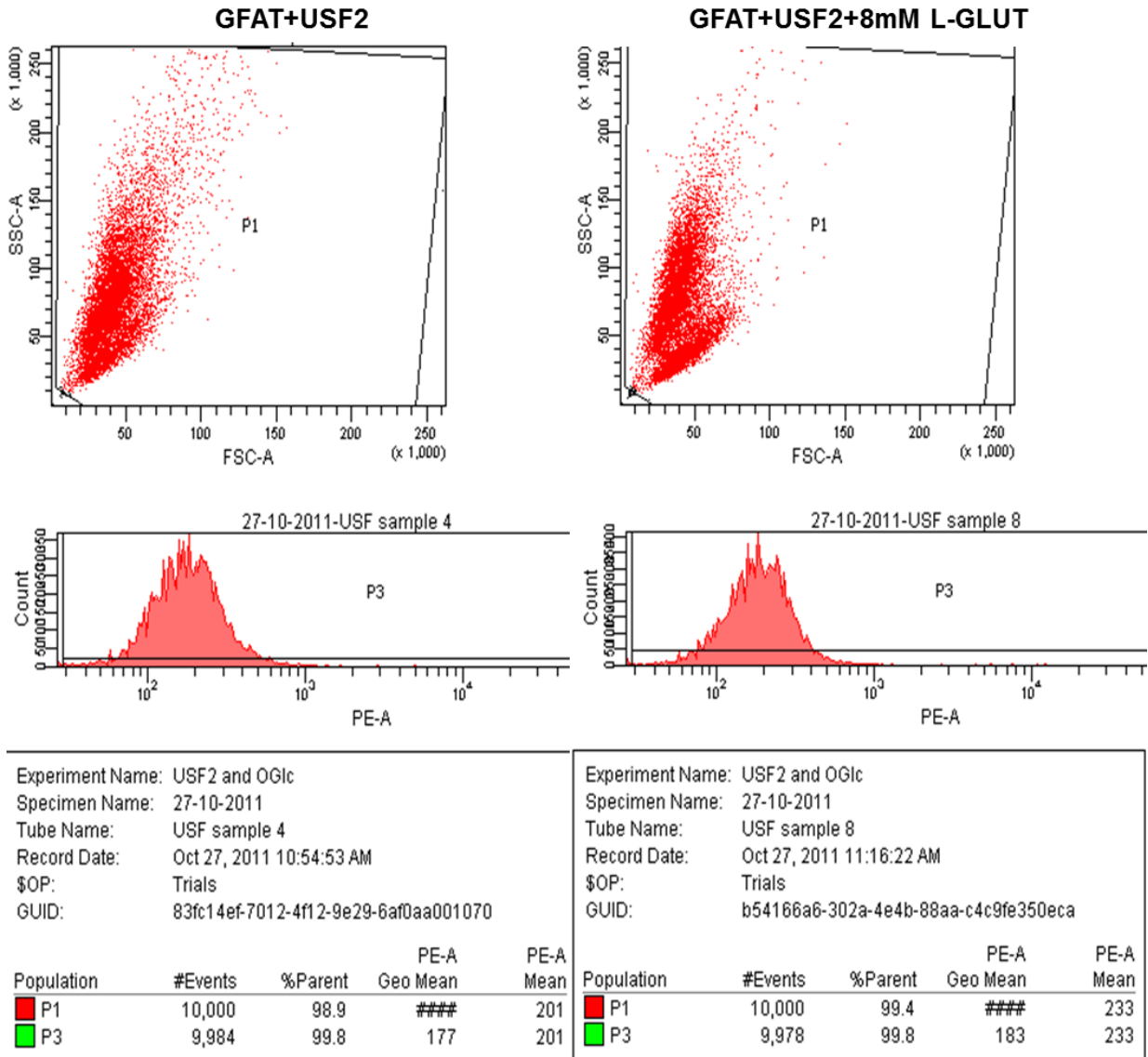


**Figure 16: The effects of L-glutamine mediated HBP flux on USF2 expression [n=10000]**

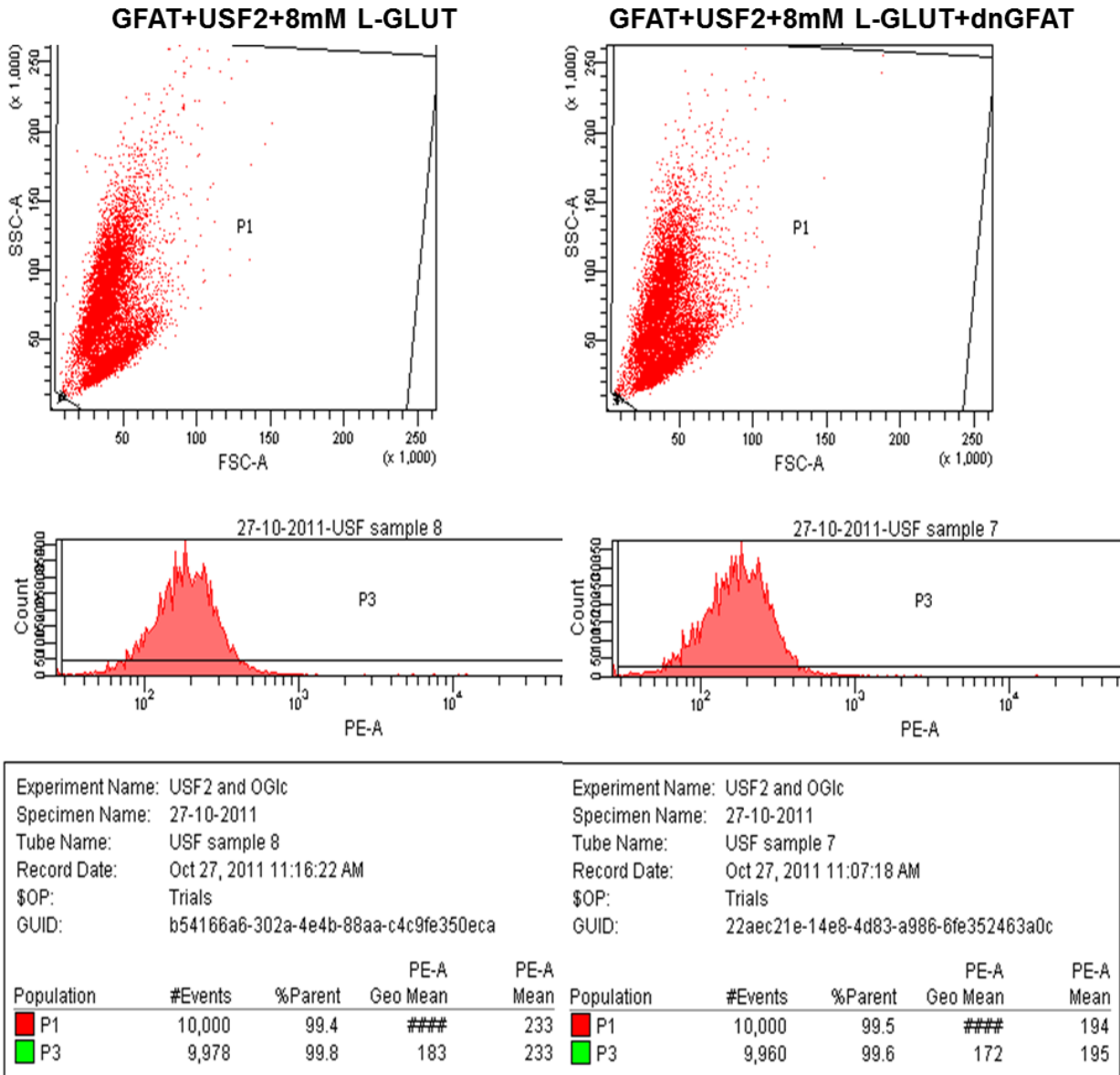


**Figure 17: The effects of HBP flux on USF2 expression can be blunted with the use of a dominant negative inhibitor of GFAT**  
 [n=10000]

### 3.3. *In Vivo* Experiments

#### 3.3.1. Animal model

Heart tissue from male Wistar rats fed a high fat and high glucose diet with added low fat diet controls were used in our *in vivo* experiments. On the day of sacrifice plasma glucose was measured from blood of a heart puncture along with glucose measured from blood of the same rats tail with a glucometer. Plasma insulin was also measured. From this the HOMA index was measured for each group of rats. It was determined that the rats were insulin resistant on day 86 of the study (Table 1 and Figure 18).

**Table 1: Measurements of glucose, insulin and HOMA on the day of sacrifice of animals in this study**

Time	Diet	rat No	Glucose* mmol/l plasma	Glucose** mmol/l full blood	INSULIN ng/ml plasma	HOMA index with plasma glucose (mg/dl)
<b>Day 0</b>	<b>LFD</b>	<b>1</b>	3.3	2.1	0.522	0.0762
		<b>2</b>	4.8	2.2	0.920	0.1979
		<b>3</b>	4.0	1.7	0.617	0.11078
		<b>4</b>	4.9	2.7	0.534	0.1158
		<b>5</b>	4.6	2.4	6.123	1.2557
		<b>6</b>		2.6		rat died before heart puncture
		<b>7</b>	3.0	3.8	0.777	0.1046
<b>Day 7</b>	<b>LFD</b>	<b>1</b>	6.22		0.523	0.1447
		<b>2</b>	5.77	4.6	0.577	0.1480
		<b>3</b>	7.17	5	0.495	0.1576
		<b>4</b>	6.20	5.2	0.654	0.1800
		<b>5</b>	6.42	4.7	1.255	0.3581
		<b>6</b>	4.72	4	0.509	0.1068
		<b>7</b>	3.71	3.9	0.659	0.1087

Time	Diet	rat No	Glucose* mmol/l plasma	Glucose** mmol/l full blood	INSULIN ng/ml plasma	HOMA index with plasma glucose (mg/dl)
<b>Day 7</b>	<b>HFD</b>	1	4.89	3.8	0.523	0.1138
		2	4.47	5.3	0.662	0.13149
		3	7.02	5	1.310	0.4089
		4	7.10	4.1	0.953	0.3008
		5	5.32	4.1	0.870	0.2058
		6	4.89	4.4	0.521	0.1133
		7	6.72	5.7	2.898	0.8649
<b>Day14</b>	<b>LFD</b>	1	6.18	5.1	1.004	0.2759
		2	8.26	5.4	2.213	0.8121
		3	5.25	4	0.502	0.1171
		4	7.39	3.5	0.799	0.2627
		5	6.21	4.3	0.509	0.1405
		6	6.60	6.1	0.740	0.2169
		7	4.96	3.9	1.506	0.3320
	<b>HFD</b>	1	6.84	5.4	0.656	0.1992
		2	5.74	4.7	0.935	0.2387
		3	7.17	5.1	0.766	0.2439
		4	6.22	5.2	1.180	0.3264
		5	9.27	7.2	6.062	2.4970
		6	6.52	6.1	1.272	0.3685
		7	5.90	4.9	1.107	0.2905
<b>Day 56</b>	<b>LFD</b>	1	5.12	4.3	3.200	0.7282
		2	5.49	4.6	2.049	0.5001
		3	7.41	6.2	2.067	0.6804
		4	4.84	3.2	1.617	0.3479
		5	5.64	4.8	1.478	0.3703
		6	5.16	4.7	2.583	0.5924
		7	5.78	3.6	1.649	0.4238
<b>Day 56</b>	<b>HFD</b>	1	8.30	6.4	5.395	1.9898
		2	5.69	4.8	1.537	0.3888
		3	6.90	4.3	2.781	0.8529
		4	6.17	4.3	3.497	0.9591
		5	6.13	4.7	1.178	0.3208
		6	9.43	6	2.608	1.0929
		7	8.32	5.8	3.125	1.1555

Time	Diet	rat No	Glucose*	Glucose**	INSULIN	HOMA index
			mmol/ plasma	mmol/l full blood	ng/ml plasma	with plasma glucose (mg/dl)
<b>Day 86</b>	<b>LFD</b>	<b>1</b>	<b>10.199</b>	<b>5.3</b>	<b>13.678</b>	<b>6.2002</b>
		<b>2</b>	6.662	4.3	1.231	0.3644
		<b>3</b>	5.944	4.8	2.104	0.5559
		<b>4</b>	5.771	4.5	0.839	0.2151
		<b>5</b>	5.612	4.5	0.871	0.2173
		<b>6</b>	6.596	5.4	1.988	0.5827
		<b>7</b>	5.612	4.9	1.873	0.4672
<b>Day 86</b>	<b>HFD</b>	1	6.503	4.6	2.100	0.6069
		2	9.402	7.3	2.049	0.8563
		3	8.258	5.7	1.725	0.6331
		4	10.718	5.6	4.742	2.2588
		5	7.207	6	2.231	0.7146
		6	7.221	5.4	2.955	0.9482
		7	7.979	5.2	13.381	4.7451

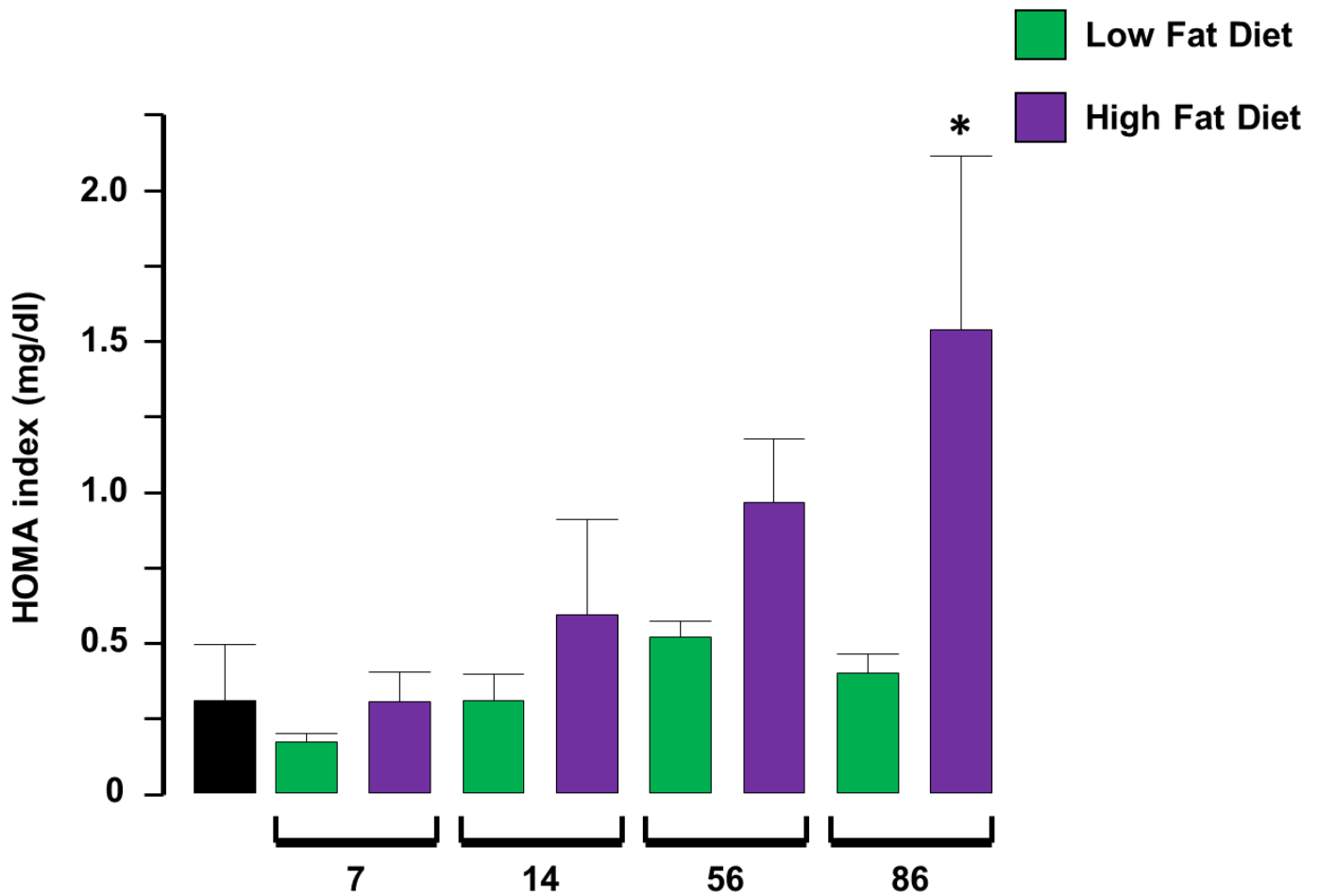


**Figure 18: HOMA index values of male Wistar rats in response to a high fat diet versus controls (low fat)**

\* $p < 0.05$  vs LF86 [n=6]

It can be seen quite clearly a gradual increase in HOMA index with time in the group of rats fed the high fat diet versus those fed normal chow (Figure 18). HOMA index reaches a significant high level in the day 86 high fat fed rats.

### 3.3.2 Real-Time Polymerase Chain Reaction

The next step was to investigate the time point for when HBP-mediated ACC $\beta$  expression is activated and lost. We isolated mRNA from rat heart tissue at various time points up to the development of insulin resistance and performed real-time PCR to measure ACC $\beta$  mRNA levels. The data revealed a time point at day 56 when ACC $\beta$  mRNA levels increased significantly in the high fat diet versus controls (Figure 19).

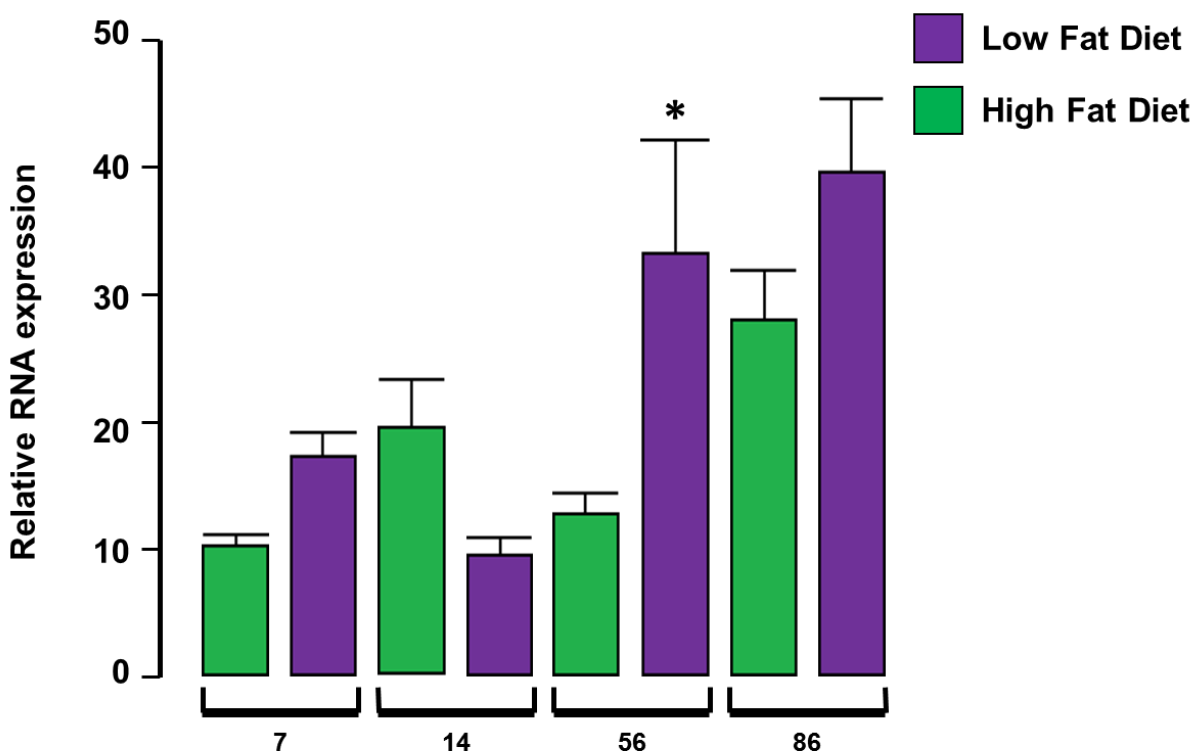
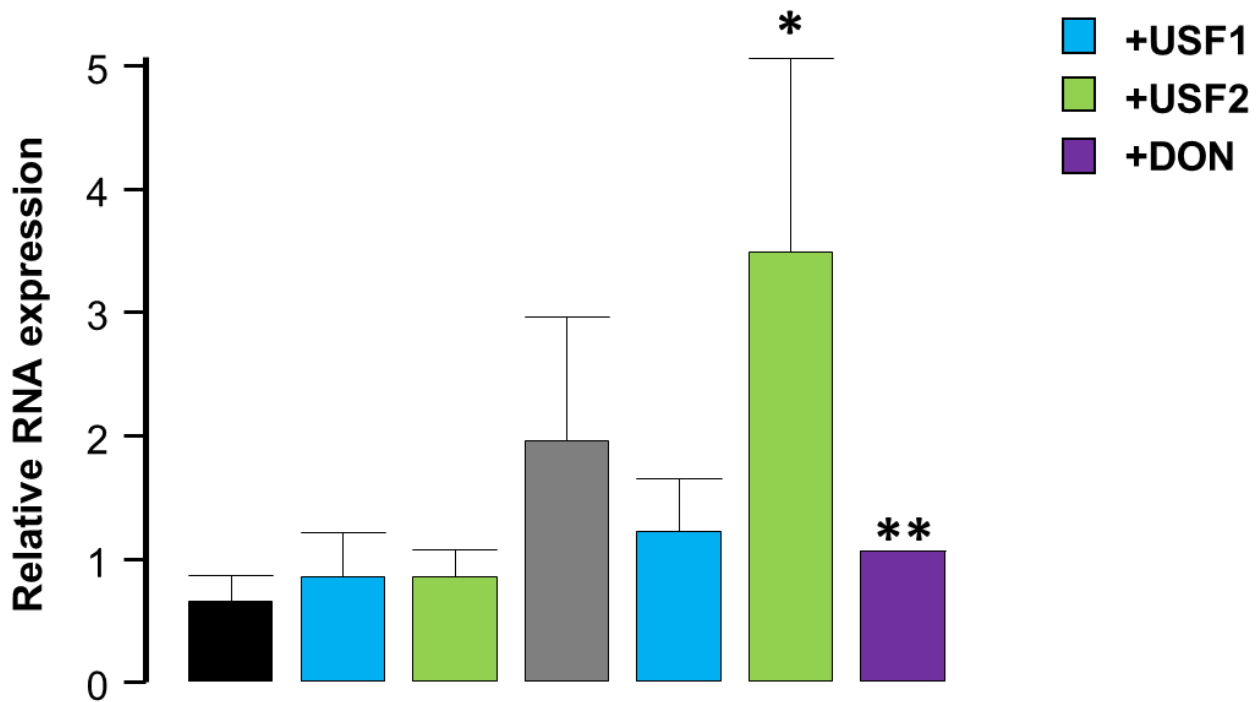


Figure 19: ACC $\beta$  expression in male Wistar rats in response to a high fat diet versus controls (low fat)

\* $p < 0.05$  vs LF56 [n=9]

We further investigated our previous experiments with transfection by looking at RT-PCR of cells transfected with USF1 and USF2 with GFAT and ACC $\beta$ . We found similar results to what was discovered in luciferase assays, with USF2 inducing ACC $\beta$  in the presence of

GFAT and this effect being lost with the addition of an inhibitor of GFAT, namely DON (6-diazo-5-oxo-l-norleucine) (Figure 20).



**Figure 20: USF2 expression in transfected H9C2 myoblasts cells**

\* $p < 0.05$  vs ACC $\beta$  + GFAT (n=6)

\*\* $p < 0.001$  vs ACC $\beta$  + GFAT + USF2 [n=6]

### 3.3.3. Chromatin immunoprecipitation of heart tissue

In optimizing the technique chromatin immunoprecipitation it was necessary to optimize sonication of samples. Bursts of 4, 8 and 12 tested with 8 bursts giving the best fragmentation of DNA (Figure 21).

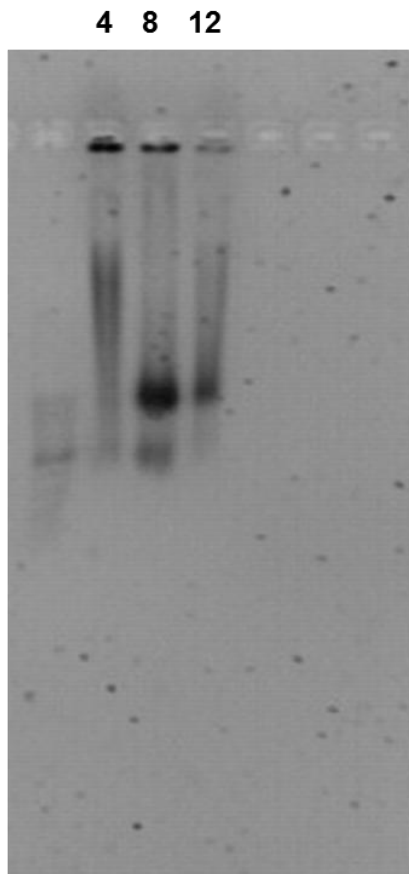


**Figure 21: DNA of sonicated of tissue from male Wistar rats with bursts 4, 8 and 12**

Heart tissue was sonicated and USF2 protein was isolated cross-linked to any DNA that was bound to it. The resulting DNA was PCR for a control primer set outside USF2 binding region of interest and a signal primer set that amplifies only the region of DNA we expect USF2 to bind. The input sample was used alongside the immunoprecipitation sample (IP) as a comparison between whole DNA of a sample before and after immunoprecipitation. We expected to find the control primers to work in the input sample and not the

immunoprecipitated sample. It was found that the control primers did not amplify any region in the IP sample (Figure 22).

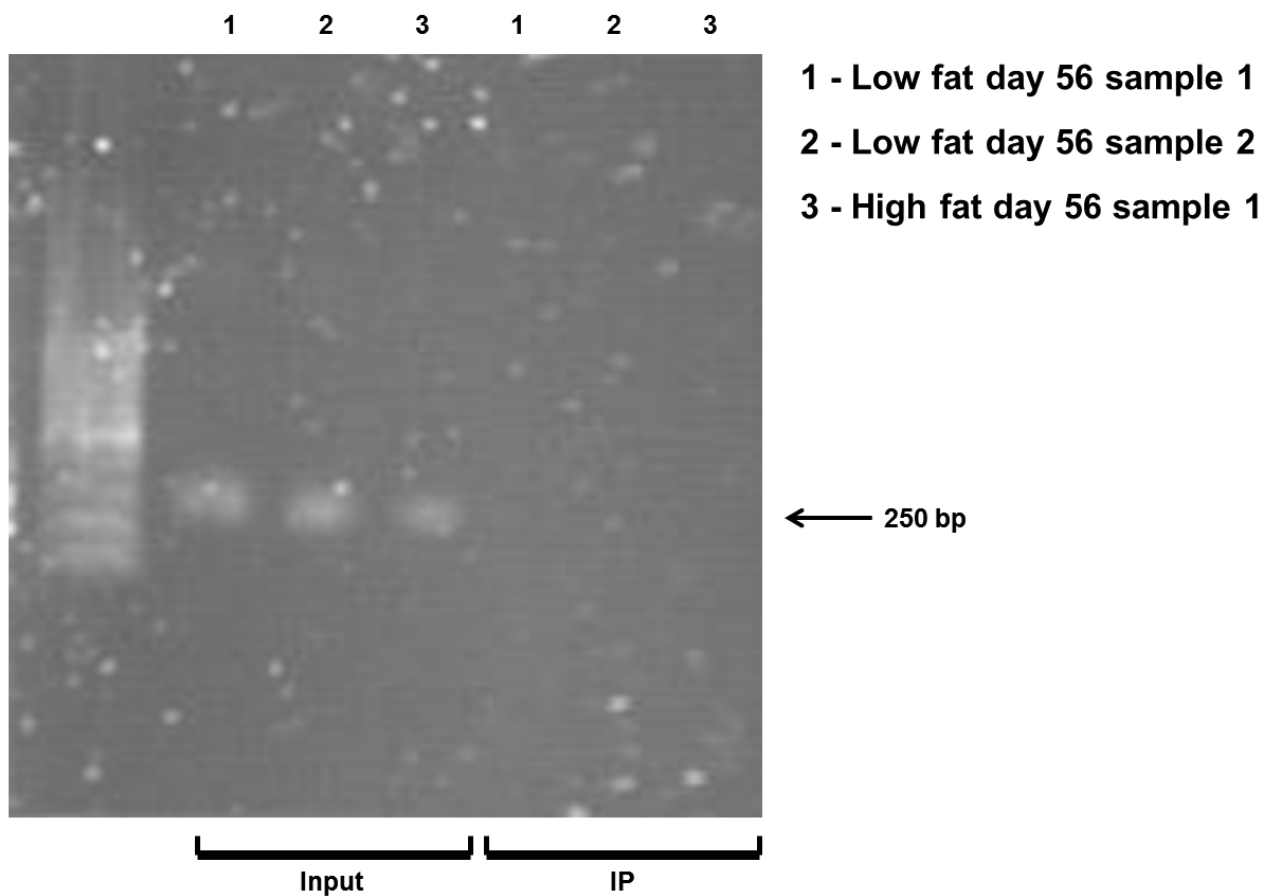


**Figure 22: ACC $\beta$  PCR of isolated DNA with ChIP of USF2 antibody using control primers outside the region of binding**

Compared to the signal primers it was seen that USF2 does bind to ACC $\beta$  in the region we expected (Figure 23). This region coincided with the region shown in our luciferase deletion constructs that was shown to be regulated by USF2 and GFAT (shown in figures 11 and 12). There was more DNA expression seen in high fat day 56 samples compared to low fat. Although, the amount of protein used between samples was normalised for protein concentration, until we perform RTPCR, this difference is relative. It is however reflected consistently in our ChIP analysis (Figure 23).

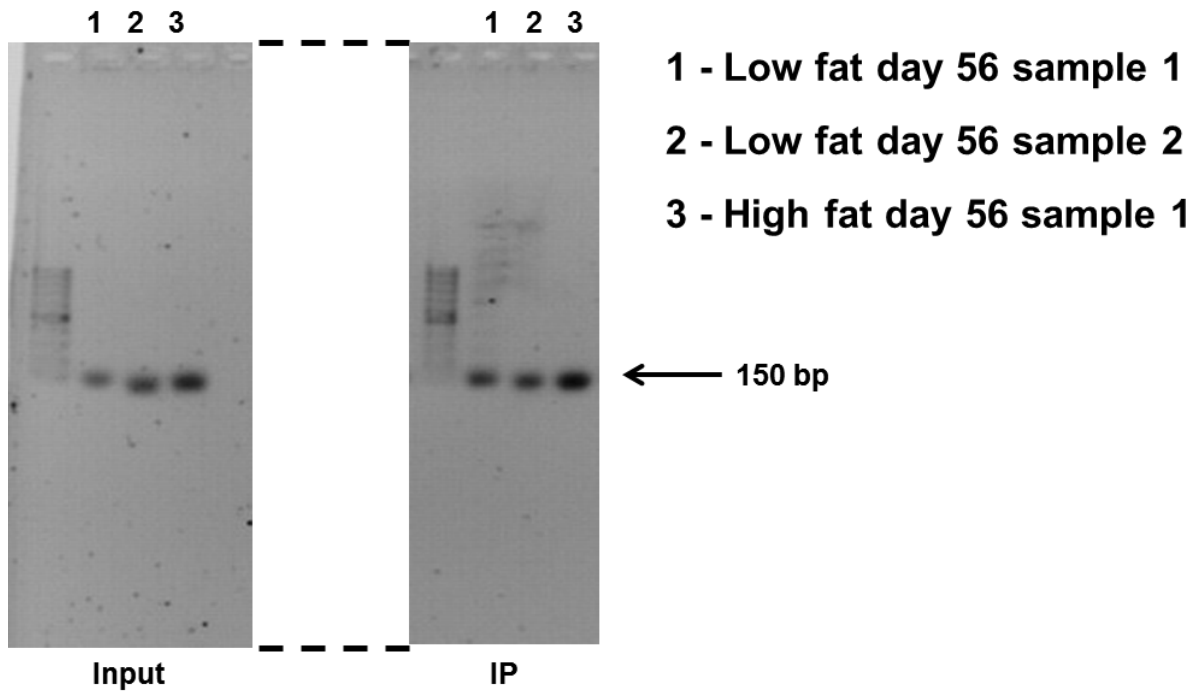


**Figure 23: ACC $\beta$  PCR of isolated DNA with CHIP of USF2 antibody using signal primers in the region of binding**

### **3.3.4. Measuring USF2 O-GlcNAcylation with Immunoprecipitation and Western blotting**

To determine if USF2 is regulated directly by O-GlcNAcylation of the hexosamine biosynthetic pathway or indirectly via another factor we immunoprecipitated USF2 and O-GlcNAc separately from high fat and low fat cardiac Wistar rat tissue. A Western blot was then performed for the opposing target, namely O-GlcNAc for USF2 IP and USF2 for O-GlcNAc IP. It was discovered that USF2 was present in the USF 2 blot but not in the O-GlcNAc IP and conversely O-GlcNAc was present in the O-GlcNAc blot but not in the USF2 IP. This would suggest that USf2 is not O-GlcNac modified in these samples (Figure 24). The significance of this was that USF2 is upregulating

ACC $\beta$  in response to hexosamine biosynthetic flux but not by O-GlcNAc modification of USF2.

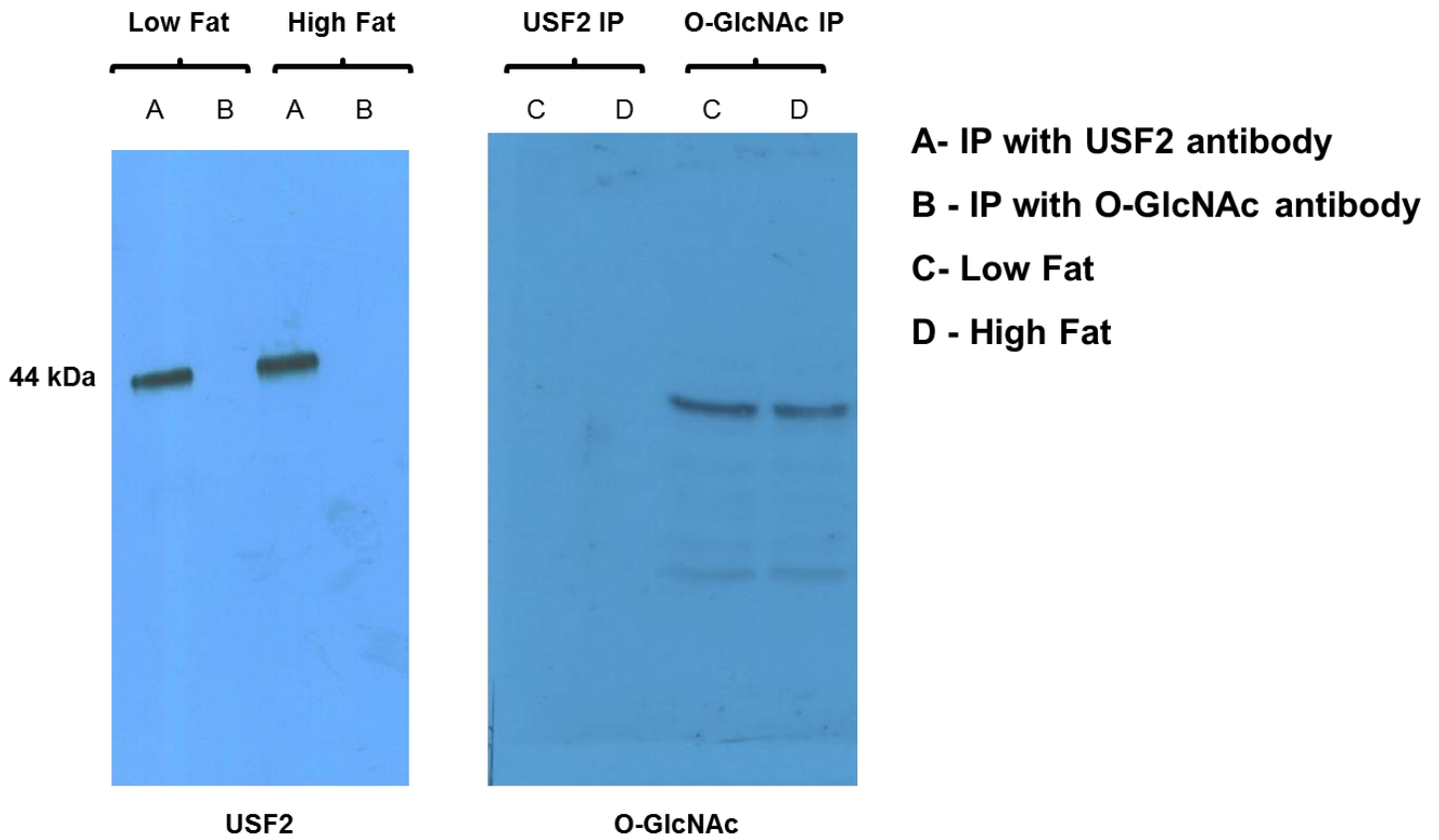


Figure 24: USF2 O-GlcNAcylation with Immunoprecipitation and Western blotting for USF2 and O-GlcNAc separately

### 3.3.5. Fatty acid measurements

Next we investigated downstream effects of the fatty acid diet on our animal model. Here we isolated total fats from the heart tissue at various time points and then measured different amounts of each fat and its carbon forms. We first analysed the totals of each fat in the samples. There was a 40% reduction in phosphatidylcholine fatty acids in the low fat diet rats versus the high fat diet ( $p < 0.05$ ) but no differences were seen in the rest of the time points (Figure 25).

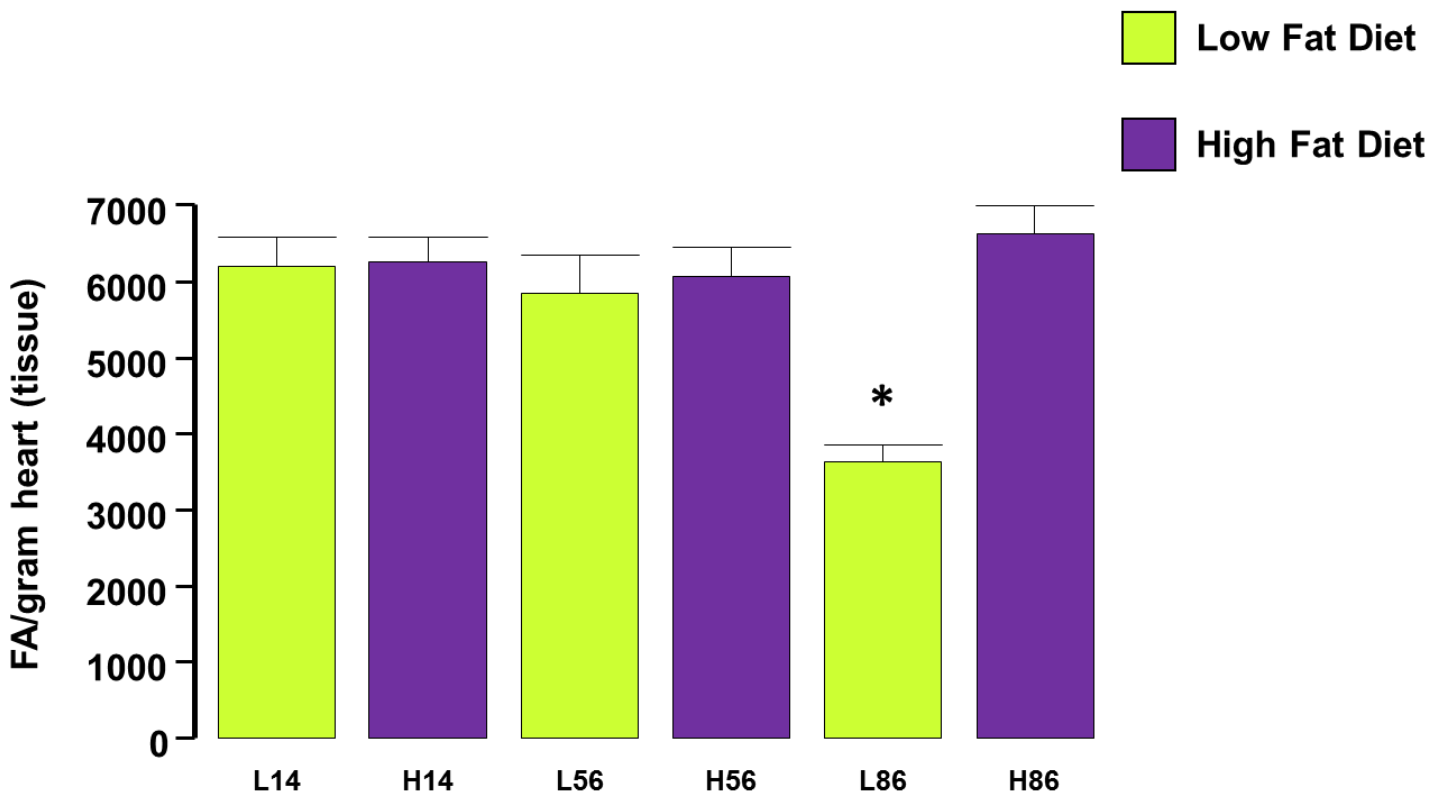


Figure 25: Total Phosphatidylcholine (PC) Fatty Acids ( $\mu\text{g}$  FA per g heart tissue)  
\* $p < 0.05$  vs All [n=6]

Interestingly, no significant differences were seen in the measurements of total phosphatidylethanolamine fatty acids in any of the samples (Figure 26).

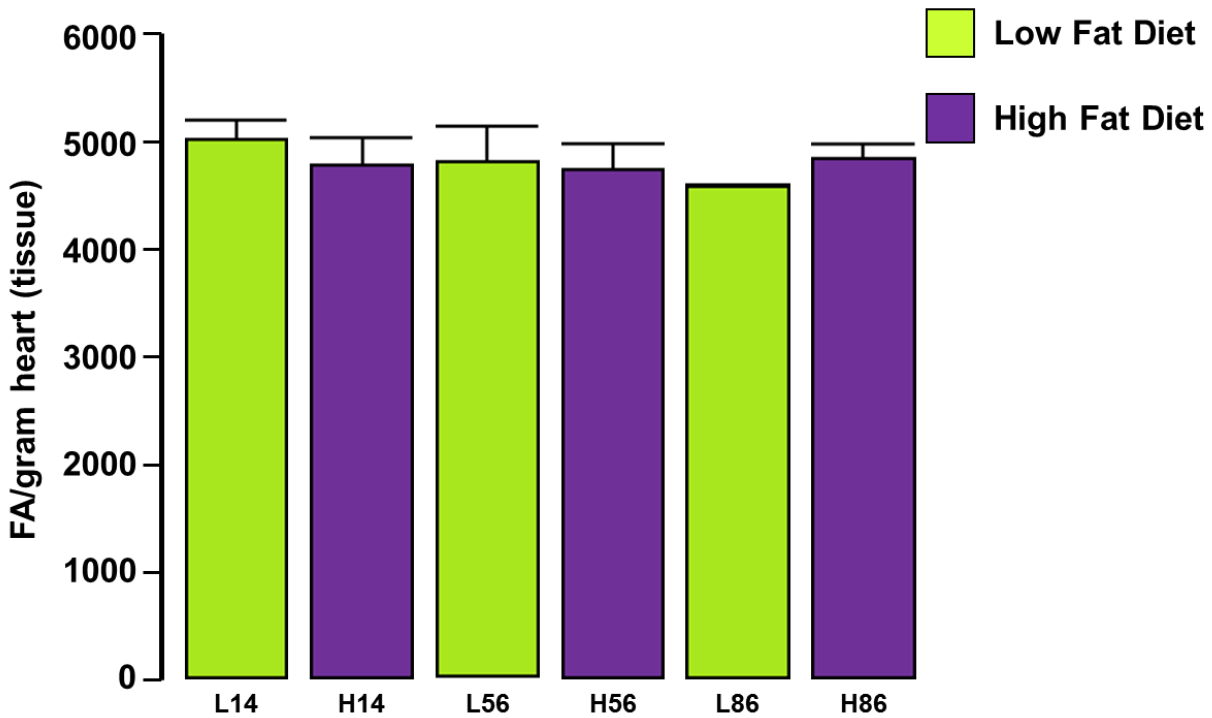


Figure 26: Total Phosphatidylethanolamine (PE) Fatty Acids ( $\mu\text{g}$  FA per g heart tissue) [n=6]

There was a large trend for phospholipid levels to be higher than controls in the day 86 high fat diet group but this was not found to be statistically significant due to lack of numbers in the low fat day 86 group (figure 27).

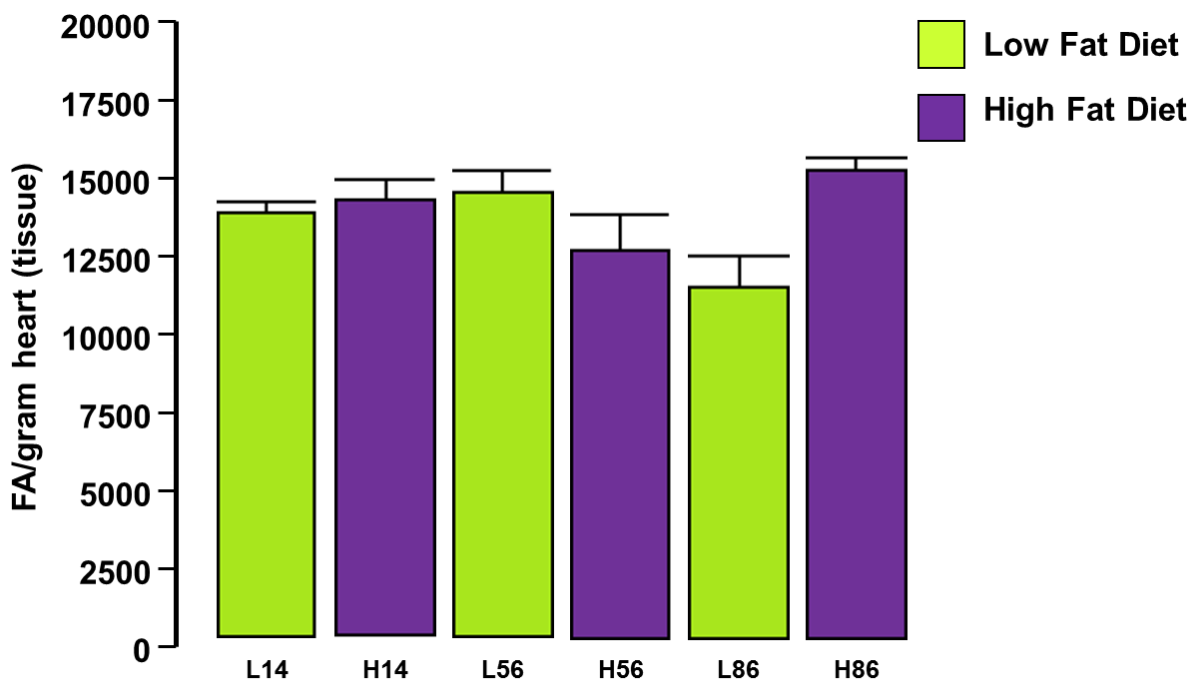


Figure 27: Total Phospholipid Fatty Acids ( $\mu\text{g}$  FA per g heart tissue) [n=6]

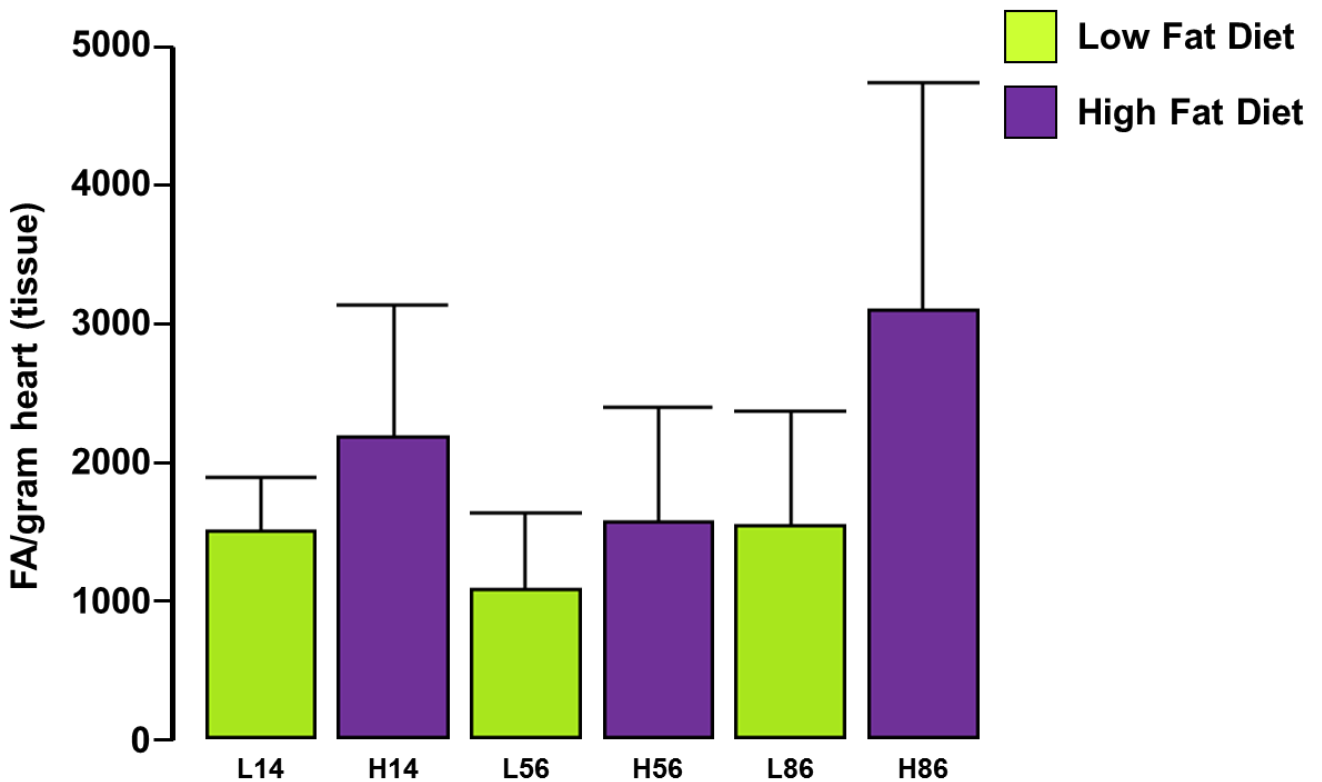
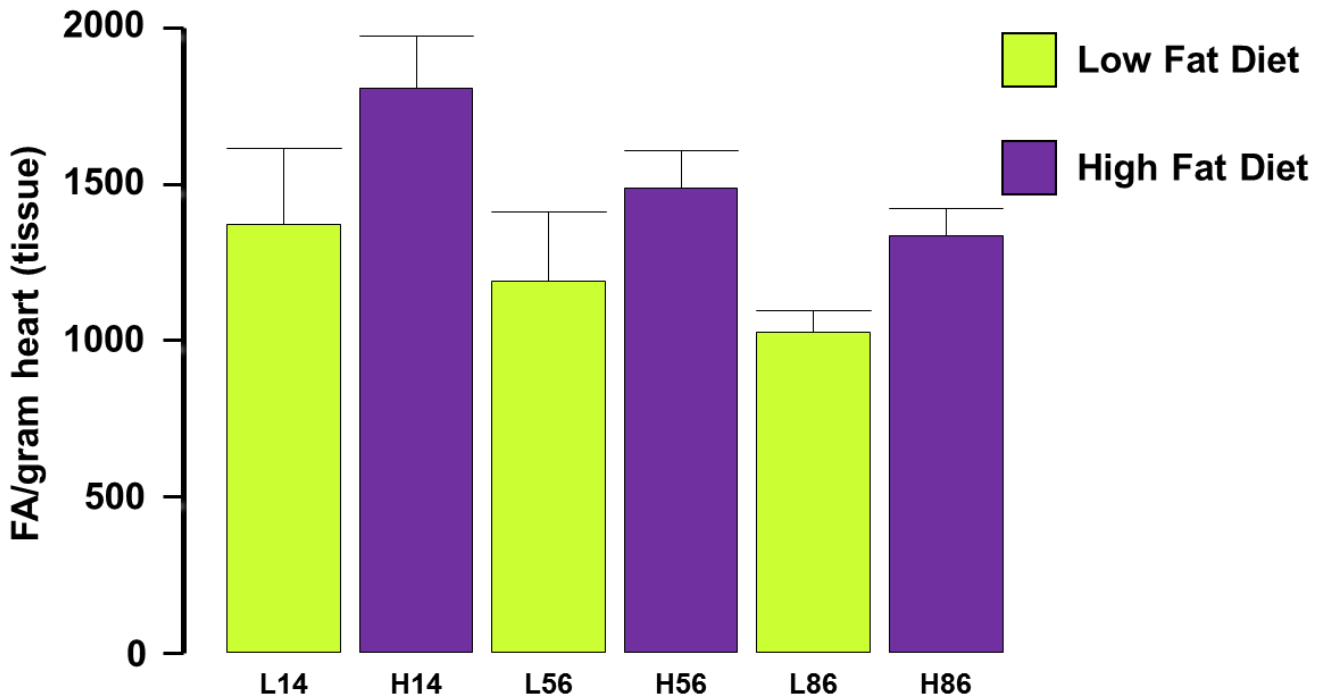


Figure 28: Total Triacylglycerol Fatty Acids ( $\mu\text{g}$  FA per g heart tissue) [n=6]

Fatty acid measurements of triacylglycerol were found to be higher in the high fat diet group than in the low fat diet group. This was seen on all the time points (Figure 28). Finally, we measured the levels of free fatty acids in the heart tissue samples. The level of free fatty acids was found to be higher in the high fat diet groups versus their controls in each time point (Figure 29). Results showed a trend towards higher fat content in the high fat hearts versus the low fat but not statistically significantly higher.



**Figure 29: Total Free Fatty Acids ( $\mu\text{g}$  FA per g heart tissue)**  
[n=6]

Fatty acid data also revealed results on the various carbon forms of each fatty acid. This data was reorganised into groups of the sum of all the saturated fatty acids (SFA – those with no double bond; x:0), sum of all monounsaturated FAs (MUFA – those with only one double bond; x:1), sum of all polyunsaturated FAs (PUFA – those with two and more double bonds; x:2), total n-6 fatty acids (Tn-6; sum of all the n-6 FAs) and total n-3 fatty acids (Tn-3; sum of all the n-3 FAs) (Table 2). This was first performed for each fatty acid and then to simplify we combined all this data into one table with just these individual groups of sums as shown in (Table 3).

**Table 2: Quantitative fatty acid composition:  $\mu\text{g}$  FA/gram heart (tissue)****Total Phospholipid Fatty Acids ( $\mu\text{g}$  FA/g heart tissue)**

Day	saturated FA	monounsaturated FA	polyunsaturated FA	total n-3 FAs	total n-6 FAs
	X:0	X:1	X: 2 or more	n-3	n-6
L14	4750.24	1143.19	7714.20	1736.43	5977.77
H14	4689.38	1253.51	8031.80	2192.04	5839.76
L56	4822.24	1223.06	8204.02	1709.55	6494.48
H56	4194.11	1150.94	7101.84	1965.10	5136.73
L86	3874.96	1060.46	6320.05	1289.38	5030.67
H86	4733.58	1270.41	8991.39	2497.38	6494.01

**Free Fatty Acids ( $\mu\text{g}$  FA/g heart tissue)**

Day	saturated FA	monounsaturated FA	polyunsaturated FA	total n-3 FAs	total n-6 FAs
	X:0	X:1	X: 2 or more	n-3	n-6
L14	534.49	325.18	447.18	69.94	377.24
H14	654.88	421.24	644.42	122.32	522.10
L56	463.77	263.57	405.49	59.59	345.89
H56	565.32	327.75	525.79	91.01	434.78
L86	367.42	248.73	360.76	56.32	304.44
H86	466.95	342.45	460.06	89.85	370.20

**Triacylglycerol Fatty Acids ( $\mu\text{g}$  FA/g heart tissue)**

Day	saturated FA	monounsaturated FA	polyunsaturated FA	total n-3 FAs	total n-6 FAs
	X:0	X:1	X: 2 or more	n-3	n-6
L14	664.81	511.02	309.51	27.98	281.53
H14	801.35	878.64	485.54	43.88	441.66
L56	421.75	397.83	241.70	15.23	226.47
H56	606.07	566.93	376.80	29.57	347.24
L86	545.34	636.34	341.01	31.86	309.16
H86	1031.14	1291.35	759.06	63.74	695.32

**Phosphatidylcholine (PC) Fatty Acids ( $\mu\text{g}$  FA/g heart tissue)**

Day	saturated FA	monounsaturated FA	polyunsaturated FA	total n-3 FAs	total n-6 FAs
	X:0	X:1	X: 2 or more	n-3	n-6
L14	2683.40	631.39	2904.60	393.27	2511.33
H14	2635.72	630.62	3020.56	538.38	2482.18
L56	2514.51	644.80	2711.88	311.21	2400.67
H56	2513.55	610.97	2961.17	569.44	2391.73
L86	1776.61	543.28	1333.21	143.98	1189.24
H86	2734.04	704.31	3208.62	582.54	2626.07

**Phosphatidylethanolamine (PE) Fatty Acids ( $\mu\text{g}$  FA/g heart tissue)**

Day	saturated FA	monounsaturated FA	polyunsaturated FA	total n-3 FAs	total n-6 FAs
	X:0	X:1	X: 2 or more	n-3	n-6
L14	1779.28	357.70	2881.22	1149.32	1731.90
H14	1505.73	364.10	2904.88	1353.53	1551.35
L56	1599.34	341.01	2840.30	1169.90	1670.40
H56	1616.95	356.64	2756.84	1383.24	1373.60
L86	1486.88	349.13	2742.05	1142.17	1599.88
H86	1528.68	399.55	2908.51	1499.47	1409.03

**Table 3: Total sum of each carbon form of fatty acids for each time point of high fat vs low fat diet (measured FA/gram heart tissue)**

Day	Sum of saturated FA X:0	Sum of monounsaturated FA X:1	Sum of polyunsaturated FA X:2 or more	total n-3 FAs n-3	total n-6 FAs n-6
L14	10412.22	2968.48	14256.70	3376.93	10879.77
H14	10287.07	3548.12	15087.20	4250.15	10837.05
L56	9821.61	2870.27	14403.38	3265.48	11137.90
H56	9496.00	3013.23	13722.44	4038.36	9684.08
L86	8051.21	2837.95	11097.09	2663.71	8433.38
H86	10494.39	4008.08	16327.63	4732.99	11594.64

The data from table 3 is represented in figure 30 and it can be seen how the levels of these different carbon forms changes over time with treatment of a high fat diet versus a low fat diet (Figure 30).

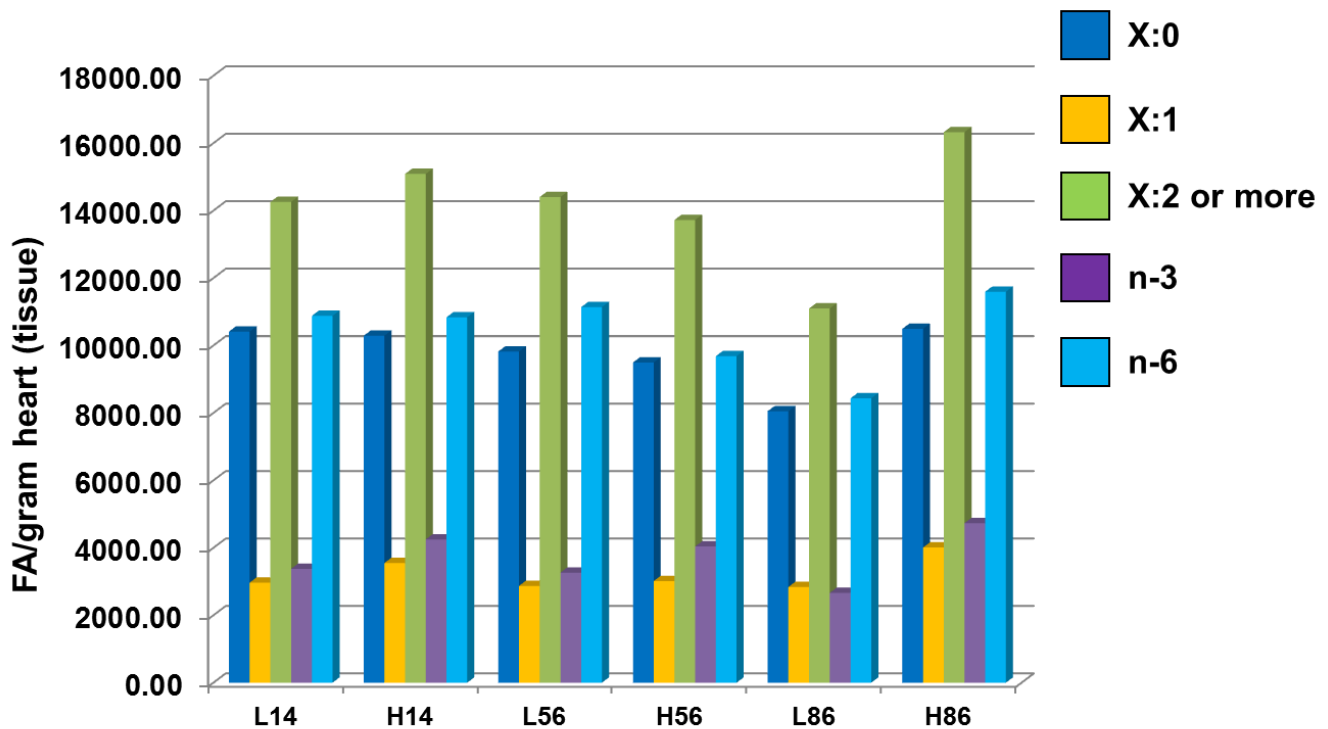


Figure 30: Total quantitative sum of fatty acid composition per µg of FA/gram heart (tissue) represented in different fatty acid subtypes [n=6]

Results show that the total level of saturated fats (X:0), polyunsaturated fats (X:2 or more) and total n-6 fatty acids (n-6) is lower in the day 86 low fat group but doesn't change in the other groups. In contrast the level of monounsaturated fats and n-3 fatty acids is consistently higher in the high fat diet versus controls (figure 26). The results from fatty acid gives a lot of insight into the outcome influences of high fat diets on fatty acid accumulation in heart tissue and together with RNA results links ACC $\beta$  levels with HOMA index values to strengthen our hypothesis that with high glucose there is an increase in flux through HBP and increase in O-GlcNAc modification of target proteins which results in ACC $\beta$  upregulation via USF2. This in turn results in a decrease in free fatty acid uptake and its accumulation in the cytosol of cells in the heart.

# **Chapter 4**

# **Discussion**

## 4.1. Discussion

In my previous study I showed that increased flux through the hexosamine biosynthetic pathway (HBP) induces cardiac ACC $\beta$  gene expression. At the end of that study we had made a novel finding that not only did HBP flux regulate ACC $\beta$  promoter activity, but that this flux was linked by a transcription factor named USF2. In this study we found that:

1. GFAT overexpression increased ACC $\beta$  promoter activity by ~75% in cardiac myoblasts. This would suggest that increased HBP flux results in O-GlcNAc modification of transcriptional targets thereby inducing ACC $\beta$  promoter activity.
2. ACC $\beta$  gene promoter activity was induced in a dose-responsive manner to increasing glutamine concentrations (glutamine being an HBP substrate). As noted when we were performing that study we had to be very specific with our growing conditions because a change in L-glutamine concentrations can influence results.
3. The regulation of ACC $\beta$  HBP-mediated promoter activity can be manipulated with the use of two dominant negative constructs (competitive inhibitors of GFAT which attenuate GFAT-mediated ACC $\beta$  promoter induction and two specific pharmaceutical inhibitors of GFAT, i.e. azaserine and 6-Diazo-5-oxo-L-norleucine, which attenuated GFAT-induced upregulation of ACC $\beta$ ).

Increased flux through the hexosamine biosynthetic pathway has been linked to an increase in glucose and glucosamine availability. An increase in HBP flux results in higher UDP-GlcNAc production and an increase in O-GlcNAc modification of a large

number of proteins and transcription factors. Researchers have continued to find more factors that are modified by this pathway. O-GlcNAc has been shown to operate in opposition to phosphorylation, glycosylating proteins that are dephosphorylated and *vice versa*. Studies have proposed that the hexosamine biosynthetic pathway functions as a cellular nutrient sensor and numerous papers have showed a correlation between increased flux through the HBP and insulin resistance. For example, Marshall et al. (1991) first proposed a role for glucose flux via the HBP in insulin resistance from a series of experiments performed in isolated rat adipocytes (78). Other studies found a correlation between the HBP and insulin resistance in rodents treated with glucose/glucosamine. Recently, increased O-GlcNAc modification has been attributed to altered glucose uptake resulting in insulin resistance. A study investigating overexpression of OGT in adipose and muscle of mice resulting in increased O-GlcNAcation showed insulin resistance and hyperleptinaemia. These studies would suggest that increased HBP flux and increased O-GlcNAcation can impact on fatty acid and glucose pathways.

In this study our aim was to investigate this mechanism and prove that this novel regulatory pathway plays a role in the development of insulin resistance in a high caloric western lifestyle. Having already established that upstream stimulatory factors (USF's) are involved in this mechanism we set up a transfection experiment to measure ACC $\beta$  response to USF1 and USF2 overexpression and found there to be a large response to USF2 but USF1 had no effect. Upstream stimulatory factors have been shown to upregulate the ACC $\beta$  gene promoter (77). However, this result was not strengthened when co-transfected with an overexpression vector of GFAT. This could be because of a threshold level of ACC $\beta$  response or the result of a lack of another

binding factor which dimerizes or binds to USF2 in a complex (Figure 5). Overexpressing USF2 would therefore have a limited response in binding due to lack of this other factor. Other studies have shown that USF's do dimerize in their mode of action (59).

To confirm that USF2 would respond to HBP flux we co-transfected a GFAT overexpressing vector with a USF luciferase reporter construct (USF-L = Upstream Stimulatory Factor TransLucent™ Reporter Vector) that contains multiple promoter binding sites for USFs. Results confirmed USF2 to be responsive to HBP flux (Figure 6). A similar result was seen by Erwin D. Schleicher et al. in 2004 where increasing O-GlcNAc modification of proteins with streptozotocin treatment, thereby increasing HBP flux, resulted in an increased mRNA and nuclear protein levels of USF-2 (127).

Flow cytometry confirmed this result by showing a strong correlation between HBP flux, O-GlcNAc modification, and USF2 expression. This was seen with modifications in L-glutamine substrate concentration and in GFAT expression with the use of a dominant negative inhibitor.

Our next focus was to find the binding site for our regulation of the ACC $\beta$  promoter. Co-transfection of the GFAT overexpression vector with truncated ACC $\beta$  promoter constructs revealed a region of interest where the ACC $\beta$  promoter was regulated by this pathway. To strengthen our hypothesis of USF2 as the transcription factor that mediates this regulation a USF2 overexpression vector was co-transfected with these same truncated ACC $\beta$  promoter constructs and it was shown that the same region of interest was being regulated by USF2.

Our focus turned further downstream of this interaction to investigate the effects of modified ACC $\beta$  activity and HBP flux on fatty acid uptake and regulation in the mitochondria in the heart. It has also been shown that an increase in O-GlcNAcation is linked to insulin resistance (5, 14, 42, 83, 92, 123). To investigate this we acquired heart tissue from an animal model of male Wistar rats fed a high fat and high glucose diet with added low fat diet controls and sacrificed at weekly time points. Day 28 rats immediately eliminated from the study as the puberty stage of a rat's growth stage would provide unreliable data. Animals stressed at the time of sacrificed would also be eliminated as we found the insulin and glucose levels to be different from non-stressed animals of the same group. Glucose and insulin measurements taken at the time of sacrifice showed the rats to be insulin resistant at day 86.

The advantage of this animal model is that we can investigate the development of metabolic syndrome. Our hypothesis asked a question as to when this effect of high glucose regulation of fatty acid pathways begin and when does it stop. Our initial assumptions were that in the event of insulin resistance glucose uptake would decrease thus a loss of HBP flux would result. This would mean that ACC $\beta$  activity would decrease unless intervened by another pathway. When we measured ACC $\beta$  mRNA levels with RT-PCR we found that at day 56 ACC $\beta$  activity was significantly higher in the high fat diet group but not in the low fat diet. At day 86 ACC $\beta$  activity the level was maintained but not significantly higher than its control. Since we don't have a time point after insulin resistance its' hard to know whether the effect was for ACC $\beta$  activity to decrease gain or maintain its level. The data from this result does however

highlight a significant correlation of time point where ACC $\beta$  activity increases at the same time where we would expect the high fat diet rats to be in metabolic syndrome.

Using RT-PCR we also investigated our previous result with luciferase assays which showed that USF2, and not USF1 is involved in the regulation of ACC $\beta$  activity by the hexosamine biosynthetic pathway. Results from this experiment supported previous results showing an increase in ACC $\beta$  activity in response to USF2 expression in the presence of GFAT and that this effect could be reduced with the addition of an inhibitor of GFAT (6-diazo-5-oxo-l-norleucine).

The next step was to prove that USF2 was binding to the ACC $\beta$  promoter. Deletion construct luciferase assay experiments showed a region close to the start codon of the ACC $\beta$  promoter where activity was lost in response to both GFAT overexpression and USF2 expression. Chromatin immunoprecipitation USF2 from high fat and low fat diet fed Wistar rat heart muscle revealed that USF2 binds to the ACC $\beta$  promoter. We investigated an hypothesis that USF2 was modified by O-GlcNAc before binding to the ACC $\beta$  promoter using flow cytometry. When experiments were performed for the flow cytometry the data was combined and measured together. Technically it can be seen as a n=1 or it can be seen as a measurement of 10000 cells. We are aware that more experiments need to be performed with this section. We were trying to find a link between O-GlcNAcylation and were under the assumption that USF2 was O-GlcNAcylated. Later the CHIP western blots proved this theory incorrect so it wasn't found to be viable to further explore this avenue. We proved that O-GlcNAc modification and USF2 expression is increased in the same cell but this can be shown in western blotting just as easily. Since USF2 isn't the protein modified there was no

need to explore this in flow cytometry. Further analysis with Western blotting showed that, although USF2 regulates ACC $\beta$  promoter activity by the hexosamine biosynthetic pathway, USF2 itself is not O-GlcNAc modified. This would indicate that there is another factor involved in the regulation of ACC $\beta$  and USF2 that is modified by HBP. Other studies have shown that USF2 is upregulated by high glucose, glycated albumin and NF- $\kappa$ B (131). Many studies have shown increased expression of USF2 by O-GlcNAc modification but none have yet focused on USF2 modification so we are unable to compare this result with other studies.

Our next step was to investigate further downstream and see whether the increase in ACC $\beta$  activity would reduce fatty acid uptake via the inhibition of CPT1 by malonyl-CoA (67, 70, 91, 102, 114, 135). Our experiments focused more on the time point's day 14, 56 and 86, i.e. time points before and after day 56 where we saw the increase in ACC $\beta$  activity. We obtained data for total fat content of saturated fatty acids, unsaturated fatty acids and phospholipids as percentage of fat and as percentage fat per gram of heart tissue, but we decided to focus more on mass of fatty acids gram of heart tissue which would make the data more normalised and comparable to each other. Phospholipid and triacylglycerol levels were generally higher in the high fat diet group indicating their uptake was skewed from being broken down by the mitochondrion. However at day 56 phospholipids were slightly lower in the high fat diet group than the low fat diet but not significantly. No differences were seen in the total phosphatidylethanolamine of these samples. The level of phosphatidylethanolamine remained level with time. This would be expected since both phospholipids and phosphatidylethanolamine fatty acids are involved in membrane structures. An interesting finding was in our low fat diet group at day 86 phosphatidylcholine levels

were at their lowest. We did have rather lower numbers of hearts compared to the other groups in the day 86 low fat group but the result is still significant. This is especially significant since this fatty acid is required for the formation of membranes too and because recent studies point to the many potential benefits of phosphatidylcholine for liver repair and found to prevent hepatocyte dystrophy and necrosis development, activate macrophage response and stimulate reparation inducing synthesis and secretion of the tumor necrosis factor.

Our data also showed a trend towards an increase in free fatty acids which is what we expected to find since in our hypothesis ACC $\beta$  activity increases malonyl-CoA production which would reduce fatty acid uptake via CPT1 into the mitochondria. This however was not significant in some groups of fatty acids. This was unexpected given the rats were fed a high fat high glucose diet. When we look at the different carbon forms of fatty acids it was the small fatty acids of n-3 and monounsaturated fats that were higher in the high fat diet groups compared to controls while the larger bulkier fatty acids showed little change. We would have expected there to have been a great increase of total fatty acids in the heart tissue given the increase in the various carbon forms but we only get a trend when we combine all the fatty acids together.

## 4.2 Conclusion

Our data reveal a novel finding, i.e. that increased flux through the hexosamine biosynthetic pathway activates USF2 and increases its expression allowing it to bind between -38/+65 and 18/+65 of the ACC $\beta$  promoter and activate it in cardiac-derived myoblasts. This increases ACC $\beta$  promoter activity seen in cardiac-derived myoblasts and mRNA levels seen in heart tissue. This effect can be seen to occur at day 56 in heart tissue during metabolic syndrome and results in insulin resistance at day 86 of male Wistar rats. We have shown that USF2 binds to the ACC $\beta$  promoter and activates it in response to the hexosamine biosynthetic pathway in a high fat and high glucose diet. This is, however, in response to another unknown regulator of USF2 which is O-GlcNAc modified or a protein which helps for a complex which regulates ACC $\beta$  as a whole. With an increase in ACC $\beta$  there is an increase in malonyl-CoA and an increase in free fatty acids due to a reduction of fatty acid uptake into the mitochondrion. This leads to intracellular lipid accumulation due to a mismatch between sarcolemmal FA uptake and mitochondrial FA oxidation. Our data shows that fatty acids are higher in the high fat diet individuals during metabolic syndrome (day 56). Subsequently, we propose that intramyocardial lipid accumulation triggers signaling pathways resulting in cell death, insulin resistance and contractile dysfunction (Figure 31).

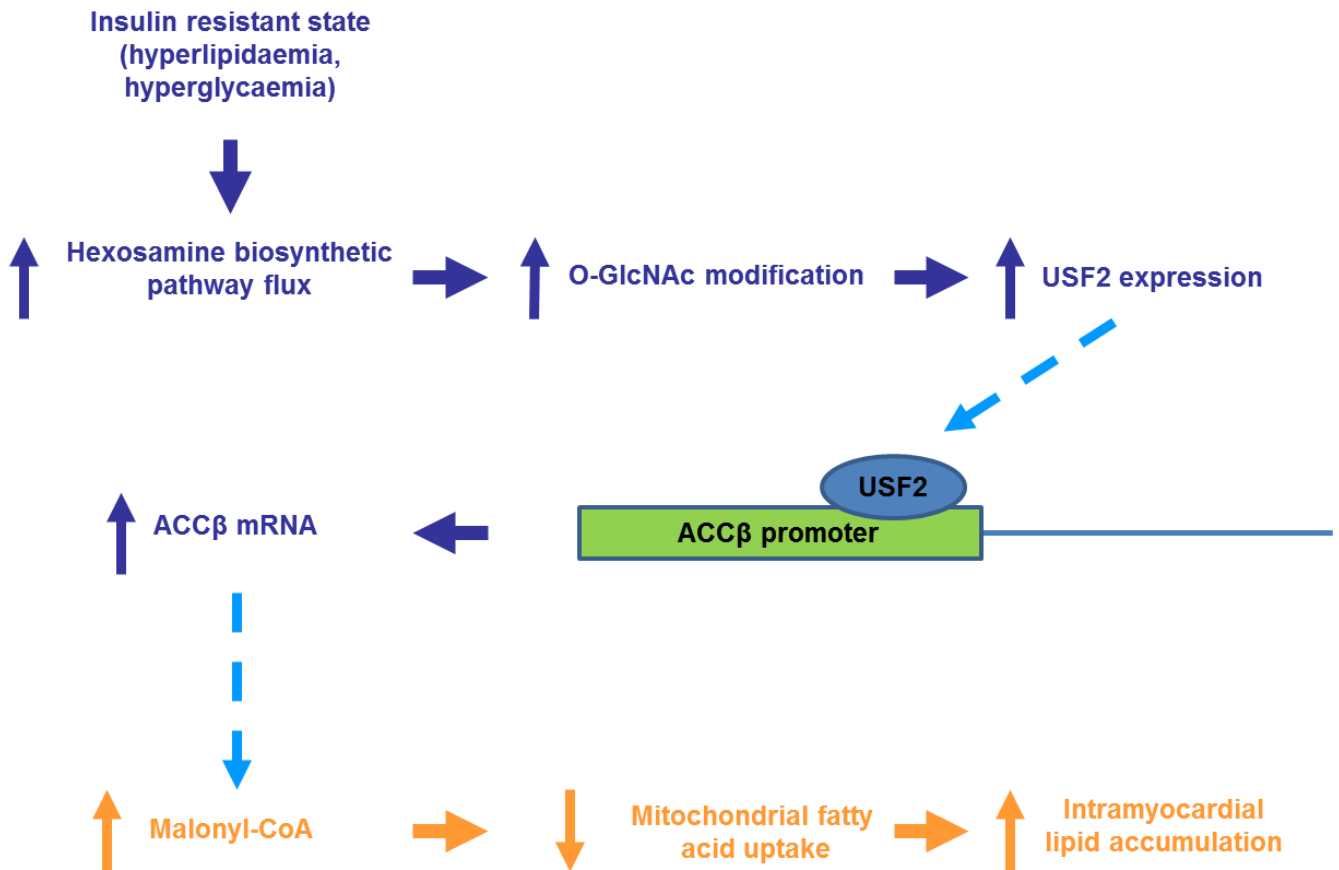


**Figure 31: Schematic diagram of hypothesis and findings.**

Data from this study can be useful in the development of drug targets in the treatment of diabetes during metabolic syndrome before insulin resistance. This novel finding also provides us with a possible target for identifying metabolic syndrome early in individuals. The main weakness to treatment of diabetes is once a patient is insulin resistant it is very difficult or impossible to rectify. It would be so much easier to treat a patient before they became insulin resistant but identifying this stage can be a challenge. We have proposed the increase flux of hexosamine pathway to be a major stepping stone during metabolic syndrome and if we can use it as a diagnostic tool to identify this stage treatment can begin before insulin resistance. It is not practical to isolate heart tissue from patients to perform this diagnosis. With this in mind, our next

focus will be to move this knowledge to skeletal muscle where insulin resistance first takes place and discover if this is present.

### **4.3. Limitations of this study**

Despite a lot of data and techniques employed there is a large amount of work that still needs to be done. Being a novel hypothesis with the hexosamine biosynthetic pathway, this study has few studies with which to compare itself. Some experiments need to be repeated a few times to ensure a higher statistical value. RT-PCR of ACC $\beta$  on cell samples would have been better over just USF2 mRNA measurements. These are being measured currently but did not make it into this thesis. Pharmaceutical inhibitors are becoming less and less reliable as more studies are published. We tried to add as much variability in our experiments to support our hypothesis but relying on dominant negative inhibitors, substrates such as glucosamine and the use of deletion constructs. This study could have used something more potent such as silencing RNA for cell work and the inclusion of oxygraphs to measure fatty acid oxidation and growing cells in a high fat and high glucose environment. Unfortunately measuring fatty acid oxidation in frozen heart tissue isn't a viable option so we couldn't measure fatty acid oxidation in tissue. A good knock out animal model of GFAT could have given us more options as well but they are very expensive to breed and there is currently only one group in the world that has one.

#### 4.4. References

1. **Abu-Elheiga L, Almarza-Ortega DB., Baldini A., and Wakil SJ.** Human acetyl-CoA carboxylase 2. Molecular cloning, characterization, chromosomal mapping, and evidence for two isoforms. *J Biol Chem* 272: 10669-10677, 1997.
2. **Abu-Elheiga L, Brinkley WR., Zhong L., Chirala SS., Woldegiorgis G., and Wakil SJ.** The subcellular localization of acetyl-CoA carboxylase2. *Proc Natl Acad Sci U S A* 97: 1444-1449, 2000.
3. **Abu-Elheiga L, Jayakumar A., Baldini A., Chirala SS., and Wakil SJ.** Human acetyl-CoA carboxylase: characterization, molecular cloning, and evidence for two isoforms. *Proc Natl Acad Sci U S A* 92: 4011-4015, 1995.
4. **Ali A, and Crowther NJ.** Body fat distribution and insulin resistance. *S Afr Med J* 95: 878-880, 2005.
5. **Arias E, Kim J., and Cartee, GD.** Prolonged incubation in PUGNAc results in increased protein O-linked glycosylation and insulin resistance in rat skeletal muscle. *Diabetes* 53: 921-930, 2004.

6. **Baron A, Zhu JS., Weldon J., Maianu L., and Garvey WT.** Glucosamine induces insulin resistance in vivo by affecting GLUT 4 translocation in skeletal muscle- Implications for glucose toxicity. *J Clin Invest* 96: 2792-2801, 1995.
7. **Bian F, Kasumov T., Jobbins KA., Minkler PE., Anderson VE., Kerner J., Hoppel CL., and Brunengraber H.** Competition between acetate and oleate for the formation of malonyl-CoA and mitochondrial acetyl-CoA in the perfused rat heart. *J Mol Cell Cardiol* 41: 868-875, 2006.
8. **Brinkmann J, Abumrad NA., Ibrahimi A., van der Vusse GJ., and Glatz JF.** New insights into long-chain fatty acid uptake by heart muscle: a crucial role for fatty acid translocase/CD36. *Biochem J* 367: 561-570, 2002.
9. **Brooks G.** Intra- and extra-cellular lactate shuttles. *Med Sci Sports Exerc* 32: 790-799, 2000.
10. **Brownlee M.** Biochemistry and molecular cell biology of diabetic complications. *Nature* 414: 813-820, 2001.
11. **Brownlee M.** The pathobiology of diabetic complications: a unifying mechanism. *Diabetes* 54: 1615-1625, 2005.

12. **Buse M.** Hexosamines, insulin resistance and the complications of diabetes: current status. *Am J Physiol Endocrinol Metab* 290: E1-E8, 2006.
13. **Buse M, Robinson KA., Gettys TW., McMahon EG., and Gluve EA.** Increased activity of the hexosamine synthesis pathway in muscles of insulin-resistant ob/ob mice. *Am J Physiol Endocrinol Metab* 272: E1080-E1088, 1997.
14. **Buse M, Robinson KA., Marshall BA., Hresko RC., and Mueckler MM.** Enhanced O-GlcNAc protein modification is associated with insulin resistance in GLUT1- overexpressing muscles. *Am J Physiol Endocrinol Metab* 283: E241-E250, 2002.
15. **Carley A, and Severson, DL.** Fatty acid metabolism is enhanced in type 2 diabetic hearts. *Biochim Biophys Acta* 1734: 112-126, 2005.
16. **Cavaghan M, Ehrmann DA., and Polonsky KS.** Interactions between insulin resistance and insulin secretion in the development of glucose intolerance. *J Clin Invest* 106: 329-333, 2000.
17. **Champattanachai V, Marchase RB., and Chatham J.** Glucosamine protects neonatal cardiomyocytes from ischemia-reperfusion injury via increases protein-associated O-GlcNAc. *Am J Physiol Cell Physiol* 292: C178-C187, 2006.

18. **Chen H, Ing BL., Robinson KA., Feagin AC., Buse MG., and Quon MJ.** Effects of overexpression of glutamine:fructose-6-phosphate amidotransferase (GFAT) and glucosamine treatment on translocation of GLUT 4 in rat adipose cells. *Mol Cell Endocrinol* 1997: 67-77, 1997.
19. **Chien K.** Alchemy and the New Age of Cardiac Muscle Cell Biology. *PLoS Biol* 3: e131, 2005.
20. **Cipollo J, Antoine Awad A., Costello CE., Robbins PW., and Hirschberg CB.** Biosynthesis in vitro of *Caenorhabditis elegans* phosphorylcholine oligosaccharides. *Proc Natl Acad Sci USA* 101: 3404 - 3408, 2004.
21. **Comer F, and Hart GW.** O-GlcNAc and the control of gene expression. *Biochim Biophys Acta* 1473: 161-171, 1999.
22. **Cooksey R, Hebert LF Jr., Zhu JH., Wofford P., Garvey WT., and McClain DA.** Mechanism of hexosamine-induced insulin resistance in transgenic mice overexpressing glutamine:fructose-6-phosphate amidotransferase: decreased glucose transporter GLUT 4 translocation and reversal by treatment with thiazolidinedione. *Endocrinology* 140: 1151-1157, 1999.

23. **Coort S, Bonen A., van der Vusse GJ., Glatz JFF., and Luiken JJFP.** Cardiac substrate uptake and metabolism in obesity and type-2 diabetes: Role of sarcolemmal substrate transporters. *Mol Cell Biol* 29: 5-18, 2007.
24. **Corden J.** Tails of RNA polymerase II. *Trends Biochem Sci* 15: 383-387, 1990.
25. **Crook E, Daniels MC., Smith TM., and McClain DA.** Regulation of insulin-stimulated glycogen synthase activity by overexpression of glutamine:fructose-6-phosphate amidotransferase in rat-1 fibroblasts. *Diabetes* 42: 1289-1296, 1993.
26. **Dahmus M.** Phosphorylation of the C-terminal domain of RNA polymerase II. *Biochim Biophys Acta* 1261: 171-182, 1995.
27. **Dyck J, and Lopaschuk GD.** AMPK alterations in cardiac physiology and pathology: enemy or ally? *J Physiol* 574: 95-112, 2006.
28. **Dyck J, Cheng JF., Stanley WC., Barr R., Chandler MP., Brown S., Wallace D., Arrhenius T., Harmon C., Yang G., Nadzan AM., and Lopaschuk GD.** Malonyl coenzyme a decarboxylase inhibition protects the ischemic heart by inhibiting fatty acid oxidation and stimulating glucose oxidation. *Circ Res* 94: e78-e84, 2004.
29. **Eaton S.** Control of mitochondrial beta-oxidation flux. *Prog Lipid Res* 41: 197-239, 2002.

30. **Essop M, Chan WY., and Taegtmeyer H.** Metabolic gene switching in the murine female heart parallels enhanced mitochondrial respiratory function in response to oxidative stress. *FEBS J* 274: 5278-5284, 2007.
31. **Federici M, Menghini R., Mauriello A., Hribalm ML., Ferelli F., Lauro D., Sbraccia P., Spagnoli LG., Sesti G., and Lauro R.** Insulin-dependent activation of endothelial nitric oxide synthetase is impaired by O-linked glycosylation of signaling proteins in human coronary endothelial cells. *Circ* 106: 466-472, 2002.
32. **Freiberg C, Pohlmann J., Nell PG., Endermann R., Schuhmacher J., Newton B., Otteneder M., Lampe T., Häbich D., and Ziegelbauer K.** Novel Bacterial Acetyl Coenzyme A Carboxylase Inhibitors with Antibiotic Efficacy In Vivo. *Antimicrob Agents Chemother* 50: 2707-2712, 2006.
33. **Garland P, and Randle PJ.** Control of pyruvate dehydrogenase in the perfused rat heart by the intracellular concentration of acetyl-coenzyme A. *Biochem J* 91: 6c, 1964.
34. **Ghisla S.** Beta-oxidation of fatty acids. A century of discovery. *Eur J Biochem* 271: 459-461, 2004.

35. **Gilde A, and Van Bilsen M.,** Peroxisome proliferator-activated receptors (PPAR s): regulators of gene expression in heart and skeletal muscle. *Acta Physiol Scand* 178: 425-434, 2003.
36. **Giordano F.** Oxygen, oxidative stress, hypoxia, and heart failure. *J Clin Invest* 115: 500-508, 2005.
37. **Gladden L.** Lactate metabolism: a new paradigm for the third millenium. *J Physiol* 558: 5-30, 2004.
38. **Grepin C, Dagnino L., Robitaille L., Haberstroh L., Antakly T., and Nemer M. A** Hormone-Encoding Gene Identifies a Pathway for Cardiac but Not Skeletal Muscle Gene Transcription. *Mol Cell Biol* 14: 3115-3129, 1994.
39. **Ha J, Lee JK., Kim KS., Witters LA., and Kim KH.** Cloning of human acetyl-CoA carboxylase-beta and its unique features. *Proc Natl Acad Sci USA* 93: 11466-11470, 1996.
40. **Hamilton J, and Kamp F.** How are free fatty acids transported in membranes? Is it by proteins or by free diffusion through the lipids? *Diabetes* 48: 2255-2269, 1999.
41. **Hammes H, Du X., Edelstein D., Taguchi T., Matsumura T., Ju Q., Lin J., Bierhaus A., Nawroth P., Hannak D., Neumaier M., Bergfeld R., Giardino I., and**

**Brownlee M.** Benfotiamine blocks three major pathways of hyperglycemic damage and prevents experimental diabetic retinopathy. *Nat Med* 9: 294-299, 2003.

42. **Hanover J, Forsythe ME., Henessey PT., Brodigan TM., Love DC., Ashwell G., and Krause M.** A *Caenorhabditis elegans* model of insulin resistance: Altered macronutrient storage and dauer formation in an OGT-1 knockout. *Proc Natl Acad Sci USA* 102: 11266-11271, 2005.

43. **Hanover J, Yu S., Lubas WB., Shin SH., Ragano-Caracciola M., Kochran J., and Love DC.,.** Mitochondrial and nucleocytoplasmic isoforms of O-linked GlcNAc transferase encoded by a single mammalian gene. *Arch Biochem Biophys* 409: 287-297, 2003.

44. **Harada N, Oda Z., Hara Y., Fujinami K., Okawa M., Ohbuchi K., Yonemoto M., Ikeda Y., Ohwaki K., Aragane K., Tamai Y., and Kusunoki J.** Hepatic De Novo Lipogenesis Is Present IN Liver-Specific ACC1-deficient Mice. *Mol Cell Biol* 27: 1881-1888, 2007.

45. **Hart G.** Glycosylation. *Curr Opin Cell Biol* 4: 1-17-1023, 1992.

46. **Hasselbaink D, Glatz JFC., Luiken JJFP., Roemen THM., and van der Vusse GJ.** Ketone bodies disturb fatty acid handling in isolated cardiomyocytes derived from control and diabetic rats. *Biochem J* 371: 753-760, 2003.
47. **Hawkins M, Angelov I., Lui R., Barzilai N., and Rosetti L.** The tissue concentration of UDP-*N*-acetylglucosamine modulates the stimulatory effect of insulin on skeletal muscle glucose uptake. *J Biol Chem* 272: 4889-4895, 1997.
48. **Hawkins M, Barzilai N., Lui R., Hu M., Chen W., and Rosetti L.** Role of the glucosamine pathway in fat-induced insulin resistance. *J Clin Invest* 99: 2173-2182, 1997.
49. **Hawkins. M, Barzilai N., Chen W., Angelov I., Hu M., Cohen P., and Rosetti L.** Increased hexosamine availability similarly impairs the action of insulin and IGF-1 on glucose disposal. *Diabetes* 45: 1734-1743, 1996.
50. **Heart E, Choi WS., and Sung CK.** Glucosamine-induced insulin resistance in 3T3-L1 adipocytes. *Am J Physiol Endocrinol Metab* 278: E103-E112, 2000.
51. **Hebert L, Daniels MC., Zhou JX., Crook ED., Turner RL., Simmons ST., Neidigh JL., Zhu JS., Baron AD., and McClain DA.** Overexpression of

glutamine:fructose-6-phosphate amidotransferase in transgenic mice leads to insulin resistance. *J Clin Invest* 98: 930-936, 1996.

52. Heese-Peck A, Cole RN., Borkhsenius ON., Hart GW., and Raikhel NV. Plant nuclear pore complex proteins are modified by novel oligosaccharides with terminal *N*-acetylglucosamine. *Plant Cell* 7: 1459-1471, 1995.

53. Herman M, and Khan BM. Glucose transport and sensing in the maintenance of glucose homeostasis and metabolic harmony. *J Clin Invest* 116: 1767-1775, 2006.

54. Hopkins T, Dyck JR., and Lopaschuk GD. AMP-activated protein kinase regulation of fatty acid oxidation in the ischaemic heart. *Biochem Soc Trans* 31: 207-212, 2003.

55. Hresko R, Heimberg H., Chi MMY., and Mueckler M. Glucosamine-induced insulin resistance in 3T3-L1 adipocytes is caused by depletion of intracellular ATP. *J Biol Chem* 273: 20658-20668, 1998.

56. Imahashi K, Pott C., Goldhaber JL., Steenbergen C., Philipson KD., and Murphy E. Cardiac-Specific Ablation of the Na<sup>+</sup>-Ca<sup>2+</sup> Exchanger Confers Protection Against Ischemia/Reperfusion Injury. *Circ Res* 97: 916-921, 2005.

57. **J Hescheler, R Meyer, S Plant, D Krautwurst, W Rosenthal and G Schultz.**

Morphological, biochemical, and electrophysiological characterization of a clonal cell

(H9c2) line from rat heart. *Circ Res.* 1991;69:1476-1486

58. **Kabashima T, Kawaguchi T., Wadzinski BE., and Uyeda K.** Xylulose 5-

phosphate mediates glucose-induced lipogenesis by xylulose 5-phosphate-activated

protein phosphatase in rat liver. *Proc Natl Acad Sci USA* 100: 5107-5112, 2003.

59. **Kasahara H, Usheva A., Ueyama T., Aoki H., Horikoshi N., and Izumo S.**

Characterization of homo- and heterodimerization of cardiac Csx/Nkx2.5

homeoprotein. *J Biol Chem* 276: 4570 - 4580, 2001.

60. **Kelly W, Dahmus ME., and Hart GW.** RNA polymerase II is a glycoprotein:

modification of the C-terminal domain by O-GlcNAc. *J Biol Chem* 268: 10416-10424,

1993.

61. **Kenchaiah D, Evans JC., Levy D., Wilson PWF., Benjamin EJ., Larson MG.,**

**Kannel WB., and Vasan RS.** Obesity and the risk of heart failure. *N Engl J Med* 347:

305-313, 2002.

62. **Kim K.** Regulation of mammalian acetyl-coenzyme A carboxylase. *Annu Rev*

*Nutr* 17: 77-99, 1997.

63. **Kim YB ZJ, Zierath JR., Shen HQ., Baron AD., and Kahn BB.** Glucosamine infusion in rats rapidly impairs insulin stimulation of phosphoinositide 3-kinase but does not alter activation of Akt/protein kinase B in skeletal muscle. *Diabetes* 48: 310-320, 1999.
64. **Komuro I, and Izumo S.** Csx: a murine homeobox-containing gene specifically expressed in the developing heart. *Proc Natl Acad Sci USA* 90: 8145 - 8149, 1993.
65. **Kreppel L, Blomberg MA., and Hart GW.** Dynamic glycosylation of nuclear and cytosolic proteins. Cloning and characterization of a unique O-GlcNAc transferase with multiple tetratricopeptide repeats. *J Biol Chem* 272: 9308-9315, 1997.
66. **Ku N, and Omary MB.** Expression, glycosylation, and phosphorylation of human keratins 8 18 in insect cells. *Exp Cell Res* 211: 24-35, 1994.
67. **Kudo N, Barr AJ., Barr RL., Desai S., and Lopaschuk GD.** High rates of fatty acid oxidation during reperfusion of ischemic hearts are associated with a decrease in malonyl-CoA levels due to an increase in 5'-AMP-activated protein kinase inhibition of acetyl-CoA carboxylase. *J Biol Chem* 270: 17513-17520, 1995.
68. **Lawrence JM, Contreras R, Chen W, and Sacks DA.** Trends in the prevalence of preexisting diabetes and gestational diabetes mellitus among a

racially/ethnically diverse population of pregnant, 1999-2005. *Diabetes Care* 31:899–

904, 2008.

69. **Lee J, Moon YA., Ha JH., Yoon DJ., Ahn YH., and Kim KS.** Cloning of human acetyl-CoA carboxylase beta promoter and its regulation by muscle regulatory factors.

*J Biol Chem* 276: 2576-2585, 2001.

70. **Lopaschuk G, Folmes CDL., and Stanely WC.** Cardiac Energy Metabolism in

Obesity. *Circ Res* 101: 335-347, 2007.

71. **Lorenz M, and Fink GR.** Life and Death in a Macrophage: Role of the

Glyoxylate Cycle in Virulence. *Eukaryot Cell* 1: 657-662, 2002.

72. **Lorenzi M.** The polyol pathway as a mechanism for diabetic retinopathy:

attractive, elusive, and resilient. *Exp Diabetes Res* 2007: 1-10, 2007.

73. **Lubas W, Frank DW., Krause M., and Hanover JA.** *O*-linked GlcNAc

transferase is a conserved nucleocytoplasmic protein containing tetratricopeptide

repeats. *J Biol Chem* 272: 9316-9324, 1997.

74. **Luiken J, Schaap FG., van Nieuwenhoven FA., van der Vusse GJ., Bonen A., and Glatz JF.** Cellular fatty acid transport in heart and skeletal muscle is facilitated by proteins. *Lipids* 34: S169-S175, 1999.
75. **Luiken J, van Nieuwenhoven FA., America G., van der Vusse GJ., and Glatz JF.** Uptake and metabolism of palmitate by isolated cardiac myocytes from adult rats: involvement of sarcolemmal proteins. *J Lipid Res* 38: 745-758, 1997.
76. **Majumdar G, Harmon A., Candelaria Martinez-Hernandez A., Raghow R., and Solomon SS.** O-glycosylation of Sp1 and transcriptional regulation of the calmodulin gene by insulin and glucagon. *Am J Physiol* 285: E584-E591, 2003.
77. **Makaula S, Adam T., and Essop MF.** Upstream stimulatory factor 1 transactivates the human gene promoter of the cardiac isoform of acetyl-CoA carboxylase. *Arch Biochem Biophys* 446: 91-100, 2006.
78. **Mao J, DeMayo FJ., Li H., Abu-Elheiga L., Gu Z., Shaikenov TE., Kodari P., Chirala SS., Heird WC., and Wakil SJ.** Liver-specific deletion of acetyl-CoA carboxylase 1 reduces hepatic triglyceride accumulation without affecting glucose homeostasis. *Proc Natl Acad Sci USA* 103: 8552-8557, 2006.

79. **Mashall S, Bacote V., and Traxinger RR.** Discovery of a metabolic pathway mediating glucose-induced desensitization of the glucose transport system. Role of hexosamine biosynthesis in the induction of insulin resistance. *J Biol Chem* 266: 4706-4712, 1991.
80. **Mashall S, Garvey WT., and Traxinger RR.** New insights into the metabolic regulation of insulin action and insulin resistance: role of glucose and amino acids. *FASEB J* 5: 3031-3036, 1991.
81. **McClain D.** Hexosamines as mediators of nutrient sensing and regulation in disease. *J Diabetes Complications* 16: 72-80, 2002.
82. **McClain D, Crook ED.** Hexosamines and insulin resistance. *Diabetes* 45: 1003-1009, 1996.
83. **McClain D, Lubas WA., Coosey RC., Hazel M., Parker GJ., Love DC., and Hanover JA.** Altered glycan-dependent signaling induces insulin resistance and hyperleptinemia. *Proc Natl Acad Sci USA* 99: 10695-10699, 2002.
84. **Miranda P, DeFronzo RA., Califf RM., and Guyton JR.** Metabolic syndrome: definition, pathology, and mechanisms. *Am Heart J* 149: 33-45, 2005.

85. **Miyake K, So WY., Poon EW., and Lam VK.** The linkage and association of the gene encoding upstream stimulatory factor 1 with type 2 diabetes and metabolic syndrome in the Chinese population. *Diabetologia* 48: 2018-2024, 2005.
86. **Molkentin JD, Lin, Q., Duncan, S. A., and Olson, E. N. (1997)** Requirement of the transcription factor GATA4 for heart tube formation and ventral morphogenesis. *Genes Dev* 11: 1061 - 1072, 1997.
87. **Neely J, Denton RM., England PJ., and Randle PJ.** The Effects of Increased Heart Work on the Tricarboxylate Cycle and its Interactions with Glycolysis in the Perfused Rat Heart. *Biochem J* 128: 147-159, 1972.
88. **O'Donnell N, Zachara NE., Hart GW., and Marth JD.** OGT-dependent X-chromosome-linked protein glycosylation is a requisite modification in somatic cell function and embryo viability. *Mol Cell Biol* 24: 1680-1690, 2004.
89. **Oh S, Lee M-Y., Kim J-M., Yoon S., Shin S., Park YN., Ahn Y-H., and Kim K-S.** Alternative usages of multiple promoters of the acetyl-CoA carboxylase gene are related to differential transcriptional regulation in human and rodent tissues. *J Biol Chem* 280: 5909-5916, 2005.

90. **Olson E, and Srivastava D.** Molecular pathways controlling heart development.

*Science* 272: 671 - 676, 1996.

91. **Onay-Besikci A, Campbell FM., Hopkins TA., Dyck JR., and Lopaschuk GD.**

Relative importance of malonyl CoA and carnitine in maturation of fatty acid oxidation

in newborn rabbit heart. *Am J Physiol Heart Circ Physiol* 284: H283-H289, 2003.

92. **Park S, Ryu J., and Lee W.** O-GlcNAc modification on IRS-1 and Akt2 by

PUGNAc inhibits their phosphorylation and induces insulin resistance in rat primary

adipocytes. *Exp Mol Med* 37: 220-229, 2005.

93. **Pettersson I, Muccioli G., Granata R., Deghenghi R., Ghigo E., Ohlsson C., and**

**Isgaard J.** Natural (ghrelin) and synthetic (hexarelin) GH secretagogues

stimulate H9c2 cardiomyocyte cell proliferation. *J Endocrinol* 175: 201-209, 2002.

94. **Pownall H, and Hamilton JA.** Energy translocation across cell membranes and

membrane models. *Acta Physiol Scand* 178: 357-365, 2003.

95. **Prentki M, and Nolan CJ.** Islet  $\beta$  cell failure in type 2 diabetes. *J Clin Invest* 116:

1802-1812, 2006.

96. **Robinson K, Sens DA., and Buse MG.** Pre-exposure to glucosamine induces

insulin resistance of glucose transport and glycogen synthesis in isolated rat skeletal

muscles. Study of mechanisms in muscle and rat-1 fibroblasts overexpressing the human insulin receptor. *Diabetes* 42: 1333-1346, 1993.

97. **Robinson K, Weinstein ML., Lindenmayer GE., and Buse MG.** Effects of Diabetes and Hyperglycemia on the Hexosamine Synthesis Pathway in Rat Muscle and Liver. *Diabetes* 44: 1438-1446, 1995.

98. **Rossetti L.** Perspective: hexosamines and nutrient sensing. *Endocrinology* 141: 1922-1925, 2000.

99. **Ruderman N, Saha AK., Vavvas D., and Witters LA.** Malonyl-CoA, fuel sensing, and insulin resistance. *Am J Physiol* 276: E1-E18, 1999.

100. **Rudnicki M, and Jaenisch R.** The MyoD family of transcription factors and skeletal myogenesis. *Bioessays* 17: 203-209, 1995.

101. **Sabourin L, and Rudnicki MA.** The molecular regulation of myogenesis. *Clinical genetics* 57: 16-25, 2000.

102. **Saddik M, Gamble J., Witters LA., and Lopaschuk GD.** Acetyl-CoA carboxylase regulation of fatty acid oxidation in the heart. *J Biol Chem* 268: 25836-25845, 1993.

103. **Saha A, Schwarsin AJ., Roduit R., Masse F., Kaushik V., Tornheim K., Prentki M., and Ruderman NB.** Activation of malonyl-CoA decarboxylase in rat skeletal

muscle by contraction and the AMP-activated protein kinase activator 5-aminoimidazole-4-carboxamide-1- $\beta$ -D-ribofuranoside. *J Biol Chem* 275: 24279-24283, 2000.

104. **Sassoon D.** Myogenic regulatory factors: dissecting their role and regulation during vertebrate embryogenesis. *Dev Biol* 156: 11-23, 1993.

105. **Schults H.** Regulation of fatty acid oxidation in heart. *J Nutr* 124: 165-171, 1994.

106. **Shafi R, Iyer SP., Ellies LG., O'Donnell N., Marek KW., Chui D., Hart GW., and Marth JD.** The O-GlcNAc transferase gene resides on the X chromosome and is essential for embryonic stem cell viability and mouse ontogeny. *Proc Natl Acad Sci USA* 97: 5735-5739, 2000.

107. **Sharon F. Clark, Sally Martin, Amanda J. Carozzi, Michelle M. Hill, and David E. James.** Intracellular Localization of Phosphatidylinositide 3-kinase and Insulin Receptor Substrate-1 in Adipocytes: Potential Involvement of a Membrane Skeleton. *The Journal of Cell Biology* Volume 140, Number 5, March 9, 1998 1211 - 1225.

108. **Shankar R, Zhu SS., and Baron AD.** Glucosamine infusion in rats mimics the beta-cell dysfunction of non-insulin-dependent diabetes mellitus. *Metabolism* 47: 573-577, 1998.
109. **Shuldiner A, John C., and McLenithan JC.** Genes and pathophysiology of type 2 diabetes: more than just the Randle cycle all over again. *J Clin Invest* 116: 1414-1417, 2004.
120. **Sirito M, Walker S., Lin Q., Kozlowski MT., Klein WH., and Sawadogo M.** Members of the USF family of helix-loop-helix proteins bind DNA as homo- as well as heterodimers. *Gene Expr* 2: 231-240, 1992.
111. **Smith T, Block NE., Rhodes SJ., Konieczny SF., and Miller JB.** A unique pattern of expression of the four muscle regulatory factor proteins distinguishes somitic from embryonic, fetal and newborn mouse myogenic cells. *Development* 117: 1125 - 1133, 1993.
112. **Spector A.** Plasma lipid transport. *Clin Physiol Biochem* 2: 123-134, 1984.
113. **Stahl A.** A current review of fatty acid transport proteins(SLC27). *Pflugers Arch* 447: 722-727, 2004.

114. **Stanely W, Morgan EE., Huang H., McElfresh TA., Streck JP., Okere IC., Chandler MP., Cheng J., Dyck JRB., and Lopaschuk GD.** Malonyl-CoA decarboxylase inhibition suppresses fatty acid oxidation and reduces lactate production during demand-induced ischemia. *Am J Physiol Heart Circ Physiol* 289: H2304-H2309, 2005.
115. **Steyn N, Bradshaw D., Norman R., Joubert J., Schneider M., and Steyn K.** Dietary changes and the health transition in South Africa: implications for health policy. *Cape Town: South African Medical Research Council, 2006.*
116. **Stryer L.** Biochemistry: Fourth Edition. *New York: Freeman and Company.* 483-628, 1999.
117. **Taegtmeyer H.** Genetics of energetics: transcriptional responses in cardiac metabolism. *Ann Biomed Eng* 28: 871-876, 2000.
118. **Torres C, and Hart GW.** Topography and polypeptide distribution of terminal *N*-acetylglucosamine residues on the surfaces of intact lymphocytes. Evidence for O-linked GlcNAc. *J Biol Chem* 259: 3308-3317, 1984.
119. **Trost S, Omens JH., Karlon WJ., Meyer M., Mestril R., Covell JW., and Dillmann WH.** Protection Against Myocardial Dysfunction After a Brief Ischemic Period

in Transgenic Mice Expressing Inducible Heat Shock Protein 70. *J Clin Invest* 101: 855-862, 1998.

120. **U. Rajamani, D. Joseph, S. Roux and M. F. Essop.** The hexosamine biosynthetic pathway can mediate myocardial apoptosis in a rat model of diet-induced insulin resistance. *Acta Physiol* 202, 151 - 157, 2011.

121. **Van Bilson M, Van der Vusse GJ., Gilde AJ., Lindhout M., and van der Lee KA.** Peroxisome proliferator-activated receptors: lipid binding proteins controlling gene expression. *Mol Cell Biol* 239: 131-138, 2002.

122. **Van der Vusse G, van Bilzen M., and Glatz JF.** Cardiac fatty acid uptake and transport in health and disease. *Cardiovasc Res* 45: 279-293, 2000.

123. **Viollet B, Lefrançois-Martinez AM., Henrion A., Kahn A., Raymondjean M., and Martinez A.** Immunochemical characterization and transacting properties of upstream stimulatory factor isoforms. *J Biol Chem* 271: 1405-1415, 1996.

124. **Vosseller K, Wells L., Lane MD., and Hart GW.** Elevated nucleocytoplasmic glycosylation by O-GlcNAc results in insulin resistance associated with defects in Akt activation in 3T3-L1 adipocytes. *Proc Natl Acad Sci USA* 99: 5313-5318, 2002.

125. **W.H.O.** Definition, Diagnosis and Classification of Diabetes Mellitus and its Complications. In: *World Health Organisation*, 1999.

126. **W.H.O.** World Health Report 2002. In: *World Health Organization*, 2002.

127. **Weigert C, Brodbeck K., Sawadogo M., Haring HU., and Schleicher ED.**

Upstream stimulatory factor (USF) proteins induce human TGF  $\beta$ 1 gene activation via the glucose-response element-1013/-1002 in mesangial cells: up-regulation of USF activity by the hexosamine biosynthetic pathway. *J Biol Chem* 279: 15908-15915, 2004.

128. **Weigert C, Brodbeck K., Sawadogo M., Haring HU.,and Schleicher ED.**

Upstream Stimulatory Factor (USF) Proteins Induce Human TGF  $\beta$ 1 Gene Activation via the Glucose-response Element -1013/-1002 in Mesangial Cells. *J Biol Chem* 279: 15908-15915, 2004.

129. **Wells L, Voseller K., and Hart GW.** Glycosylation of nucleocytoplasmic proteins: signal transduction and O-GlcNAc. *Science* 291: 2376-2378, 2001.

130. **Wild S, Roglic G., Green A., Sicree R., and King H.** Global prevalence of diabetes estimates for the year 2000 and projections for 2030. *Diabetes Care* 27: 1047-1053, 2004.

131. **Wilson P, D'Agostino RB., Sullivan L., Parise H., and Kannel WB.** Overweight and obesity as determinants of cardiovascular risk: the Framingham experience. *Arch Intern Med* 162: 1867-1872, 2002.
132. **Winz R, Hess D., Aebersold R., and Brownsey W.** Unique structural features and differential phosphorylation of the 280-kDa component (isozyme) of rat liver acetyl-CoA carboxylase. *J Biol Chem* 269: 14438 - 14445, 1994.
133. **Yamashita H, Takenoshita M., Sakurai M., Bruick RK., Henzel WJ., Shillinglaw W., Arnot D., and Uyeda K.** A glucose-responsive transcription factor that regulates carbohydrate metabolism in the liver. *Proc Natl Acad Sci USA* 98: 9116-9121, 2001.
134. **Yanzhang Li, and Shuxia Wang.** Glycated albumin upregulates upstream stimulatory factor 2 gene transcription in mesangial cells. *Am J Physiol Renal Physiol* 299: F121 - F127, 2010.
135. **Young M, Goodwin GW., Ying J., Guthrie P., Wilson CR., Laws FA., and Taegtmeyer H.** Regulation of cardiac and skeletal muscle malonyl-CoA decarboxylase by fatty acids. *Am J Physiol Endocrinol Metab* 280: E471-E479, 2001.

136. Yuan H, Wong LS., Bhattacharya M., Ma C., Zarafani M., Yao M., Schneider M., Pitas RE., and Martins-Green M. The effects of second-hand smoke on biological processes important in atherogenesis. *BMC Cardiovasc Disord* 7: 1-16, 2007.

137. Zachara N, and Hart GW. Cell signaling, the essential role of O-GlcNAc! *Biochim Biophys Acta* 1761: 599-617, 2006.

138. Zhang S, and Kim, KH. Acetyl-CoA carboxylase is essential for nutrient-induced insulin secretion. *Biochem Biophys Res Commun* 229: 701-705, 1996.

# **Chapter 5**

# **Appendix**

**Appendix 1:**

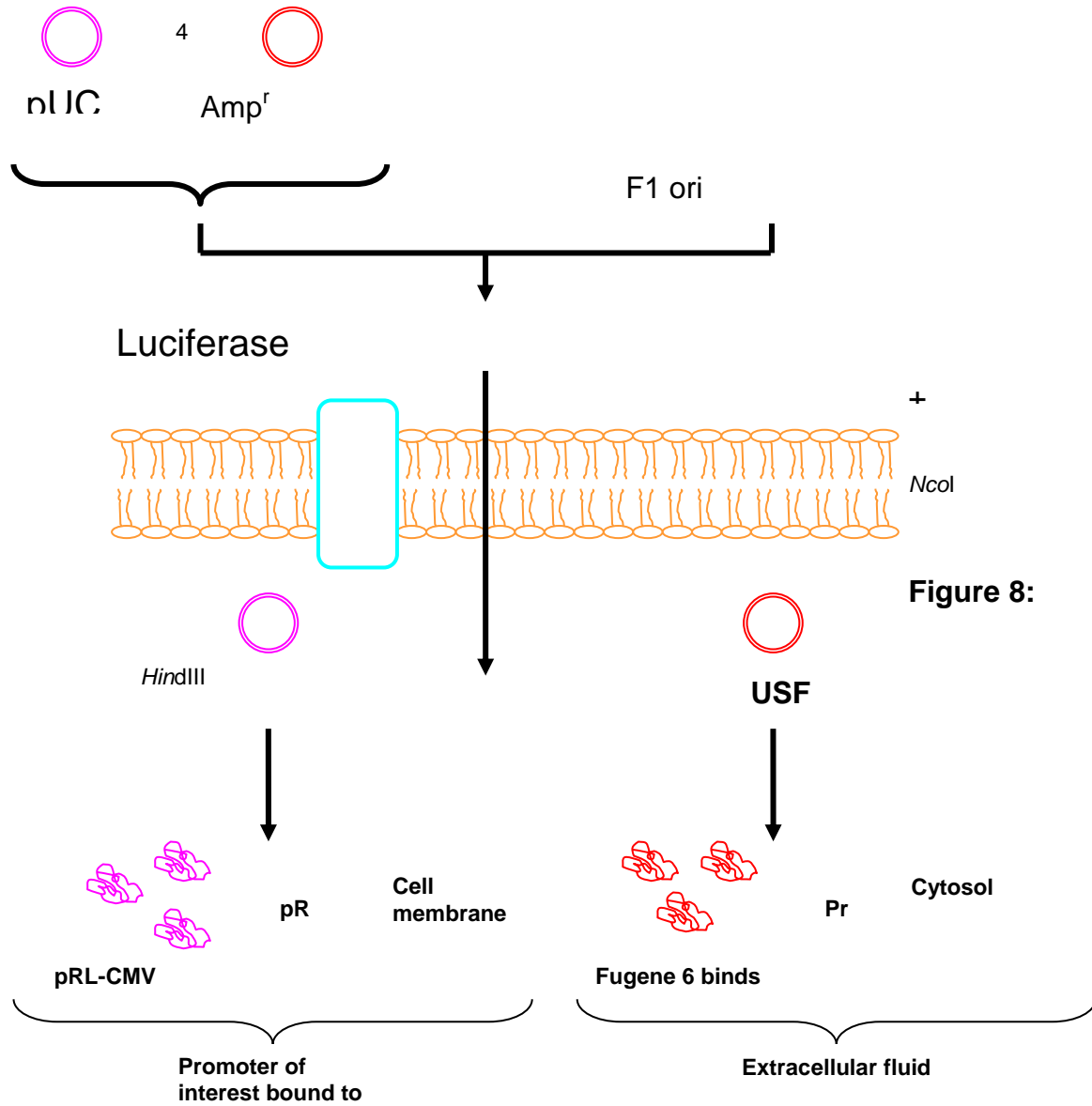
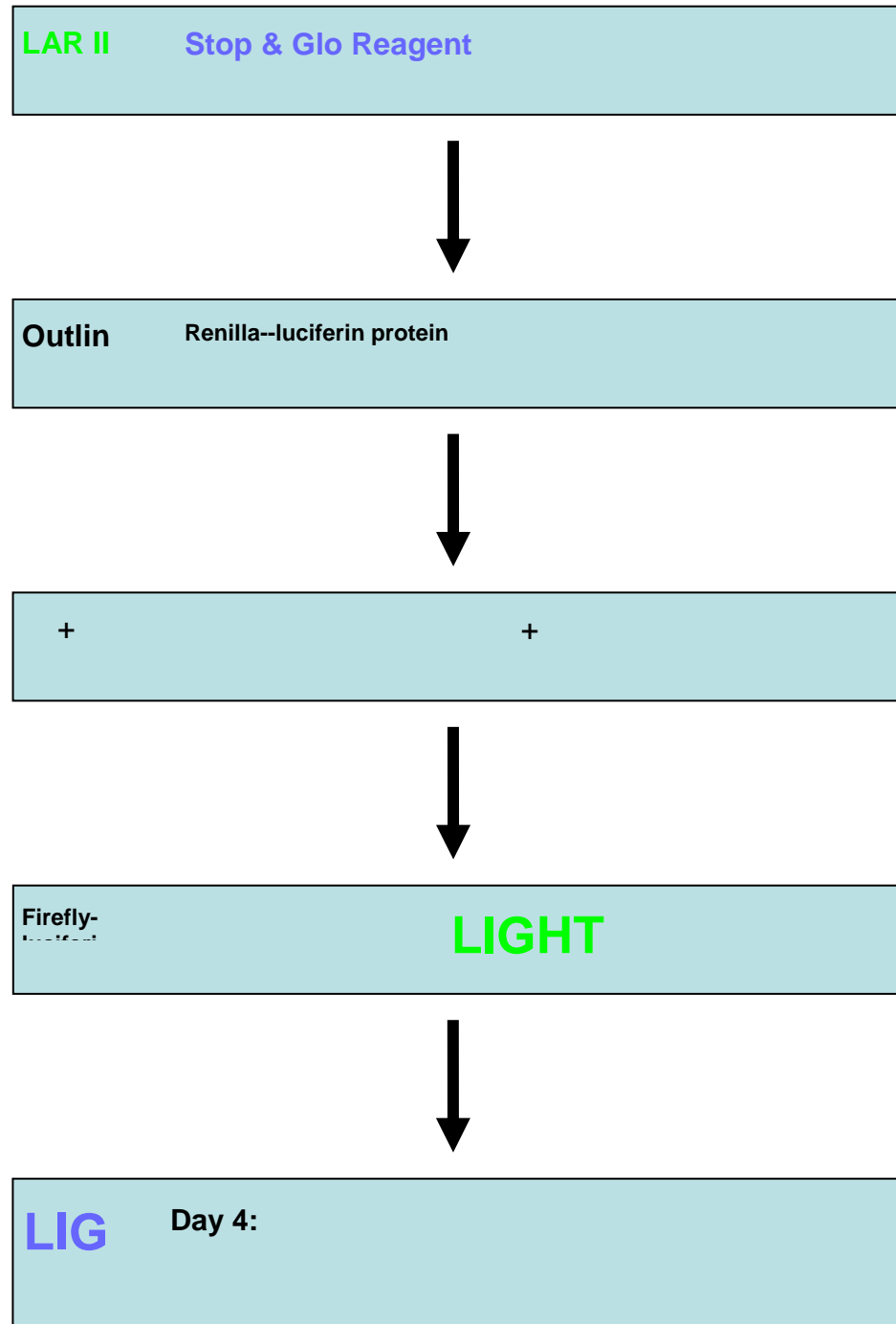


**Figure 8:**

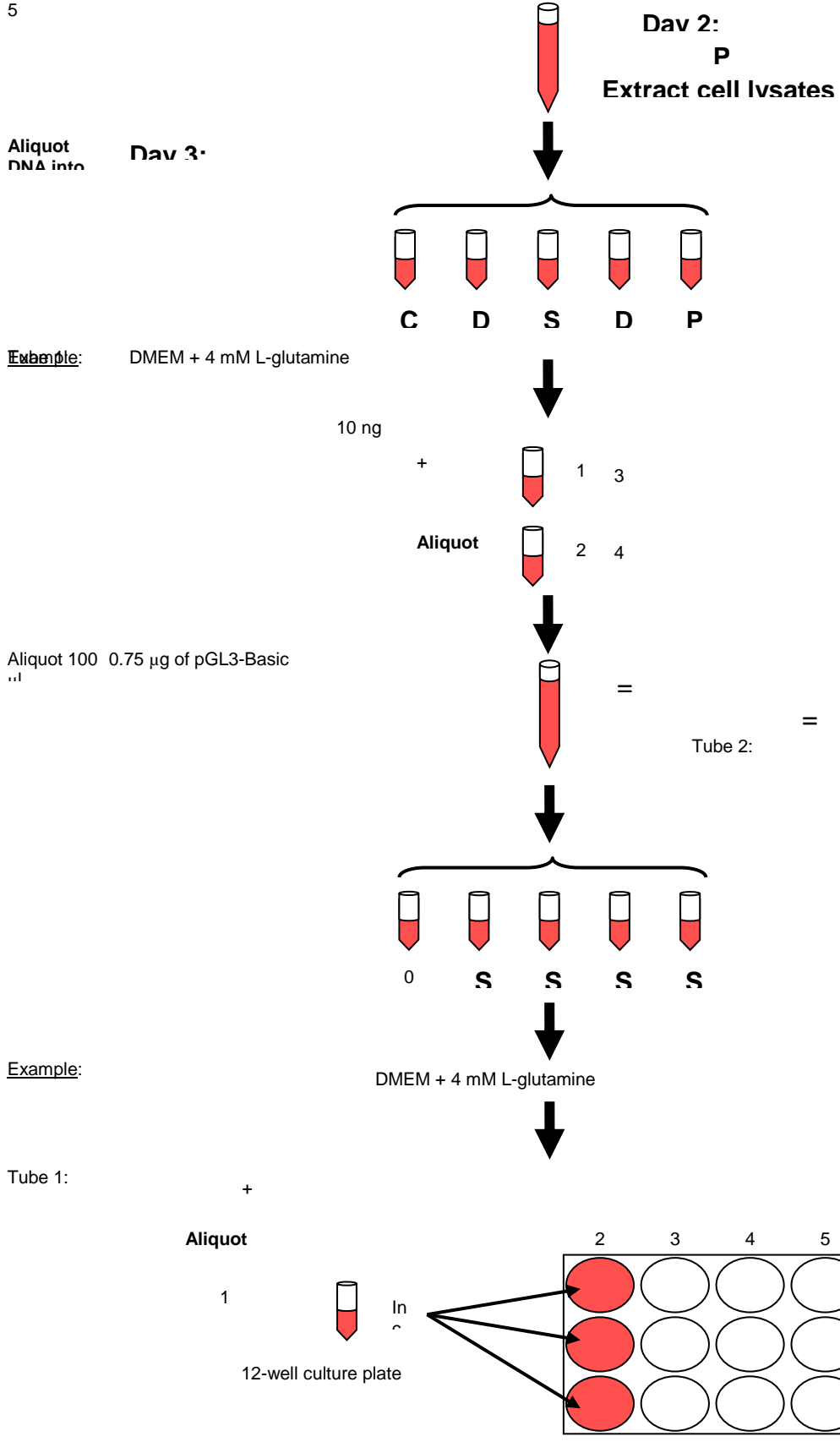
**Fugene 6 Transfection Reagent**

## Appendix 2: Outline of transfection schedule.



## Appendix 3: Outline of day 2 transfection procedure.

5



## Appendix 4: Outline of day 4 lysate extraction

Leave plate on a shaker for 15 minutes at room temperature



Extract lysates and place each into separate microfuge tubes and store at -80°C

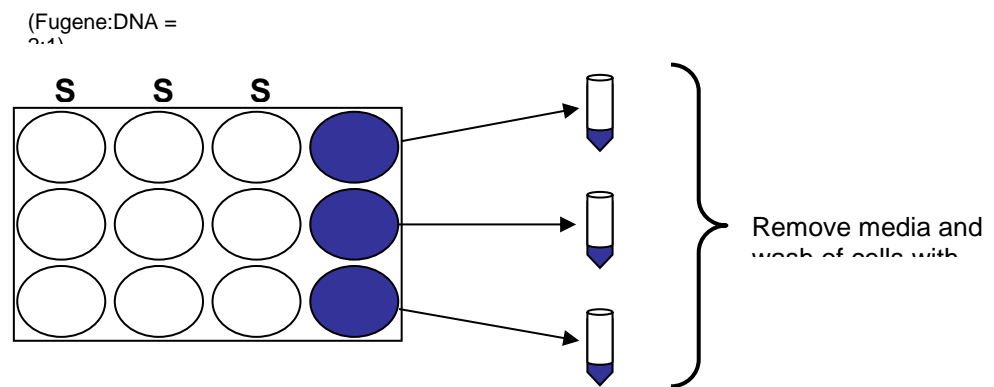


Add 200 µl of Passive Lysis Buffer from Dual-Luciferase Reporter Assay Kit in each well of 12-well culture plate



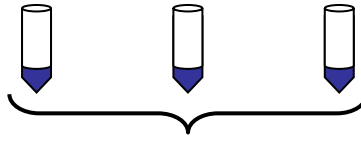
Example:

4



## Appendix 5: Performing the luciferase assay on day 5

**Step 1:**



Store at -80°C

**Step 2:**

1



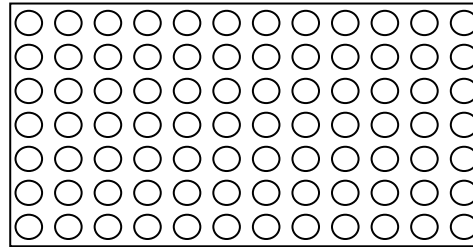
**Step 3:**

2



**Step 4:**

3



Thaw samples in

4



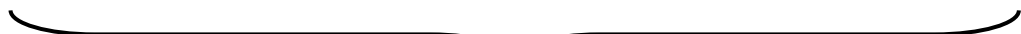
Vortex samples and then centrifuge at 12,000 rpm at 4°C for 2 minutes



Aliquot 10 µl of each sample onto a 96-well luminometer plate



Place in luminometer with reagent 1 and reagent 2



Samples from Day 4

## **Appendix 6: Procedure for extraction of RNA using Aurum total RNA fatty and fibrous tissue kit** (Protocol from Bio-RAD Laboratories, Hercules, California, USA)

1. Measure the amount of starting material. Note that the Aurum total RNA fatty and fibrous tissue kit is designed to process up to the amounts indicated below (per column):

- (i)  $1 \times 10^7$  cultured mammalian cells grown in suspension
- (ii) One 102 cm plate mammalian cultured cells grown in monolayer
- (iii)  $2.4 \times 10^9$  of Gram-positive or Gram-negative bacteria
- (iv)  $3.0 \times 10^7$  of yeast
- (v) 100 mg of animal tissue (a 4 mm cube of most animal tissue weighs 70–85 mg)
- (vi) 100 mg of plant tissue
- (vii) 50 mg filamentous fungi

**Warning:** Processing larger amounts of starting material may lead to column clogging and reduced RNA purity. It is crucial that the appropriate amount of starting material be used. For samples that are known to be rich in RNA, it is highly recommended that less than the maximum amount of starting material be used so that the binding capacity of the column is not exceeded. In addition, complete disruption and homogenization of the starting material is critical to prevent column clogging and reduced RNA yields.

2. Disrupt and homogenize the sample. Below are recommended procedures for disruption and homogenization.

**Note:** Incomplete disruption will clog the column in subsequent steps and result in reduced yields of total RNA.

### **Fresh Tissue**

Fresh tissues can be processed in PureZOL immediately after dissection. Alternatively, freshly dissected tissue can be immediately frozen in liquid nitrogen and processed using instructions for frozen tissue. Transfer up to 100 mg of freshly dissected tissue into a 2.0 ml microcentrifuge tube and add 1 ml of PureZOL. Disrupt the sample for 30–60 seconds using a rotor-stator or bead mill homogenizer (refer to manufacturer instructions for details). Although not as effective, passing the tissue sample through an 18-gauge needle and syringe can be used for sample disruption if a homogenizer is not available. Pass the sample through the needle and syringe until no more solid tissue is left in the lysate. The sample volume should not exceed 10% of the volume of PureZOL used for disruption. Proceed to step 3.

### **Frozen Tissue**

Grind the frozen tissues to a fine powder with a mortar and pestle under liquid nitrogen. Avoid thawing the sample by periodically adding liquid nitrogen to the mortar. Weigh up to 100 mg of tissue and transfer the sample into a 2.0 ml microcentrifuge tube. Add 1 ml of PureZOL and disrupt for 30-60 seconds using a rotor-stator or bead

mill homogenizer (refer to manufacturer's instructions for details). Alternatively, take a small chunk of the frozen tissue (up to 100 mg) and drop it into 1 ml of PureZOL reagent and immediately homogenize the sample. Although not as effective, passing the tissue sample through an 18-gauge needle and syringe can be used for sample disruption if a homogenizer is not available. Pass the sample through the needle and syringe until no more solid tissue is left in the lysate. The sample volume should not exceed 10% of the volume of PureZOL used for disruption. Proceed to step 3.

Cells grown in a monolayer should be lysed with PureZOL directly in the culture dish. Aspirate the culture medium and immediately add 1 ml of PureZOL to a 10 cm<sup>2</sup> dish. Pass the lysate through a pipette several times. The amount of PureZOL added is dependent on the area of culture dish (1 ml per 10 cm<sup>2</sup>) and not on cell number. Insufficient volumes of PureZOL may result in DNA contamination. Proceed to step 3.

**Note:** Do not wash cells prior to the addition of PureZOL as this could increase the possibility of mRNA degradation.

### **Suspension Cells (Mammalian, Plant, Bacterial, or Yeast)**

Pellet the cells by centrifuging at 3,000-5,000 x g for 2 minutes. Immediately lyse by adding 1 ml of PureZOL to 1 x 10<sup>7</sup> cultured mammalian and plant cells, 2.4 x 10<sup>9</sup> of Gram-positive or Gram-negative bacteria, or 3.0 x 10<sup>7</sup> of yeast (equivalent to 3 OD•ml of yeast). Pass the lysate through a pipet or an 18-gauge needle and syringe several times. To improve the efficiency of the cell lysis process, a rotor-stator homogenizer or a bead mill homogenizer is recommended to disrupt the cell walls of yeast and

bacteria. Bacteria and yeast lysate can also be heated to 55°C for 10 minutes prior to adding chloroform to increase the effectiveness of lysis by PureZOL. Proceed to step 3.

**Note:** Do not wash cells prior to the addition of PureZOL as this could increase the possibility of mRNA degradation.

3. Once the sample has been disrupted in PureZOL, incubate the lysate at room temperature for 5 minutes to allow the complete dissociation of nucleoprotein complexes.

**Note:** Following the disruption step, the sample can be stored at -70°C for at least 1 month. To process frozen lysates, samples should be thawed at room temperature. If necessary, heat samples to 37°C in a water bath for 5–10 minutes to completely dissolve salts. Avoid extended treatment at 37°C, which can cause chemical degradation of the RNA.

It is recommended that lysate from tissues that are rich in fat, polysaccharides, proteins, and extracellular material be centrifuged at 12,000 x g for 10 minutes at 4°C following the 5 minute incubation at room temperature. This step removes any solid insoluble debris that was left after the disruption step. Transfer the supernatant into a new 2.0 ml microcentrifuge tube without aspirating the pellet, then proceed to step 4. For lipid-rich samples, avoid transferring the excess fat that collects as a top layer. Carryover of the solid debris can cause column clogging and affect RNA sample purity.

4. Add 0.2 ml of chloroform to the lysate, then cover and shake vigorously for 15 seconds. Do not vortex!

5. Incubate for 5 minutes at room temperature while periodically mixing the sample.

6. Centrifuge at 12,000 x g for 15 minutes at 4°C.

Following centrifugation, the mixture will separate into 3 phases: an upper, colorless aqueous phase; a white interphase; and a lower, red organic phase. RNA is found exclusively in the aqueous phase, while DNA and proteins remain in the interphase and organic phase. The volume of the aqueous phase should be approximately 600 µl, or 60% of the volume of PureZOL used in the initial disruption.

If removal of contaminating DNA is a requirement, prepare DNase I enzyme by following steps a-b below while centrifuging the samples for phase separation: **a.** DNase I is provided as a lyophilized powder. If the DNase has already been reconstituted, skip to step b. Otherwise, reconstitute the DNase I by adding of 250 µl of 10 mM Tris, pH 7.5 (not provided) to the vial and mix by pipetting up and down briefly. Do not vortex! See Section 5, Materials and Equipment Required (Not Provided in the Kit), on how to prepare 10 mM Tris, pH 7.5. **b.** For each column to be processed, mix 5 µl of reconstituted DNase I with 75 µl of DNase dilution solution in a 1.5 ml microcentrifuge tube. Scale up proportionally if processing more than one column. Once diluted with DNase dilution solution, do not refreeze for later use.

7. Without disturbing the interphase, immediately transfer the aqueous phase to a 2.0 ml microcentrifuge tube.

**Note:** It is crucial that none of the interphase or organic phase be transferred with the aqueous phase. Some of the aqueous phase should be left behind to avoid the risk of contaminating the RNA with contaminants such as phenol, which can interfere with downstream applications.

8. Add an equal volume (approximately 600  $\mu$ l) of 70% ethanol (not provided) to the tube and mix thoroughly by pipetting up and down.

9. At this time, warm the elution solution to 70°C in a water bath for use in step 19.

10. Attach an Aurum total RNA binding mini column to a luer fitting of the column adaptor plate on the Aurum vacuum manifold or to a compatible vacuum manifold. Refer to Figures 4B and 4C for setup. The vacuum source should be turned off, and the vacuum regulator should be completely open.

11. Pipet 700  $\mu$ l of the RNA sample into the RNA binding mini column. Turn the vacuum on and adjust to –20" to –23" Hg by closing the vacuum regulator. Continue to apply vacuum until all of the RNA sample have passed through the column. Open the vacuum regulator until the gauge indicates 0" Hg.

12. Repeat step 11 for the remainder of the sample. The Aurum total RNA fatty and fibrous tissue kit supplies RNase-free DNase I to be used to treat samples for complete removal of contaminating genomic DNA. If removal of genomic DNA is not a requirement, proceed directly to step 15. Otherwise, perform on-column DNase I digest by proceeding to step 13.

13. Add 700 µl of low-stringency wash solution (already supplemented with ethanol) to the RNA binding column and close the vacuum regulator dial until the gauge indicates –20" to –23" Hg. Continue to apply the vacuum until the low-stringency wash solution has passed through the column. Open the vacuum regulator until the gauge indicates 0" Hg.

14. Remove any contaminating genomic DNA from the RNA sample using steps a–c described below.

- a. Add 80 µl of the diluted DNase I to each column processed, making sure to add the DNase to the center of the membrane stack at the bottom of each column.
- b. Allow the DNase digest to incubate at room temperature for 15 minutes.
- c. When the DNase digestion is complete, centrifuge columns for 30 seconds at >12,000 x g. Discard the digest buffer from the wash tube and place the column back into the same wash tube.

15. Add 700 µl of high-stringency wash solution to the RNA binding mini column and close the vacuum regulator dial until the gauge indicates –20" to –23" Hg. Continue to

apply the vacuum until the high-stringency wash solution has passed through the column. Open the vacuum regulator until the gauge indicates 0" Hg.

16. Add 700  $\mu$ l of low-stringency wash solution (already supplemented with ethanol) to the RNA binding column and close the vacuum regulator dial until the gauge indicates –20" to –23" Hg. Continue to apply the vacuum until the low-stringency wash solution has passed through the column. Open the vacuum regulator until the gauge indicates 0" Hg.

17. Transfer the RNA binding mini column to a 2.0 ml capless tube (provided). Centrifuge for 2 minutes at >12,000 x g to remove the residual wash solution.

**Note:** The elution solution should be at 70°C before proceeding with the elution step.

18. Transfer the RNA binding column to a 1.5 ml microcentrifuge tube (provided).

19. Pipet 40  $\mu$ l (or 30  $\mu$ l)† of the warmed elution solution onto the center of the membrane at the bottom of the RNA binding column.

† **Note:** When isolating total RNA from small amounts of starting material (<10 mg of tissue or 500,000 cells), perform a single elution with 30  $\mu$ l of warmed elution solution.

**Do not perform step 22.**

20. Incubate 1 minute for complete soaking and saturation of the membrane.

21. Centrifuge for 2 minutes at  $>12,000 \times g$  to elute the total RNA.

22. Repeat steps 19 and 20 using 40  $\mu\text{l}$  of the elution solution if the starting amount of starting material is more than 10 mg of tissue or 500,000 cells.

**Note:** The eluted total RNA samples can be used immediately in downstream applications. Alternatively, the RNA sample can be aliquoted and stored at  $-20^{\circ}\text{C}$  for 1 month or at  $-70^{\circ}\text{C}$  for 1 year

## Appendix 7: Normal antibody Western blotting and detection

Buffers used:

10x Tris Buffer Saline (TBS): (5 litres)

121 g Tris

40 g NaCl

pH solution to 7.6

TBS-T Wash Buffer: Add 10 ml of 10x TBS to 90 ml of ultrapure or distilled water and then add 1 ml of Tween-20.

Blocking Buffer: Add 5 mg of milk powder (Elite skim milk powder) to 100 ml of TBS-T.

Procedure:

1. Remove PVDF (Millipore, Billerica, USA) membrane from the transfer apparatus and wash the membrane 3 times with TBS-T for 5 minutes.
2. Block nonspecific sites on the membrane by completely immersing the membrane with the blocking membrane (approximately 50 ml) at room temperature (RT) overnight at 4°C.
3. Prepare a 1:3,000 dilution of the GFAT antibody in blocking buffer.

4. Incubate the blot overnight at 4°C. We used 17 µl of primary antibody in 5 ml of blocking buffer in a 50 ml Falcon tube and left the membrane to incubate overnight at 4°C.
5. Wash the membrane six times by completely immersing in TBS-T wash buffer (approximately 50 ml) and agitating for 5 minutes.
6. Prepare approximately 1:2,000 dilution of goat anti-rabbit-horse radish peroxidase in blocking buffer. For 5 ml of blocking buffer we added 5 µl of secondary antibody.
7. Remove wash buffer, add the diluted secondary antibody and incubate for 1 hour at room temperature with gentle shaking.
8. Wash the membrane six times by completely immersing the membrane in TBS-T wash buffer (approximately 50 ml) and shaking for 5 minutes.
9. Wash the membrane for 15 minutes with TBS.
10. Add 0.5 ml of ECL Reagent 1 to the membrane and then add ECL reagent 2 to the membrane. Make sure to spread the ECL reagents over the whole membrane. Incubate for 1 minute at room temperature while continuously washing the ECL reagent mixture over the membrane.

11. Remove membrane from ECL reagent and place in a plastic membrane protector (we used two pieces of acetate).
12. Place the protected membrane in a film cassette with the protein side facing up.
13. The membrane was exposed to Hyperfilm (Amersham, Buckinghamshire, UK) in a dark room for up to  $\pm 7$  minutes and then placed in developer for  $\pm 30$  seconds. The film was washed and fixed.

## Appendix 8: Stripping protocol

1. Make up the following solution:

100 mM  $\beta$ -Mercaptoethanol: 700 ml/100 ml

2% SDS: 20 ml/100 ml (from 10% stock)

62.5 mM Tris-HCl pH 6.7: 0.757 g/100 ml

Make up to 100 ml with H<sub>2</sub>O

2. Incubate membrane in solution at 60°C for 30-60 min with occasional agitation.

3. Wash the membrane in TBS-Tween before blocking in 5% milk.

## **Appendix 9:**

### **Chloroform/ methanol extraction of tissue samples - (Quantitative) for the determination of lipid, total protein, total phospholipid and phospholipid fractions:**

This method can be used for liver, artery and aorta intima and heart muscle tissue samples

#### **Reagents:**

1. 0.9% Saline
2. Chloroform +0.01% BHT
3. Methanol + 0.01% BHT
4. Saline saturated with CMS (0.9%; m/v in H<sub>2</sub>O)
5. Distilled methanol
6. Liquid nitrogen
7. Distilled water

### **Equipment and instruments needed:**

1. Mortar and pestle
2. Scalpel and tweezers
3. Filter paper (Whatman no.1)
4. Extraction tubes
5. Gilson (1ml)
6. Blue tips
7. Whirly machine
8. Mechanical shaker
9. Analytical scale
10. Nitrogen evaporator

### **Method:**

1. Resuspend sample in normal saline on ice.
2. Rinse with clean saline and dry with filter paper.
3. Cut into small pieces and blot dry. Use a sample size of approximately  $\pm 150$  mg.
4. Freeze-dry sample with liquid nitrogen in the mortar and grind with a pestle until it forms a powder.
5. Weigh out  $\pm 100$  mg sample in extraction tube and record exact weight.
6. Add 500  $\mu\text{L}$  saline to sample and mix slowly.
7. Add 3 ml a methanol and butylated hydroxytoluene (BHT) solution and mix slowly.
8. Add 6 ml a chloroform and BHT solution and mix slowly.

9. Tighten caps well. Do not expose the sample to air as this will oxidise the fatty acids in the sample.
10. Shake for 30 minutes on a mechanical shaker at room temperature.
11. Place the tube with the sample on a test tube rack in a heated water bath and blow nitrogen in tube until the liquid is evaporated away, replace cap careful not to expose the sample to air and store at 4°C.

Lipid determination: (for neutral and phospholipid classes)

**Reagents:**

1. Saline saturated with CMS
2. CMS+BHT
3. Distilled methanol
4. BBOT
5. C:M (2:1)+BHT

**Equipment and instruments needed:**

1. Whirly machine
2. Pipette (2 ml)
3. Pipette (10 ml)
4. Pasteur pipettes
5. Round bottom flasks

6. Filter paper (Whatman no.1) using small, medium and large according to funnel.
7. Stand
8. Glass funnels
9. Buchi vacuum rotary (45°C)
10. Pipette aids
11. Vacuum pump
12. Tweezers
13. Mechanical shakers
14. Spotting tubes
15. Nitrogen evaporator

**Method:**

1. Attached round bottomed flask and funnel to a stand.
2. Place two filter papers in funnel and wet with methanol.
3. See that they fit snugly onto the bottom.
4. Transfer the extracted sample in CM 2:1 by means of a pasteur pipette into the funnel and apply vacuum pressure.
5. Rinse the stopper into the funnel with 5ml CM (2:1), and apply vacuum pressure.
6. Replace the top filter back into the extraction tube with a tweezer.
7. Add 3 ml methanol+BHT and whirly.
8. Add 6 ml chloroform+BHT and whirly.
9. Cap and shake on a mechanical shaker for 10 minutes.

10. Pour contents of tube over onto funnel, rinse the stopper with 5 ml CM (2:1) and apply vacuum pressure.
11. Pipette 5 ml CM (2:1) into extraction tube, washing down the sides. Transfer the contents to the funnel with a pasteur pipette and apply vacuum pressure. Repeat once more.
12. Finally rinse inside of funnel with 2 ml methanol and apply vacuum pressure.
13. Remove the round bottomed flask from the funnel and dry extract on a buchi apparatus.
14. When extract is dry, cool off shortly in a ice bath.
15. Add 2 ml of CMS , dissolve lipids by swirling the flask, and transfer over into a spotting tube with a pasteur pipette.
16. Repeat step 15 - four times.
17. Add 2ml saline saturated with CMS, fill tube with nitrogen, cap and mix the contents of tube by turning the tube upside down 15 times.
18. Leave to stand until phases separates and then discard top layer with a pasteur pipette.

For storing: Fill the tube with nitrogen, cap and store at 4<sup>0</sup>C.

Spotting :

**Reagents:**

Solvent 1- SOP: GC/20/08

Solvent 2- Boric acid solvent SOP: GC/20/08

Transmethylating solution

Hexane

**Equipment and instruments needed:**

Waterbath (45°C)

Hamilton syringe (100 µL, 500 µL)

TLC-plates (silica jel 60, Merck art no 5721) -activate the plates before use.

Glass tubes

Block (70°C)

Glass tank

Nitrogen evaporator

**Method:**

1. Evaporate sample in a waterbath under nitrogen.
2. Wash down inside of tube with 1 ml CMS, dry under nitrogen and repeat once more.
3. Put tubes on ice, and make up to x µL with syringe (x = number of samples).
4. Pre-equilibrate a filter paper lined separation tank with solvent 1 for at least 10 minutes before use.
5. Spot x µL for neutral and phospholipids and develop the spotted plate in solvent 1 for 15 minutes (x = number of samples).
6. Dry the plate under nitrogen for 10 minutes.
7. Pre-equilibrate a filter paper lined separation tank with solvent 2 for at least 25 minutes before use.

8. The separated neutral lipids are located by spraying the plate with BBOT (dissolved in chloroform /methanol, 1:1, v/v).
9. Mark the separated components, with the help of the appropriate standard, under an UV-light and scrape of the spots into glass tubes.
10. Add 2 ml trans-methylating solution to samples, cap and put in the block (70°C) for 2 hours.
11. After scraping of the neutral lipids, dry the plate for 30 minutes under nitrogen.
12. For the separation of the phospholipids, develop the same plate in a separate tank with solvent 2 for 30 minutes.
13. Dry the plate for at least 25 minutes under nitrogen.
14. Mark the phospholipids spots and scrape off carefully.
14. After transmethylation of the neutral lipids cool samples at room temperature.
15. Add 2 ml hexane, apply nitrogen and store at 20°C.
16. Samples are now ready to be processed for GC analysis, except for the CE that has to be spotted again for the methyl esters.